The Role of Neural Crest in Vertebrate Evolution:

Tissue-specific Genetic Labeling in Zebrafish (*Danio rerio*) Reveals Neural Crest Contribution to Gills, but Not to Scales

Dissertation
der Mathematisch-Naturwissenschaftlichen Fakultät
der Eberhard Karls Universität Tübingen
zur Erlangung des Grades eines Doktors
der Naturwissenschaften
(Dr. rer. nat.)

vorgelegt von
Alessandro Mongera
aus Trento
(Italien)

Tübingen
2013

Tag der mündlichen Qualifikation: 09.12.2013

Dekan: Prof. Dr. Wolfgang Rosenstiel
1. Berichterstatter: Prof. Dr. Christiane Nüsslein-Volhard
2. Berichterstatter: Prof. Dr. Rolf Reuter
3. Berichterstatter: Dr. Didier Stainier

to my friends

Contents

Abstract

During vertebrate evolution, the development of an active, predatory lifestyle and an increased body size coincided with the appearance of many morphological innovations. Among these vertebrate-specific phenotypic features, a major role in promoting the massive radiation of this animal group has been played by a new, true head. The neural crest (NC), an embryonic population of multipotent cells that first appears within the chordate phylum, is a major ontogenetic source for the vertebrate head and its contribution to the cranial skeleton has been intensively studied in different model organisms. However, this head is not exclusively formed by a skull protecting a centralized nervous system and a jaw for water influx control and prey capture, but also by gills that serve as a new respiratory organ. The role of NC in the expansion of the respiratory surface of the gills has been so far neglected. In particular, the embryonic origin of pillar cells, the functional and structural core of the gill filaments, is unclear, although it has been suggested that they may derive from the lateral plate mesoderm, from endothelial cells, or from smooth muscles.
During my doctoral studies, I used genetic lineage labeling to first address the contribution of NC to the gills of adult zebrafish. I generated a tamoxifen-inducible sox10:ER^{T2}-Cre

line and labeled NC cells by inducing Cre/loxP-dependent recombination at embryonic stages. In the gills, intriguingly, we observed labeled primary and secondary filaments. In particular, pillar cells, which mechanically support the filaments and form gill-specific capillaries, have a NC origin. This result points to a critical role of NC in facilitating more efficient gas exchange and thus uncovers a novel, direct involvement of this embryonic tissue in the evolution of respiratory systems during vertebrate evolution.

Within the phylum Chordata, vertebrates evolved also the ability to produce a mineralized skeleton, which represents along with the expanded gills another important innovation. This skeleton, which supports the body, allows locomotion, and protects internal organs, can be divided into a superficial dermal skeleton (integumentary skeleton) and a more internal endoskeleton. Bones forming the dermal skeleton (dermal bones) do not derive from cartilaginous tissues but form directly from intramembraneous ossifications; bones of the endoskeleton (endochondral bones), on the contrary, develop from pre-formed cartilage and replace it. While during tetrapod evolution and the conquest of land a post-cranial integumentary skeleton has been lost in many lineages and only the dermal bones of the skull were maintained, the trunk in fish remains covered by a large variety of diverse skeletal elements, which are generally referred to as 'scales'. Structural and ontogenic similarities with NC-derived teeth and cranial dermal bones have led to the widely accepted view that scales may derive from NC and not from mesoderm likewise parts of the neurocranium and the complete axial endoskeleton. I tested this hypothesis by Cre/loxP-based genetic labeling and found that sox10:ER^{T2}-Cre-dependent recombination does not lead to substantial mark-

ing of post-cranial integumentary skeletal elements, suggesting a non-NC origin for these tissues. By using a mesoderm-specific Cre-driver line and performing transplantation experiments and transposon-mediated clonal analysis I found a mesodermal origin for scale-forming osteoblasts, thus *i)* supporting the notion of a non-skeletogenic trunk NC *in vivo* and *ii)* rejecting a long-standing, but not yet experimentally tested, influential assumption.

Zusammenfassung

Während der Evolution der Wirbeltiere ging die Entwicklung von räuberischer Ernährungsweise und wachsender Körpergröße mit der Entstehung vieler neuer Körperstrukturen einher. Zu diesen vertebratenspezifischen Strukturen gehört insbesondere die Entwicklung des Kopfes mit Schädel und Kiefer, die eine zentrale Rolle bei der massiven Zunahme der Formenvielfalt der Wirbeltiere gespielt hat. Die Neuralleiste, eine Anlage multipotenter embryonaler Zellen, die neu im Phylum der Chordatiere erscheint, ist die primäre ontogenetische Quelle für den Kopf der Wirbeltiere. Der Beitrag der Neuralleiste zur Bildung der Knochen des Kopfes wurde in unterschiedlichen Modellorganismen intensiv untersucht. Der neue Kopf der Vertebraten besteht neben dem Schädel, der das zentrale Nervensystem schützt, und dem Kiefer, der den Wasserstrom regelt und zum Fang der Beute dient, auch aus Kiemen, die als neues Atmungsorgan fungieren. Die Rolle der Neuralleiste bei der Entstehung der Kiemen, die eine entscheidende Vergrößerung der Oberfläche für den Gasaustausch darstellen, wurde bislang wenig untersucht. Insbesondere ist die embryologische Herkunft der Pillarzellen, welche die funktionale und strukturelle Basis der Kiemenlamellen bilden, noch unklar. Es wurde bisher angenommen, dass sie aus dem Seitenplattenmesoderm, den en-

dothelialen Zellen oder der glatten Muskulatur entstehen.
Während meiner Doktorarbeit habe ich eine genetische, klonale Analyse durchgeführt, um den Beitrag der Neuralleiste an der Bildung adulter Strukturen, besonders der Kiemen, im Zebrabärbling zu untersuchen. Eine Tamoxifen-induzierbare sox10: ER^{T2}-Cre-Linie wurde generiert. Mit dieser wurde in Neuralleistenzellen im embryonalen Stadium Cre/loxP-abhängige Rekombination in einem Reportergen induziert. Die resultierenden Klone markieren Neuralleistenzellen und ihre Nachkommen. In den Kiemen konnte ich eine Markierung primärer und sekundärer Kiemenlamellen nachweisen. Insbesondere wurden Pillarzellen, welche die Lamellen mechanisch unterstützen und kiemenspezifische Kapillaren bilden, markiert und damit gezeigt, dass diese von der Neuralleiste abstammen. Dieses Resultat zeigt, dass die Neuralleiste bei der Entwicklung der Kiemen eine wichtige Rolle spielt und direkt an der Evolution des effizienteren Atmungsystems der Wirbeltiere beteiligt ist.
Im Phylum der Chordaten haben Wirbeltiere die Fähigkeit entwickelt, mineralisiertes Knochengewebe, aus dem das Skelett besteht, zu bilden,. Dieses Skelett, das den Körper stützt, ermöglicht eine differenzierte Fortbewegung und beschützt auch die inneren Organe. Es besteht aus dem äußeren Dermalskelett und dem tiefergelegenen Innenskelett (Endoskelett). Knochen, die das Dermalskelett bilden (Hautknochen), entstehen nicht aus Knorpelgewebe, sondern durch dermale Ossifikation. Knochen des Endoskeletts (enchondrale Knochen) hingegen entwickeln sich aus vorgeformtem Knorpel und ersetzen ihn im Laufe der Entwicklung. Während der Evolution ist in den meisten Landwirbeltieren das postkraniale Dermalskelett verloren gegangen, lediglich die Dermalknochen des Schädels sind erhalten geblieben. Dagegen ist bei Fischen der Rumpf von Schup-

pen, die aus Dermalknochen bestehen, bedeckt. Strukturelle und ontogenetische Ähnlichkeiten mit den aus der Neuralleiste stammenden Zähnen und kranialen Hautknochen haben zur weitverbreiteten Annahme geführt, dass Schuppen auch aus der Neuralleiste entstammen und nicht aus dem Mesoderm, wie andere Teile des Neurokraniums und das axiale Endoskelett. Ich habe diese Hypothese durch genetische, klonale Analyse überprüft und herausgefunden, dass die durch sox10:ER^{T2}-Cre hervorgerufenen Rekombinationen nicht zu einer wesentlichen Markierung von postkranialen dermalen Skelettelementen führen. Durch klonale Analyse mit einer mesodermspezifischen Cre-Linie sowie Transplantationsexperimenten und Transposon-basierter Markierung habe ich gezeigt, dass die schuppenbildenden Knochenzellen einen mesodermalen Ursprung haben. Damit konnte ich die bisher ungeprüfte Hypothese, dass Schuppen aus der Neuralleiste abstammen, widerlegen und zeigen, dass die knochenbildene Rolle der Neuralleiste auf Strukturen des Kopfes beschränkt ist.

CHAPTER 1

Introduction

1.1 Neural crest as a source of vertebrate innovations

The neural crest (NC) is an embryonic population of multipotent cells that first appears within the phylum Chordata and represents the ontogenetic source of a large variety of vertebrate innovations [Gans and Northcutt, 1983]. In contrast to endoderm, mesoderm, and ectoderm, this tissue is not defined as a distinct population of cells at the onset of gastrulation; however, NC gives rise to such a vast range of cell types that it has been regarded as the *fourth germ layer*. According to this notion, vertebrates are quadroblastic animals, e.g. animals with four germ layers, as opposed to non-vertebrate chordates, which are characterized by three germ layers and thus possess a triploblastic embryonic organization likewise the rest of *Bilateria* [Hall, 2000].
In zebrafish, NC cells (NCCs) are first induced during neurula

stages at the level of the dorsal neural tube, where they subsequently undergo delamination and epithelial-to-mesenchymal transition (EMT). Following EMT, the newly formed population of mesenchymal cells, located at the interface between the neural tube and the overlying ectoderm, starts soon to migrate along two major routes: a lateral route, between the skin and the lateral aspect of somites, and a ventral route, between the neural tube and the medial aspect of somites. Although different NC-derived cell types arise during early phases of the ontogeny of this tissue, it is still a matter of debate whether NC specification into different cell lineages occurs generally before, during, or after migration, at the location where cells will reside [Hall, 2000].

NC can be divided, along the antero-posterior axis, into 5 major populations [Hall, 2009]: *i)* cranial NC (CNC), which gives rise to sensory neurons of the cranial nerves, odontoblasts forming the teeth, osteoblasts of the dermal skull, chondroblasts of the jaws, and pigment cells; *ii)* cardiac NC (CarNC)(from somites 1-3), which forms smooth muscles of the great arteries and contributes to the aortico-pulmonary septum in the heart; *iii)* vagal NC (VNC)(from somites 1-7), which gives rise to enteric ganglia of the gut; *iv)* trunk NC (TNC)(posterior to somite 6), which differentiates into pigment cells, sensory neurons forming the dorsal root ganglia (DRGs), neurons of the sympathetic system, and chromaffin cells of the adrenal medulla; and *v)* sacral NC (SNC)(posterior to somite 28), which gives rise to enteric neurons predominantly in the hindgut.

Since its discovery by His, the diverse fates of NC cells have been a matter of profound interest [His, 1868]. While the NC origin of cranial and spinal ganglia has been easily accepted because of the ontogenic association of these multipotent cells

to the neurogenic ectoderm, the notion of a NC-derived head mesenchyme has been initially rejected [Hall, 2009]: according to the germ-layer theory, developed in the 19th century by many influential naturalists [Pander, 1817; Huxley, 1849; Lankester, 1873], mesoderm was indeed the exclusive source of skeletal tissue. A NC origin for odontoblasts and cartilage of the craniofacial and pharyngeal arch skeletons has been first claimed by Platt, on the basis of experiments conducted in the mudpuppy *Necturus maculosus* [Platt, 1893, 1894]. These results remained controversial until supporting evidence for a non-mesodermal origin of a large set of cranial skeletal elements has been finally provided in independent studies and in different organisms [Landacre, 1921; Stone, 1929; de Beer, 1947; Hörstadius, 1950].

While many vertebrate-specific structures have been shown over the years to derive from NC cells [Le Douarin and Kalcheim, 1999; Hall, 2009], a possible NC origin for gills, which are a prominent feature of the new head of vertebrates, has never been a subject of investigation. This lack of attention is remarkable because it stands in contrast with the general acceptance of the 'new head' theory framework, which regards NC as the major embryonic source of a large set of vertebrate innovations [Gans and Northcutt, 1983]. Although the cartilaginous gill arch endoskeleton [Landacre, 1921] and the muscolo-connective walls of pharyngeal blood vessels [Le Lievre and Le Douarin, 1975] have long been recognized as NC derivatives, the embryonic origin of gill pillar cells, which represent the functional core of the gills and are the major player in the expansion of the respiratory surface, was unknown [Hughes and Morgan, 1973].

Similarly, also the embryonic origin of the post-cranial integu-

mentary dermal skeleton, which in fish is formed by scales and fin rays, was not clear. In spite of a lack of experimental evidence, this skeletal elements have been widely regarded as *bona fide* NC derivatives, for at least three reasons: *i)* a large set of dermal bones forming the skull have a NC origin, thus showing that this embryonic tissue has the potential to differentiate in bone-forming cells of the integument [Le Douarin and Kalcheim, 1999; Hall, 2009]; *ii)* scales are similar to teeth, which are well established NC derivatives [Smith and Hall, 1990]; *iii)* the 'new head' theory, previously mentioned, has been really influential, dictating the theoretical framework of many research programs in the field of vertebrate evolution [Gans and Northcutt, 1983].

1.2 Tools for cell lineage tracing

1.2.1 Non-genetic labeling

Many techniques to define the fates of NC cells have been developed [Le Douarin and Kalcheim, 1999]. Extirpation, for example, is based on the surgical removal of the dorsal neuroepithelium or neural folds and on the analysis of the deficiencies caused by the operation: tissues that do not form are likely to derive from the removed cell population. This technique does not require a labeling step and has been also used for NC fate mapping in jawless fish and teleosts [Langille and Hall, 1988, 1986], although it possibly leads to an overestimation of the contribution to post-embryonic structures of such removed tissues. Interactions between tissues are generally important in

diverse morphogenetic processes, thus the complete or partial absence of a structure may depend on the removal of a non-lineage-related tissue that serves as instructive developmental signal and not on the actual removal of its own, direct embryonic source [Le Douarin and Kalcheim, 1999].
Besides extirpation, specific markers and labeling tools that allow these cells to be identified throughout ontogeny, after different rounds of cell division and differentiation, are generally a prerequisite. Indeed, vital dye injections into premigratory NC cells have represented a widely used alternative to neural tube extirpation. This technique allows for an elevated precision in targeting specific cells, thus avoiding the high false positive rate that can possibly be encountered in extirpation experiments. However, it does not permit to trace NC to adult structures, as the dye gets diluted after few rounds of cell divisions [Le Douarin and Kalcheim, 1999]. The most commonly used reagents are the lipophilic dyes DiI and DiO [Selleck and Stern, 1991; Lumsden, 1991; Schilling and Kimmel, 1994] and the lysinated rhodamine dextran (LRD) [Schilling and Kimmel, 1994; Warga and Kimmel, 1990; Bronner-Fraser and Fraser, 1988; Collazo et al., 1993]. While DiI and DiO are incorporated into the membranes, LRD enters the cell and offers thus a more unambiguous means to precisely label specific cells and their progeny [Collazo et al., 1993].
This short-term labeling technique has been replaced in avians by the quail-chick marker system, which allows for long-term tracing of embryonic tissues, and in particular of NC, to post-embryonic and adult organs [Le Douarin, 1974; Le Douarin and Kalcheim, 1999]. This system consists in the grafting of a portion of the neural tube and the associated neural folds (the embryonic origin of NC) between quail and chick embryos. Spe-

cifically, a fragment of the neural tube of the recipient (usually the chick embryo) is surgically removed using a microscalpel, while the notochord and the paraxial mesoderm are left *in situ*. A similar neural tube fragment is obtained from the donor (usually the quail embryo), treated with trypsin in order to dissociate residual mesodermal cells lying on its surface, and grafted into the host [Le Douarin and Kalcheim, 1999]. Donor cells from quail, after NC migration and differentiation, were recognized initially by the morphology of the nuclei and subsequently by species-specific antibodies that exclusively bind to quail epitopes [Le Douarin and Kalcheim, 1999]. Although the quail-chick chimeras permit to trace NC cells throughout ontogeny, this technique presents some disadvantages: *i)* grafting experiments require non-trivial manipulation skills; *ii)* the system is specific for avians and therefore not useful to perform comparative analysis in other animal models; *iii)* contamination from other embryonic tissues, e.g. mesodermal cells in NC grafts, are difficult to control.

A modified version of this technique has been developed in zebrafish and consists in transplanting at embryonic stages donor cells constitutively expressing a fluorophore into *wild type* host embryos. Placed in specific positions, these transplanted progenitors give rise to organs and structures that retain the original labeling. Although this system allows in principle for long-term fate mapping of any tissue and cell population, a major caveat is represented by the difficulty of targeting a single, specific embryonic region during the grafting. This kind of manipulation leads often to multiple clones that may not share a common lineage.

Extirpation, vital dye injections, the quail-chick marker system and transplantation experiments are still important tools

to define the embryonic source of post-embryonic and adult structures; however, as previously described, they have disadvantages that are difficult to overcome. In the last decades, a new technique to genetically label individual cells and their clonal progeny has been developed: taking advantage of an endogenous mechanism developed by the bacteriophage P1, this genetic system allows for specific and permanent labeling of cell lineages in mouse [Orban et al., 1992], zebrafish [Bertrand et al., 2010], and chick [Yokota et al., 2011].

1.2.2 Cre/loxP-mediated genetic labeling

The Cre/loxP system is a site-specific recombination system which is based on two components: a Cre recombinase and a pair of short DNA sequences called loxP sites. The Cre recombinase is able to recognize the loxP sequences and to drive their recombination, whose outcome depends on the original orientation of the two sites: if they have identical orientation, the recombination will cause a deletion event; if they have opposite orientation, an inversion of the flanked DNA will be produced. This simple mechanism can be employed to cause deletions and insertions in cell lines and transgenic animals. Originally developed to induce genetic modifications in cell culture [Sauer and Henderson, 1988], this system became soon a fundamental tool for gene knock-out and knock-in also in mouse [Orban et al., 1992]. Applied to mouse, this system required two transgenic lines, carrying two different genetic insertions: *i)* a line expressing the Cre recombinase under the control of a tissue-specific promoter; and *ii)* a line carrying loxP sites inserted in specific endogenous loci or as parts of an

ubiquitously expressed transgenic insertion (loxP cassette). In knock-out strategies, the loxP sites are usually inserted in loci flanking specific exons, whose deletion by Cre-mediated recombination may cause a premature stop and thus a non-functional protein product. In knock-in strategies, the loxP sites are instead inserted as parts of a transgenic cassette which usually contains a promoter for ubiquitous or tissue-specific expression and an inverted coding sequence for a desired protein. The loxP sites flank this sequence, which only after recombination-mediated inversion can encode for a functional product. This product is either a protein of interest for mis- or overexpression experiments or a marker for cell lineage tracing. Importantly, this system is widely used to permanently label specific cells and their progeny, as the Cre-mediated recombination leads to genetic modifications that are stably inherited within clonal lineages.

The major caveat of this system in its original design was the full dependency of the recombination events on the temporal domain of the promoter used to drive the Cre recombinase, which leads to two important problems: *i)* impossibility to study in knock-in experiments late phenotypes if the tissue-specific promoter acts also earlier during development leading to lethality or substantial defects; *ii)* marking of tissue which does not originate from the cells of interest if the promoter, throughout development, drives transgene expression also in other cell types. To overcome these issues a modified version of the system, which allows for a tight temporal control of recombination, has been conceived [Metzger et al., 1995]. Specifically, the Cre recombinase has been engineered in a way that its nuclear translocation, and thus its activity, occurs only after tamoxifen treatment. The Cre/loxP technology has been

recently employed to trace embryonic population of cells to post-embryonic or adult structures also in zebrafish [Bertrand et al., 2010; Hans et al., 2009, 2011]. For example, using a zebrafish Cre-driver line specific for the embryonic vascular endothelium, it was shown that hematopoietic stem cells derive from the aortic endothelium [Bertrand et al., 2010]. Notably, although the system has become popular for genetic cell tracing also in this model organism, it has been not yet fully developed for knock-in strategies.

1.3 The gills

According to the 'new head' theory, the evolution of a true head, largely of NC and placodal origin, has accompanied the shift from filter-feeding to active predation, driving vertebrate radiation [Gans and Northcutt, 1983]. While a proto-NC can be found in the tunicate *Ciona intestinalis* [Abitua et al., 2012], this tissue acquires its full repertoire of features only at the protochordate-vertebrate transition, concomitantly with the development of the new vertebrate lifestyle. Important features of the vertebrate head are a skull protecting and accommodating a centralized nervous system and paired sense organs, a jaw for water influx control and prey capture, and gills as respiratory organs [Gans and Northcutt, 1983]. Although the NC contribution to the cranial skeleton has been intensively studied in different model organisms [Hall, 2000; Le Douarin and Kalcheim, 1999], its role in the expansion of the respiratory surface of the gills has been neglected.
Gills are the primary site of aquatic respiration in all the

fish groups (Agnatha, Chondrichthyes, Actinopterygii). Aerial-breathing species may use, in addition to gills, the skin or the swim bladder [Evans et al., 2005]. The vertebrate gills are characterized by primary and secondary gill filaments (lamellae) that consist of a highly complex vasculature surrounded by respiratory epithelium. These tissues are connected to, and supported by, the pharyngeal arches. In cephalochordates and urochordates, which represent the vertebrate sister group, gills are simple structures with reduced size, leading to a small ratio between respiratory surface area and body volume [Evans et al., 2005]. Particularly, in the cephalochordate amphioxus, the gills are formed by thin bars that are vertically oriented along the walls of the pharynx. These bars contain blood vessels and neurons, are supported by an internal rod of collagen, and are covered by a ciliated epithelium [Evans et al., 2005]. During evolution, respiration shifted from these ciliated epithelia to complex gill organs which, coupled to muscular ventilation, greatly increased gas exchange capacity, thus contributing to the development of more active life styles and of larger body sizes [Evans et al., 2005; Gans and Northcutt, 1983].

Although important elements of the gills such as the cartilaginous gill arch endoskeleton and the walls of pharyngeal blood vessels are long established NC derivatives [Landacre, 1921; Le Lievre and Le Douarin, 1975], the embryonic origin of gill pillar cells, another major components of the gill organ, remains unclear [Hughes and Morgan, 1973]. Pillar cells represent the functional and structural core of the gill filaments in that they support mechanically the respiratory epithelium and form capillary beds for blood perfusion [Hughes and Morgan, 1973]. Notably, they are also thought to control gas exchange by modulating the volume of vessel lumina via specific cyto-

plasmic processes [Smith and Chamley-Campbell, 1981; Evans et al., 2005]. Over the years, it has been suggested that pillar cells may derive from the lateral plate mesoderm or hypomere [Gans and Northcutt, 1983], from endothelial cells [Bietrix, 1895], or from smooth muscles forming the blood vessels entering the primary filaments [Datta Munshi and Singh, 1968]. I used genetic lineage labeling to address the contribution of NC to the gills of adult zebrafish. Although the relevance of the 'new head' theory for the interpretation of vertebrate evolution, this important feature of the vertebrate head has never formally proposed as a NC derivative and no studies directed to deciphering its embryonic origin have been produced.

1.4 The post-cranial integumentary skeleton

Within the phylum Chordata, vertebrates evolved the ability to produce mineralized tissues [Sire et al., 2009]. In the 'new head' theory, Northcutt and Gans regarded neural crest (NC) as the *bona fide* ontogenetic source for a large set of vertebrate-specific traits [Gans and Northcutt, 1983]. In the light of this theory, structural and ontogenic similarities with NC-derived teeth and dermatocranial bones of the skull, have led to the widely accepted view that components of the post-cranial integumentary skeleton such as scales, scutes and bony plates may derive from NC and not from mesoderm as the axial endoskeleton [Sire et al., 2009; Smith and Hall, 1990]. Notably, it has been further proposed that the appearance of post-cranial dermal bones may predate, at the protochordate-vertebrate

transition, the evolution of axial endochondral bones [Smith and Hall, 1990]. Therefore, the NC-derived skeleton might have played a more significant role than the mesoderm-derived skeleton in driving the early phases of vertebrate radiation. The view of a NC origin for these bony elements, however, has not been confirmed and contradicts the notion of an opposition between a *skeletogenic* cranial NC and a *non-skeletogenic* post-cranial NC [Hall, 2000]. Classical experiments in chick embryos have shown for instance that TNC cells grafted in cranial regions are able to form a large set of CNC derivatives but not NC-derived cartilaginous or bony elements of the skull [Nakamura and Ayer-le Lievre, 1982].

The post-cranial integumentary skeleton of aquatic vertebrates provides protection and improves the mechanics of locomotion [Sire et al., 2009]. Scales of fish, as opposed to the epidermis-derived scales of reptiles and birds, are skeletal elements that form in the dermis [Sire and Akimenko, 2004]. Despite their structural and morphological diversity, these structures, which can be generally referred to as 'scales', are thought to share a common evolutionary predecessor, the odontode, and are thus considered homologous [Huysseune and Sire, 1998; Sire and Huysseune, 2003; Reif, 1982]. Odontodes are mineralised, multi-layer functional units consisting of attachment bone, dentine and, in specific cases, enamel/enameloid in the outermost surface. Developing from a single ontogenetic source, e.g. the dermal papilla, odontodes are found either attached to dermal bone or freely in the skin [Smith and Hall, 1990].

Among the different types of scales found in extant fish, only placoid scales of Chondrichthyes such as sharks and rays feature the original organization of odontodes whereas the other scale types represent substantial modifications. In particular,

scales in teleost fish, referred to as elasmoid scales, are highly derived structures [Sire and Akimenko, 2004]. Notably, the modification and reduction of the integumentary skeleton represents an evolutionary trend during vertebrate radiation [Sire et al., 2009]. The highly simplified structure of elasmoid scales, which are the most common post-cranial dermoskeletal element among living vertebrates [Sire et al., 2009], and the general lack of structural details at the tissue level compromise the possibility to easily identify homologies with more ancient scale types [Sire et al., 2009]. Analysis of the development of scale tissues and informations about their embryonic origin would be helpful to define the evolutionary relationships between different exoskeletal components [Sire et al., 2009].

Tracing the embryonic origin of scales is complicated by the late onset of their development. In zebrafish, scales form approximately at 30 days post-fertilization (dpf) along the lateral line and then expand giving rise to a species-specific squamation pattern [Sire and Akimenko, 2004]. To overcome this problem and shed more light on a possible NC contribution to the scales of zebrafish, I have used stable genetic lineage tracing based on tamoxifen-inducible ER^{T2}, transplantation experiments and transposon-based clonal analysis. Surprisingly, I found that mesoderm-derived cells participate in zebrafish scale formation by giving rise to scale-forming osteoblasts.

CHAPTER 2

Results

Publication 1:

Mongera A., Singh A.P., Levesque M.P., Chen Y.Y., Konstantinidis P., and Nüsslein-Volhard C. (2013). **Genetic lineage labeling in zebrafish uncovers novel neural crest contributions to the head, including gill pillar cells.** *Development* 140(4):916-25.

Extensive fate mapping of NC has been performed in many organisms representative of different vertebrate taxa, with a focus on chick, frog, and mouse [Le Douarin and Kalcheim, 1999; Bronner-Fraser and Fraser, 1988; Collazo et al., 1993; Chai et al., 2000; Le Douarin, 1986]. Many structures arise at post-embryonic or adult stages; therefore long-term labeling techniques are required to uncover their ontogenic source. The gills

were lost very early in the evolution of tetrapods, making the Cre/loxP system developed in mouse and chick-quail graftings unsuitable for this purpose. In zebrafish and in medaka, short-term labeling techniques such as vital dye injections [Schilling and Kimmel, 1994; Li et al., 2003; Wada et al., 2005] and long-term techniques such as transplantation and ablation [Langille and Hall, 1988] have been employed to trace NC cells in the larvae. However, these methods have severe limitations as far as adult structures are concerned, as the label does not persist through adulthood or unspecific marking is more difficult to control.

To overcome these limitations I generated a transgenic line driving the inducible ER^{T2}-Cre recombinase under the control of the NC-specific *sox10* promoter. This promoter has been shown to be specific for NC cells and oligodendrocytes in early development [Carney et al., 2006]. Crossing the Cre-driver line to multiple reporter lines with different loxP cassettes, I first showed that the recombination occurs under tight control of externally supplied tamoxifen, which acts allowing the nuclear localization of the ER^{T2}-Cre [Metzger et al., 1995]. Further, I found that at larval stages recombined tissue comprises well established NC derivatives, such as the viscerocranium, glia wrapping the primary motor axons, and pigment cell precursors. In metamorphic and adult fish, many cranial and trunk derivatives were labeled, such as the taenia marginalis, the epiphyseal bar, the ethmoid plate, the trabeculae, sympathetic neurons, dorsal root ganglia, neurons of the enteric nervous system, melanophores, xanthophores, and iridophores [Le Douarin and Kalcheim, 1999; Hall, 2009].

Besides confirming in a teleost species the NC origin of structures that have been known to derive from this embryonic tis-

sue from studies carried on in other organisms, I showed that:

i) the entire opercular series, which forms a dermoskeletal flap improving suction feeding and fluid movement control through mouth and gills, receives contribution from NC;

ii) many cell types forming the barbels, tentacle-like chemosensory structures protruding from the integument of the mouth region, have a NC origin;

iii) the border between NC and mesoderm contribution in the skull roof (NC/mesoderm interface), which is formed by the frontal and parietal dermal bones, is located in the anterior region of the frontals;

iv) in the gill filaments, smooth muscles of the blood vessel tunica media and, more interestingly, pillar cells are NC derivatives.

As the definition of NC origin rests on the specificity of the *sox10* promoter, I validated these new findings inducing recombination with a second, NC-specific promoter from the *crestin* locus [Luo et al., 2001; Chen, 2011]. Notably, the entire set of novel NC-derived structures has been confirmed.

Development 140, 916-925 (2013) doi:10.1242/dev.091066

Genetic lineage labeling in zebrafish uncovers novel neural crest contributions to the head, including gill pillar cells

Alessandro Mongera[1,*], Ajeet P. Singh[1], Mitchell P. Levesque[1,‡], Yi-Yen Chen[1,§], Peter Konstantinidis[2] and Christiane Nüsslein-Volhard[1,*]

SUMMARY

At the protochordate-vertebrate transition, a new predatory lifestyle and increased body size coincided with the appearance of a true head. Characteristic innovations of this head are a skull protecting and accommodating a centralized nervous system, a jaw for prey capture and gills as respiratory organs. The neural crest (NC) is a major ontogenetic source for the 'new head' of vertebrates and its contribution to the cranial skeleton has been intensively studied in different model organisms. However, the role of NC in the expansion of the respiratory surface of the gills has been neglected. Here, we use genetic lineage labeling to address the contribution of NC to specific head structures, in particular to the gills of adult zebrafish. We generated a *sox10:ER^{T2}-Cre* line and labeled NC cells by inducing Cre/loxP recombination with tamoxifen at embryonic stages. In juvenile and adult fish, we identified numerous established NC derivatives and, in the cranium, we precisely defined the crest/mesoderm interface of the skull roof. We show the NC origin of the opercular bones and of multiple cell types contributing to the barbels, chemosensory organs located in the mouth region. In the gills, we observed labeled primary and secondary lamellae. Clonal analysis reveals that pillar cells, a craniate innovation that mechanically supports the filaments and forms gill-specific capillaries, have a NC origin. Our data point to a crucial role for the NC in enabling more efficient gas exchange, thus uncovering a novel, direct involvement of this embryonic tissue in the evolution of respiratory systems at the protochordate-vertebrate transition.

KEY WORDS: Neural crest, Pillar cells, Cre/loxP, Zebrafish, Cranial neural crest, Gill

INTRODUCTION

The evolution of a true head has been proposed as a major step in the protochordate-vertebrate transition, enabling the shift from filter feeding to active predation (Northcutt and Gans, 1983). The vertebrate head that has been assembled stepwise over evolutionary time displays functional characteristics that serve prey detection and capture but also enable a more efficient respiratory metabolism (Gans and Northcutt, 1983). Indeed, a predatory lifestyle requires a higher metabolic rate, which in turn establishes a positive selective pressure for enhanced gas exchange and distribution. To increase gas exchange capacity, respiration shifted during evolution from ciliated epithelia along the walls of the pharynx to complex gill organs attached to the branchial arches. Craniates, which include vertebrates and hagfishes, developed gills with highly organized filamentous structures that enable a massive expansion of the surface area involved in respiration (Evans et al., 2005).

The 'new head' theory of Northcutt and Gans proposes that many morphological and functional innovations of vertebrates develop from the neural crest (NC), the epidermal placodes or the lateral plate mesoderm (Northcutt and Gans, 1983). Although the original claims of this theory regarding the origin of NC and placodes have been subsequently refuted, a huge body of work has confirmed the important role of NC in accelerating vertebrate evolution (Northcutt, 2005; Yu et al., 2008; Abitua et al., 2012). NC is a pluripotent embryonic tissue that differentiates into numerous cell types, such as osteoblasts and chondroblasts in the skull, neurons of the peripheral nervous system, Schwann cells and pigment cells (Hörstadius, 1950; Le Douarin, 1986; Le Douarin and Dupin, 2012). Further, NC is suggested to have played a crucial role in vertebrate brain development by promoting forebrain viability, a prerequisite for brain expansion (Etchevers et al., 1999).

Although the NC origin of the cartilaginous gill arch endoskeleton (Landacre, 1921) and of the walls of pharyngeal blood vessels (Le Lièvre and Le Douarin, 1975) is long established, the embryonic origin of gill pillar cells, which represent the functional and structural core of the gill lamellae, is unclear (Hughes and Morgan, 1973). It has been suggested that this important component of the gill filaments might derive from the lateral plate mesoderm (Northcutt and Gans, 1983), from endothelial cells (Bietrix, 1895) or from smooth muscles (Datta Munshi and Singh, 1968).

Extensive fate mapping of NC has been performed in many organisms representative of different vertebrate taxa (Le Douarin and Kalcheim, 1999), notably by transplantation experiments creating chick-quail chimeras (Le Douarin, 1986), vital dye injection in the premigratory NC of chick and frog (Bronner-Fraser and Fraser, 1988; Collazo et al., 1993), tissue extirpation in medaka and lampreys (Langille and Hall, 1988a; Langille and Hall, 1988b), and genetic lineage labeling using Cre/loxP-mediated recombination in mice (Chai et al., 2000; Jiang et al., 2002). However, a more detailed map for adult structures in hagfishes, lampreys and ray-finned fishes (actinopterygians) would be extremely valuable, as important structures of the 'new head', such as the gills, were lost very early in the evolution of tetrapods with the acquisition of a terrestrial lifestyle. In zebrafish and medaka, vital dye injection, expression of reporter genes and transplantation experiments have been employed to follow the migration of NC-

[1]Max-Planck-Institut für Entwicklungsbiologie, 72076 Tübingen, Germany. [2]Institut für Spezielle Zoologie und Evolutionsbiologie mit Phyletischem Museum, Friedrich-Schiller-Universität Jena, 07743 Jena, Germany.

*Authors for correspondence (alessandro.mongera@tuebingen.mpg.de; christiane.nuesslein-volhard@tuebingen.mpg.de)
‡Present address: University of Zurich Hospital, 8091 Zurich, Switzerland
§Present address: GeneTex International Corporation, 300 Hsinchu, Taiwan

Accepted 12 December 2012

derived cells in the larva (Langille and Hall, 1988a; Schilling and Kimmel, 1994; Li et al., 2003; Wada et al., 2005). However, these methods have severe limitations as far as adult structures are concerned, as the label becomes diluted or transgene expression does not persist through adulthood.

To overcome these limitations and to permanently and specifically label NC cells and their derivatives in zebrafish, we generated a transgenic line expressing tamoxifen-inducible Cre recombinase under the control of the *sox10* promoter (Carney et al., 2006). *Sox10* is expressed specifically in the NC at early stages of development (Dutton et al., 2001). We induced Cre/loxP-mediated recombination in various reporter lines during embryonic development and identified in larval, juvenile and adult fish numerous established NC derivatives, including multiple elements of the cranial skeleton, peripheral nervous system components, pigment cells and glia, thus confirming the specific expression of the *sox10* promoter in NC cells during the time of induction.

Moreover, we were able to define the NC/mesoderm interface in the zebrafish frontoparietal bones, which are dermoskeletal elements whose origin across vertebrate taxa is still debated (Couly et al., 1993; Gross and Hanken, 2008a; Noden and Trainor, 2005), and to demonstrate a NC contribution to other head structures of uncertain origin.

Strikingly, we observed labeled gill filaments, including primary and secondary lamellae. In particular, we discovered labeled pillar cells, which represent a craniate innovation that provides the basis for the surface expansion of the gills (Evans et al., 2005). Pillar cells form capillary beds for blood perfusion and have mechanosensory properties (Smith and Chamley-Campbell, 1981; Evans et al., 2005). We propose that the development of this atypical NC-derived cell type at the protochordate-vertebrate transition led to the appearance of a more complex gill organ, supporting the relevance of the 'new head' theory to the evolution of the respiratory system.

MATERIALS AND METHODS

Transgenic lines

To generate *Tg(cmlc:GFP-sox10:ER^{T2}-Cre)* (abbreviated to *sox10:ER^{T2}-Cre*), the *(−4.9kb)sox10* promoter (Carney et al., 2006) was subcloned into a pTol2-*cmlc:GFP* plasmid and the ER^{T2}-Cre coding sequence (Metzger et al., 1995) was PCR amplified and inserted by in-fusion reaction (Clontech) downstream of the promoter region. For *Tg(rps9:loxP-DsRed2-loxP-EGFP)* (abbreviated to *rps9:switch*), the *EF1α* promoter in the pTol-*EF1α*:loxP-DsRed2-loxP-EGFP plasmid (Hans et al., 2009) was replaced with a 3 kb promoter region of the Fugu *rps9* gene (ENSTRUG00000015896.1). Primers used: 5′-AGAATCAC-CGTGGGTGAGGAG-3′ and 5′-GGCGGCTTAATTGTGCCTGCA-3′. In addition, the following reporter lines were used: *Tg(β-actin2:loxP-STOP-loxP-DsRed-express)* (abbreviated to *β-actin:switch*) (Bertrand et al., 2010); *Tg(ubi:loxP-EGFP-loxP-mCherry)* (abbreviated to *ubi:switch*) (Mosimann et al., 2011); *Tg(EF1α*:loxP-DsRed2-loxP-EGFP) (abbreviated to *EF1α:switch*) (Hans et al., 2009); *Tg(hsp70l:loxP-DsRed2-loxP-nlsEGFP)* (abbreviated to *hs:R to nG*) (Knopf et al., 2011); *Tg(crestin:Gal4-UAS-GFP)* (Y.-Y. Chen, PhD thesis, Eberhard Karls Universität Tübingen, 2011); and *Tg(−4725sox10:Cre)* (Rodrigues et al., 2012).

For early NC tracing (within the first 3 days), the best line is *EF1α:switch*, as the expression level is high at early stages. For metamorphic and adult fish, the best 'ubiquitous' line in our experience is *ubi:switch*, followed by *β-actin:switch*, which generally leads to a more patchy labeling.

Cre induction

Fish carrying the *sox10:ER^{T2}-Cre* transgene were crossed to the different reporter lines and 16-hpf embryos were dechorionated and treated with 5 μM 4-hydroxytamoxifen (4-OHT; Sigma, H7904) for 8 hours unless otherwise specified. Control embryos were incubated in a corresponding dilution of ethanol.

UAS:Cre injection

Tg(crestin:Gal4-UAS-GFP;β-actin:switch) embryos at the 1-cell stage were injected with different concentrations (1-10 ng/μl) of a pTol2 vector containing the Cre coding sequence downstream of a 4xUAS site.

Image acquisition and processing

Images were taken using a Zeiss LSM 5 Live confocal microscope and a Leica M205 FA stereomicroscope and processed using Imaris (Bitplane), ImageJ (NIH) and Adobe Photoshop. For confocal imaging of adult gills, fish were fixed for 1 hour in 4% paraformaldehyde. The head was mounted in 0.4% agarose for imaging after the removal of the operculum. Adult maxillary barbels were surgically removed and mounted in 1% agarose for imaging.

Cryosectioning and immunohistochemistry

After fixation, juvenile fish (1 mm) were washed with PBS and incubated in 10%, 20% and 30% sucrose solutions. The samples were then incubated in 1:1 30% sucrose:OCT Compound (Tissue-Tek) for 30 minutes and then in OCT overnight. Fish were frozen in cryomolds and 20 μm cryosections were obtained with a CH3050 cryostat (Leica). Cryosections were treated with 100% methanol for 10 minutes to improve adherence to the slides. Sections were rehydrated in PBST (PBS with 0.1% Tween 20), and blocked in 10% sheep serum in PBST for at least 1 hour at room temperature. The primary antibody [rabbit anti-DsRed (Clontech) at 1:200] was incubated overnight at 4°C in 10% sheep serum in PBST. Sections were then washed with PBST and incubated with the secondary antibody [anti-rabbit-Cy3 (Dianova) at 1:400] for 2 hours at room temperature. Sections were washed several times with PBST and nuclei visualized by adding DAPI (Sigma) to PBST in the last washing step.

RESULTS

sox10:ER^{T2}-Cre allows inducible labeling of NC in zebrafish

We generated a *sox10:ER^{T2}-Cre* transgenic line by fusing the NC-specific *(−4.9kb)sox10* promoter to the tamoxifen-inducible Cre recombinase coding sequence [Fig. 1A (1)]. To test the system prior to NC differentiation, we created a reporter line that ubiquitously drives a red-to-green switchable cassette under the control of the Fugu *(−3)rps9* promoter [Fig. 1A, before (2) and after (3) recombination]. The recombination was induced in double-transgenic embryos carrying the Cre driver construct and the reporter cassette by adding 4-hydroxytamoxifen to the water for 8 hours [16-24 hours postfertilization (hpf)], when NC delamination and early migration occur (Fig. 1B). At this time period, the *sox10* promoter is reported to be specific for NC cells and oligodendrocytes (Simon et al., 2012; Carney et al., 2006). To assess the controllability and the potential leakiness of the system, we compared induced and uninduced embryos at 36 hpf. After induction we found many GFP$^+$ cells resulting from Cre-induced recombination in the branchial arch region (Fig. 1C), in the dorsal neural tube, around the otic vesicles (Fig. 1E) and along the walls of the dorsal aorta and the ventral notochord (Fig. 1G). Uninduced embryos lacked GFP$^+$ cells in these areas (Fig. 1D,F,H).

We then induced clones in the well-established *β-actin:switch* reporter line, which has already been shown to effectively trace embryonic cell populations to later stages of development and to adulthood (Bertrand et al., 2010). We analyzed the developing viscerocranium in larvae at 4 days postfertilization (dpf). In this

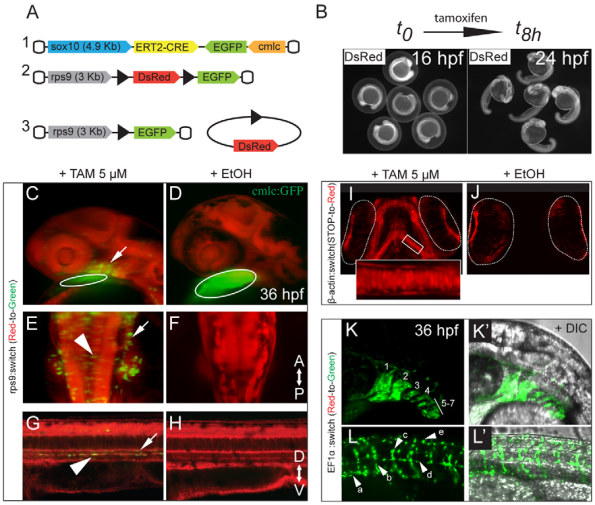

Fig. 1. An inducible Cre/loxP-based genetic system for long-term fate mapping of zebrafish NC. (**A**) Schematic of the two constructs used to generate (1) a NC-specific *ER^{T2}-Cre* driver line [*(−4.9kb)sox10* zebrafish promoter] and (2) a ubiquitous reporter line [*(−3kb)rps9* promoter from *Takifugu rubripes*] that enables detection of the recombination events during the early phases of NC differentiation. (3) *DsRed* excision after Cre-mediated recombination. (**B**) Time window for tamoxifen induction (16-24 hpf). (C-H) *Tg(sox10:ER^{T2}-Cre;rps9:switch)* embryos at 36 hpf, treated with tamoxifen (C,E,G) or with ethanol as control (D,F,H). (C-L′) Maximum intensity projections (MIPs) of confocal stacks. (**C**) GFP^{+} recombined cells in the branchial arch region (arrow) and cmlc:GFP marker (circled). (**E**) Hindbrain area with recombined cells in the otic epithelium (arrow) and along the dorsal neural tube, characterized by an epithelial, pre-delamination shape (arrowhead). (**G**) Sagittal section of the trunk with GFP^{+} melanoblasts and sympathetic neuron precursors flattened along the dorsal aorta walls (arrowhead) and the ventral notochord (arrow). (**D**,**F**,**H**) In the uninduced controls, no recombined cells are detectable. (**I**,**J**) Developing viscerocranium in 4-dpf *Tg(sox10:ER^{T2}-Cre;β-actin:switch)* larvae showing labeled chondrocytes that are absent in the control. The eyes, which show red autofluorescence, are circled. (**K-L′**) *Tg(sox10:ER^{T2}-Cre;EF1α:switch)* induced embryos (36 hpf) showing (K,K′) labeled pharyngeal arches (1-7) and (L,L′) pigment precursors (a), motor axon glia (b), dorsal root ganglia (DRG) progenitors (c), glia along the lateral line (d) and dorsal melanoblasts (e). The anteroposterior (AP) and dorsoventral (DV) axes are indicated.

region, chondroblasts were labeled in induced larvae (n=10; Fig. 1I), whereas no DsRed^{+} cells were detected in uninduced controls (n=10; Fig. 1J). Next, we analyzed the specificity of our system for NC derivatives using the *EF1α:switch* line and observed specific marking of pharyngeal arches 1-7 (Fig. 1K,K′) and of pigment precursors, peripheral nervous system glia, dorsal root ganglia (DRG) progenitors, lateral line Schwann cells and dorsal melanoblasts (Fig. 1L,L′, a-e, respectively). Induction of Cre at later time points (4 dpf) and for shorter periods (1-2 hours) results in isolated clones restricted to one or a few cell types, such as pigment cells (supplementary material Fig. S1A,D; n=50). These clones become smaller when the induction is performed at juvenile stages (i.e. 20 dpf; n=46; supplementary material Fig. S1B). Lack of labeling in adults of uninduced fish carrying both transgenes (supplementary material Fig. S1C) suggests that reporter expression was under tight control of the externally supplied tamoxifen.

Taken together, these results show that the *sox10:ER^{T2}-Cre* line allows for rigorous control of the onset of tamoxifen-dependent recombination events in NC cells. In line with the previously characterized *(−4.9)sox10:GFP* reporter (Carney et al., 2006), our *sox10:ER^{T2}-Cre* is occasionally expressed in a few random skeletal muscle progenitors in the trunk, which appear through adulthood as labeled clones (data not shown). These rare clones (on average one per flank), along with their clonally related recombined tissues, were not considered further in this analysis.

NC-derived structures in the trunk

To assess the NC contribution to postembryonic structures, we first analyzed labeled tissues in established postcranial NC derivatives of metamorphic juvenile fish (20 dpf) in which recombination had been induced at embryonic stages as described above (Fig. 2). We detected sympathetic ganglia (Fig. 2A), neurons of the enteric nervous system (Fig. 2B) and DRG (Fig. 2C). Moreover, we found sensory neurons innervating the body periphery, such as the pectoral and the caudal fins (Fig. 2D,D′, respectively). Glia providing myelination to axons in the peripheral nervous system were also marked (Fig. 2E-F′). We then searched for labeled chromatophores and found clones of iridophores, melanophores and xanthophores (Fig. 2G-I′). In several cases, we found labeled melanophores in proximity to recombined glial cells that surround the DRG (Fig. 2J, arrowheads).

In the heart of metamorphic switched fish we found many labeled cells, of which at least some show overlap with *cmlc:GFP*$^{+}$ cells, indicating that they are contractile cardiomyocytes (Kwan et al., 2007) (Fig. 2K,K′). In zebrafish, by means of cell

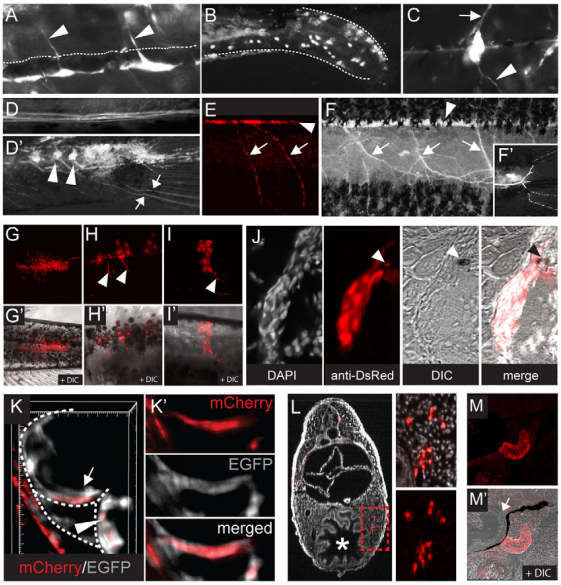

Fig. 2. Detection of postcranial NC derivatives. (**A-D′**) Lateral perspectives of epifluorescent acquisitions of DsRed$^+$ components of the peripheral nervous system in induced *Tg(sox10:ER^{T2}-Cre;β-actin:switch)* metamorphic fish. (A) Sympathetic ganglia (white) located along the ventral walls of the dorsal aorta (the dorsal walls are highlighted by the dashed line) and axonal projections (arrowheads) towards the spinal chord. (B) Neurons located in the most posterior region of the gut (dashed lines), close to the anus, forming the enteric nervous system. (C) DRG with afferent (arrow) and efferent (arrowhead) projections. (D,D′) Somatosensory projections innervating the pectoral fin (D) and the caudal fin (D); indicated are two of the most posterior DRG in the caudal region (arrowheads) and their projections entering the fin region (arrows). (**E-F′**) DsRed$^+$ glia cells in induced *Tg(sox10:ER^{T2}-Cre;β-actin:switch)* metamorphic and adult fish. MIP of confocal stacks showing glia cells along the lateral line nerve (arrowhead) and the axonal projections innervating the neuromasts (arrows) in metamorphic (E) and adult (F) zebrafish. (F′) Lateral line glia in the caudal fin. (F,F′) Epifluorescence pictures. (**G-I′**) MIP of confocal stacks showing pigment cells in induced *Tg(sox10:ER^{T2}-Cre;β-actin:switch)* metamorphic fish: (G,G′) iridophore clone, (H,H′) melanophore clone with glia cells (arrowheads) and (I,I′) xanthophore clone with glia cells (arrowhead). (**J**) Confocal image of transverse cryosection and anti-DsRed antibody staining showing a labeled melanophore (arrow) close to labeled glia cells wrapped around the DRG. (**K,K′**) Heart region of induced metamorphic fish carrying the *ubi:switch* transgene as a reporter. (K) 3D view of confocal stacks showing cmlc:GFP$^+$ cardiomyocytes (gray) and mCherry$^+$ cells (red, arrow and arrowhead) in the heart. (K′) Confocal section of the region indicated in K by the arrow, showing colocalization between an mCherry$^+$ cell and a GFP$^+$ cardiomyocyte. (**L**) Confocal image of transverse cryosection and anti-DsRed antibody staining showing an induced *Tg(sox10:ER^{T2}-Cre;β-actin:switch)* metamorphic fish. Labeled adrenomedullary cells in the liver (red, inset). The gut is indicated by the asterisk. (**M,M′**) Confocal image of sagittal cryosection and anti-mCherry antibody staining showing the pronephric duct region of an induced *Tg(sox10:ER^{T2}-Cre;ubi:switch)* metamorphic fish. (M) mCherry$^+$ cells populate the epithelial walls of the pronephric duct. (M′) The arrow indicates the otic capsule in the posterior chondrocranium.

transplantation and different labeling techniques, a NC contribution to cardiomyocytes has already been demonstrated (Sato and Yost, 2003; Li et al., 2003). We also observed clones in the adrenomedullar region (Fig. 2L) and in the epithelial walls of the pronephros (Fig. 2M,M′), confirming the NC contribution to these internal organs (Collazo et al., 1993).

Taken together, these data show that our inducible Cre/loxP-based genetic labeling system enables the detection of a large set of trunk NC derivatives in juvenile and adult fish. With the rare exception of spurious muscle clones, we did not detect any tissue with an established non-NC origin. The *sox10:ER^{T2}-Cre*-induced recombination may thus be used as a potent tool to uncover the NC origin of other postembryonic structures.

Analysis of labeled head structures reveals a NC contribution to frontal but not parietal bones

Next, we surveyed labeled chondrocranial and cartilaginous viscerocranial elements of the developing skull in 5-dpf larvae (Schilling et al., 1996; Piotrowski et al., 1996) and in 15- to 20-dpf fish (Fig. 3; Table 1). In the neurocranium, we detected recombined tissues in the ethmoid plate (Fig. 3A, e), trabeculae (Fig. 3A, t), taenia marginalis anterior (Fig. 3B, tma) and posterior (Fig. 3B, tmp), epiphyseal bar (Fig. 3B, eb) and in the otic capsule (Fig. 3C), whereas the basilar plate (parachordalia) and the anterior basicranial commissure were devoid of labeled cells. In the viscerocranium, we found a NC contribution to all its components (Fig. 3D,E).

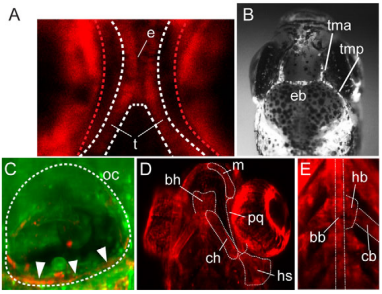

Fig. 3. NC-derived elements in the developing chondrocranium and viscerocranium. (**A**) Confocal section of recombined tissue in the ethmoid plate (e) and the trabeculae (t) of a 5-dpf *Tg(sox10:ER^{T2}-Cre;ubi:switch)* larva. The red dashed lines highlight the autofluorescence of the eyes. (**B**) Epifluorescent image of labeled elements of the dorsal neurocranium in 15-dpf *Tg(sox10:ER^{T2}-Cre;β-actin:switch)* fish: taenia marginalis anterior (tma), taenia marginalis posterior (tmp) and epiphyseal bar (eb). (C-E) MIP of confocal stacks. (**C**) Recombined cells in the forming ventral cartilage of the otic capsule (oc, arrowheads) in 5-dpf *Tg(sox10:ER^{T2}-Cre;ubi:switch)* larvae. (**D**) Labeled viscerocranial elements in the mandibular region [Meckel's cartilage (m), palatoquadrate (pq)] and in the hyod region [hyosymplectic (hs), ceratohyal (ch), basihyal (bh)] of 5-dpf *Tg(sox10:ER^{T2}-Cre;ubi:switch)* larvae. (**E**) Labeled basibranchial (bb), hypobranchial (hb) and ceratobranchial (cb) elements of 5-dpf *Tg(sox10:ER^{T2}-Cre;ubi:switch)* larvae.

In the head of metamorphic and adult fish we identified, by *in vivo* confocal imaging, neurocranial, viscerocranial and dermatocranial skeletal elements (Fig. 4; supplementary material Fig. S2). We decided to focus our attention on those structures that are still debated in the literature among different vertebrate taxa. Identifying their embryonic origin in zebrafish will be of great importance in deciphering key steps of vertebrate evolution.

First, we looked at the otic capsule and at the viscerocranium to confirm at later stages what we found in the larvae. A NC origin for the otic capsule cartilage has been shown previously in *Xenopus*, chicken and mice (Gross and Hanken, 2008b; Le Lièvre, 1978; Noden, 1983; Cubbage and Mabee, 1996; O'Gorman, 2005), whereas extirpation/vital dye labeling experiments did not demonstrate a NC contribution to this structure in lamprey, medaka or toads (Langille and Hall, 1988a; Langille and Hall, 1988b; Olsson and Hanken, 1996). Notably, in the neurocranium of juvenile zebrafish, we detected labeled chondroblasts and osteoblasts in the otic capsule and in the structure that contributes to the formation of the inner ear (Fig. 4A-A″).

In the viscerocranium, Meckel's cartilage, along with other important viscerocranial elements, is labeled, as expected (Fig. 4B). Remarkably, we detected labeled cells in the basihyal and the basibranchial (Fig. 4B′), two cartilages that form the hyobranchial skeleton. Unlike in zebrafish, NC does not seem to contribute to these bones in lissamphibians (Olsson and Hanken, 1996).

In the dermatocranium, we show that NC contributes to the entire opercular series, consisting of the opercle, inter-, sub- and preopercle (Fig. 4C,D). The vault series of dermal bones forming the roof of the skull consists of paired frontals and parietals. Both NC and mesoderm are known to contribute to frontoparietal bones. Intriguingly, we find that in zebrafish the frontals are labeled only in the anterior center of ossification (Fig. 4E, arrowhead; Fig. 4F) and the parietals (n=100, using three different reporter lines) are devoid of recombined osteoblasts (Fig. 4E, outlined by the dashed frame). The extent of their contribution defines a NC/mesoderm boundary in the skull, for which empirical data are inconsistent across vertebrate taxa (Gross and Hanken, 2008a). Our data point to a NC/mesoderm boundary in the frontal bones, at the border between the anterior and the posterior ossification centers.

NC contributes to the barbels

Barbels are whisker-like tactile organs that protrude from the integument of the mouth region. The embryonic origin of the fibroblast-like cells that synthesize the extracellular rod matrix is unknown. As barbels have been recently used as a model for adult organ regeneration (LeClair and Topczewski, 2010), we sought to determine whether NC contributes to barbel development.

We detected labeled cells at the core of the maxillary barbels, surrounded by specialized epithelial cells (Fig. 4G). Specifically, we identified labeled nerve fibers (Fig. 4H, asterisks, red channel) in the region of the lymphatic (Fig. 4H, arrow, green channel) and blood vessels (Fig. 4H, arrowhead, green channel). Notably, we

Table 1. List of chondrocranial and viscerocranial elements that form the developing skull with detected/undetected contribution from the NC

Division	Region	Element	NC contribution
Neurocranium	Base	Parachordal (pc)	Not detected
		Anterior basicranial commissure (abc)	Not detected
		Trabecula (t)	Yes
		Ethmoidal plate (e)	Yes
	Orbito-temporal	Epiphyseal bar (eb)	Yes
		Taenia marginalis anterior (tma)	Yes
		Taenia marginalis posterior (tmp)	Yes
	Otic	Otic capsule (oc)	Yes
Viscerocranium	Mandibular	Meckel's cartilage (m)	Yes
		Palatoquadrate (pq)	Yes
	Hyoid	Basihyal (bh)	Yes
		Ceratohyal (ch)	Yes
		Hyosymplectic (hs)	Yes
	Branchial	Basibranchial (bb)	Yes
		Hypobranchial (hb)	Yes
		Ceratobranchial (cb)	Yes

Abbreviations as in Fig. 3.

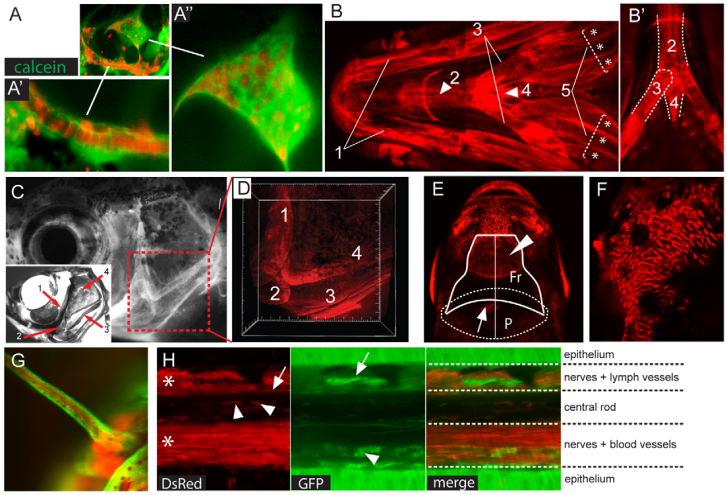

Fig. 4. Detection of contested cranial NC derivatives. (**A-A″**) MIP of confocal stacks showing labeled cartilaginous and bony elements in the otic capsule: chondroblasts and osteoblasts in the ventral cartilage (A′) and in the inner ear structures (A″). (**B**) MIP of confocal stacks (ventral view) showing labeled viscerocranial structures: (1) Meckel's cartilage (paired), (2) the basihyal (unpaired), (3) the ceratohyal (paired), (4) the basibranchial (unpaired) and (5) the branchiostegal rays (paired), with individual rays marked with an asterisk. (**B′**) Confocal section from B showing labeled (2) basihyal (unpaired), (3) ceratohyal (paired) and (4) basibranchial (unpaired) elements. (**C**,**D**) Epifluorescent image of mCherry^{+} osteoblasts forming the opercular series in *Tg(sox10:ER^{T2}-Cre;ubi:switch)* adult fish (C) and Alizarin Red-stained skull (lateral view) in a 3-month-old zebrafish showing the four bones forming the opercular series: (1) preopercle, (2) interopercle, (3) subopercle and (4) opercle (inset). (D) 3D view of confocal stacks (boxed region in C), which shows positive cells in all the bones composing the opercular series. (**E**) Frontal (Fr) and parietal (P) bones. Epifluorescence image showing recombined osteoblasts in the rostral part of the frontals (arrowhead), whereas the parietals are devoid of labeled osteoblasts (arrow indicates a pigment cell clone). (**F**) MIP of confocal stacks showing labeled osteoblasts in the anterior region of the frontals. (**G**) MIP of confocal stacks of a maxillary barbel in induced adult fish showing recombined tissues in the core of the tactile organ. (**H**) Confocal section showing, in the red channel, labeled nerves (asterisks), fibroblast-like cells in the rod matrix (arrowheads) and flattened cells along the dorsal aspect of the rod (arrow). In the green channel, a non-switched lymphatic vessel (arrow) and blood vessel (arrowhead) are indicated. In the merge panel, the different layers composing the barbels are shown.

found labeled fibroblast-like cells embedded in the matrix of the central rod (Fig. 4H, arrowheads, red channel) and labeled flattened cells along the dorsal aspect of the rod (Fig. 4H, arrow, red channel). Interestingly, similar mesenchymal, fibroblast-like cells have been proposed to play a crucial role in blastema formation during fin regeneration (Knopf et al., 2011).

Pillar cells are NC derived

Finally, we focused on the gill organ and observed labeled gill filaments, including primary and secondary lamellae (Fig. 5A,B). In the primary lamellae, smooth muscle cells of the blood vessel tunica media are labeled (Fig. 5C, arrows) and are located in close contact with the endothelium, which is labeled by the *flk:GFP* transgene (Lawson and Weinstein, 2002) (Fig. 5C′). In the secondary lamellae, we found labeled pillar cells (Fig. 5D,E). Pillar cells are highly specialized, with autoregulatory contractile properties that offer mechanical support to the respiratory epithelium (Fig. 5D, green), and enable an adaptation of the lamellar surface to the oxygen content of water (Bettex-Galland and Hughes, 1973; Hughes and Morgan, 1973). Pillar cells are arranged in parallel columns and, with their cytoplasmic processes (Fig. 5D, arrowhead) supporting the respiratory epithelium (Fig. 5D, green), form lumina (Fig. 5E, arrowheads) that give rise to capillary networks through which blood perfuses and gas exchange occurs (Fig. 5F) (Hughes and Morgan, 1973).

In our experimental set-up, the definition of NC origin rests entirely on the specificity of the *sox10* promoter. Although we did identify most of the previously known NC derivatives in the floxed clones, the discovery of new structures requires independent confirmation. We therefore induced recombination with an alternative NC promoter from the *crestin* locus (Luo et al., 2001) (Y.-Y. Chen, PhD thesis, Eberhard Karls Universität Tübingen, 2011) by injecting *UAS:Cre* DNA into *Tg(crestin:gal4-UAS:GFP;β-actin:switch)* embryos at the 1-cell stage. We detected, among previously identified NC derivatives (data not shown), labeled barbels (supplementary material Fig. S3), gill pillar cells and smooth muscles (Fig. 5G). Moreover, we identified these structures using a non-inducible *sox10:Cre* line with a longer (7.2 kb) promoter fragment and a different genomic insertion site (Rodrigues et al., 2012) (data not shown).

DISCUSSION

The appearance of NC was fundamental to subsequent vertebrate evolutionary history, tremendously accelerating the emergence

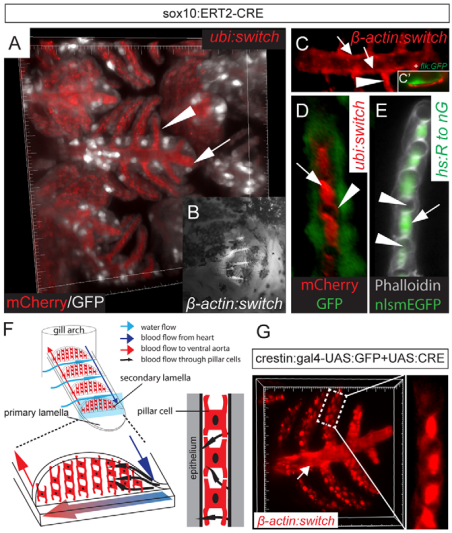

Fig. 5. NC origin of gill pillar cells. (A-E) Recombined cells in the primary and secondary lamellae of the gills. (**A**) 3D view of confocal stacks showing the gill lamellae in an induced *Tg(sox10:ER^{T2}-Cre;ubi:switch)* adult fish: non-NC-derived tissues are in gray (GFP), whereas NC-derived tissues in the primary (arrow) and in the secondary (arrowhead) lamellae are in red (mCherry). (**B**) Epifluorescence image of DsRed^{+} cells in the primary and secondary lamellae in an induced *Tg(sox10:ER^{T2}-Cre;β-actin:switch)* adult fish. (**C**) Confocal section of labeled smooth muscles of the blood vessel tunica media in the primary lamellae (arrows) and pillar cell in contact with the smooth muscle layer (arrowhead). (**C′**) flk:GFP^{+} endothelium in the gills surrounded by NC-derived smooth muscles. (**D**) Confocal section of a secondary lamellae showing recombined mCherry^{+} pillar cells surrounded by non-recombined GFP^{+} epithelial cells in an induced *Tg(sox10:ER^{T2}-Cre;ubi:switch)* adult fish. The arrow indicates the pillar cell body, whereas the arrowhead marks a cytoplasmic process connecting two neighboring pillar cells. (**E**) MIP of confocal stacks showing a phalloidin-stained (gray) secondary lamella with the GFP^{+} pillar cell nuclei of an induced *hs:R to nG* adult fish. The pillar cell nuclei (arrow) are located between adjacent lumina (arrowheads). (**F**) Schematic of gill lamellae and pillar cells demonstrating the flow of blood through the organ. (**G**) MIP of confocal stacks of recombined lamellae using the *crestin* promoter, showing labeled smooth muscles (arrow) and pillar cells (inset).

of a predatory lifestyle and the exploitation of unexplored ecological niches. Although NC contribution to multiple cell types is well documented in different model organisms (Gross and Hanken, 2008a), the lack of a comprehensive analysis of NC-derived adult structures in actinopterygians leaves a gap in our understanding of important evolutionary transitions. Key innovations that endowed vertebrates with predatory capacity were the acquisition of muscular ventilation coupled with respiratory surface expansion, the emergence of a skull vault and a dorsoventrally articulated jaw. We have developed and employed a genetic long-term labeling method to uncover a potential NC origin of evolutionarily important cell types and tissues of previously unrecognized or debated origin in zebrafish, a model teleost. In particular, in the present study we focused on the gill respiratory system and showed that, by giving rise to gill pillar cells, NC might have expedited respiratory surface expansion and muscular ventilation.

NC-driven expansion of the respiratory surface at the protochordate-vertebrate transition

At the protochordate-vertebrate transition, the acquisition of a predatory lifestyle was facilitated by a massive expansion of the respiratory surface in the gills and the switch from ciliary to muscular ventilation (Northcutt and Gans, 1983). Recent paleontological analysis of cristozoan fossils such as *Haikouella lanceolata* and *Yunnanozoon lividum* suggests a precraniate history of ‘crest animals’. These fossils are characterized by paired gill rays and jointed, widely spaced branchial arches, but do not possess a skull (Chen, 2008; Chen et al., 1999; Holland and Chen, 2001; Mallatt and Chen, 2003). Although many structures directly involved in prey capture have been shown to derive from NC, the embryonic origin of the new, expanded respiratory organ, which according to the recent paleontological interpretation seems to predate the appearance of the skull, has not been investigated. Our demonstration of a NC origin for gill pillar cells reinforces the importance of this embryonic tissue in the evolution of respiratory systems and, possibly, in the radiation of precraniate crest animals at the protochordate-vertebrate transition.

Pillar cells are found in the gills of hagfishes (Mallatt and Paulsen, 1986; Elger, 1987), lampreys (Youson and Freeman, 1976), chondrichthyans and osteognathostomes (Evans et al., 2005). However, cephalochordates lack specialized gill cells that increase the respiratory surface area. Instead, this group has rather simple collagen bars located in the pharynx atrium, and gas exchange occurs through ciliated epithelial cells (Welsch, 1975; Baskin and Detmers, 1976). Thus, pillar cells are a craniate synapomorphy and, as they provide the structural basis for the new expanded gill organ, represent a key innovation in vertebrate evolution. Pillar cells form small channels to conduct blood through the gills and possess the ability to expand or contract their cytoplasmic processes to control blood flow (Bettex-Galland and Hughes, 1973). This contraction/expansion activity also regulates the distance between neighboring secondary lamellae, thereby modulating water flow through the gills. The development of this atypical vertebrate-specific cell type is still poorly understood. Observations of cellular microanatomy and tissue ontogeny (Datta Munshi and Singh, 1968), supported by the expression of smooth muscle myosin (Smith and Chamley-Campbell, 1981), suggest a derivation of pillar cells from the smooth muscles forming the blood vessels of the primary lamellae. Cephalic NC is known to give rise to avian and mammalian smooth muscle cells of the blood vessels of the face and forebrain but not to the endothelium (Etchevers et al., 2001; Le Lièvre and Le Douarin, 1975; Yoshida et al., 2008). Our finding that, in addition to the smooth muscles of the pharyngeal arches, those forming the primary lamellae also have a NC origin supports the hypothesis that pillar cells evolved from this tissue rather than from endothelial cells, as originally proposed (Bietrix, 1895).

NC contribution to cranial skeletal elements and barbels in zebrafish

The contribution of cranial NC to the frontal and parietal bones is contentious and studies using different model systems and labeling techniques have led to inconsistent results (Couly et al., 1993;

Noden and Trainor, 2005; Gross and Hanken, 2008a). For example, fate mapping in *Xenopus* using fluorescent dextran labeling suggested that cranial NC contributes to the entire length of the frontoparietal bones (Gross and Hanken, 2005), whereas studies in mouse using *Wnt1-Cre*-mediated genetic labeling suggested that NC does not contribute to the parietal bones (Jiang et al., 2002). Moreover, analysis of quail-chick chimeras has led to conflicting conclusions regarding a NC contribution to these dermatocranial elements in the avian skull, defining the NC-mesoderm boundary at the border between the anterior and posterior regions of the frontals (Noden, 1978; Evans and Noden, 2006) or extending NC contributions to both frontal and parietal bones (Couly et al., 1993).

The frontal and parietal bones of the zebrafish are anatomically similar to their mammalian counterparts and start to ossify at 3-4 weeks postfertilization (Cubbage and Mabee, 1996; Quarto and Longaker, 2005). We find that NC contributes to the anterior but not to the posterior ossification center of the frontals. Further, we find no contribution to the parietals, allowing us to suggest that the NC/mesoderm boundary in zebrafish lies in the frontal bones, between the anterior and the posterior ossification center, as has been shown in chicken (Noden, 1978; Evans and Noden, 2006) and mice (Jiang et al., 2002). Differences in the location of the NC/mesoderm boundary could also be attributed to species-specific factors, although we cannot rule out a possible contribution of experimental methodology to conflicting conclusions.

The embryonic origin of the otic capsule is debated. These paired bones accommodating the inner ear are considered to be a novelty of craniates and are absent in early crest animals (Chen, 2008; Gross and Hanken, 2008a; Mallatt and Chen, 2003). Studies in birds and mammals have shown a NC contribution to the otic capsule (Le Lièvre, 1978; O'Gorman, 2005; Noden, 1983). Previous studies using NC extirpation/vital dye labeling did not find a NC contribution to the otic capsules in lamprey (Langille and Hall, 1988b), medaka (Langille and Hall, 1988a) and oriental fire-bellied toad (Olsson and Hanken, 1996), although the otic capsules in *Xenopus* were shown to receive a contribution from the cranial NC (Gross and Hanken, 2008b). These studies have led to the view that NC contribution to the otic capsule must predate the divergence of the mammalian and avian lineages (O'Gorman, 2005; Gross and Hanken, 2008a). We show that NC contributes to the otic capsule in zebrafish and could thus be a trait shared among vertebrates. In this regard, it is interesting to note that mutants with NC defects often have ear phenotypes in zebrafish (Kelsh et al., 1996; Whitfield et al., 1996).

Elegant fossil and molecular genetic analyses suggest that gnathostome jaw evolution occurred in a stepwise fashion, facilitated by skull reorganization and altered epithelial-mesenchymal interactions among pre-existing molecular programs (Gai et al., 2011; Shigetani et al., 2002). We find that, as in other vertebrates, the complete lower jaw is NC derived. Contrary to observations in amphibians (Olsson and Hanken, 1996), the zebrafish hypobranchial skeleton is also NC derived.

The opercular flap, which consists of multiple flat dermal bones, is also NC derived, as shown in the present study. The evolution of the opercular series has facilitated a novel mechanism for the depression of the mandible (Lauder, 1980a; Lauder, 1980b; Lauder, 1982), allowing an improvement in suction feeding through better control over fluid movement (Lauder, 1980a). The NC origin of the opercular series, as conclusively shown using our long-term labeling approach, was previously assumed on the basis of its dermal bone composition and the expression of specific transgenes (Kimmel et al., 2010). Recent findings demonstrating the presence of an embryonic operculum in amniotes have rekindled interest in this structure, which was presumed to have been lost completely with the evolution of tetrapods and the emergence of a terrestrial lifestyle (Richardson et al., 2012).

We also find a NC contribution to zebrafish barbels. Barbels are tentacle-like chemosensory structures that arose independently many times during actinopterygian evolution (LeClair and Topczewski, 2010). Poor homology in terms of embryonic development and cellular composition across different vertebrate taxa complicates phylogenetic comparisons and makes it difficult to trace the evolutionary history of these sensory structures (Fox, 1999). In the barbels of recombined fish we detected fibroblast-like cells in the matrix of the rod and flattened cells along its dorsal aspect. These two cell types are likely to be involved in the production of the connective tissue of the supporting central rod. Barbels are an attractive model for understanding tissue regeneration in adult organs (LeClair and Topczewski, 2010). That central components of these structures have a NC origin raises the intriguing possibility of studying the potential role of NC-derived adult tissues in organ repair.

sox10:ER^{T2}-Cre as a tool to understand the evolution of developmental mechanisms underlying emergence of the vertebrate body plan

Very little is known about the cellular and molecular events underlying NC-driven diversification of the vertebrate body plan. This is due, in part, to a dearth of tools to allow consistent and long-term labeling of NC derivatives. Inducible *sox10:ER^{T2}-Cre* recombination allows NC long-term labeling in a spatiotemporal manner: the spatial domain of Cre-mediated recombination is restricted by the *sox10* promoter and the temporal domain is under tamoxifen control. In the future, the *sox10:ER^{T2}-Cre* line will also enable the genetic manipulation of NC and its derivatives. For example, taking advantage of the new FlipTrap and FlEx technologies (Trinh et al., 2011; Ni et al., 2012), it will be possible to specifically manipulate particular genes in cell lineages that fall into the spatiotemporal domain of the *sox10:ER^{T2}-Cre* transgene. This will greatly improve our understanding of how these populations of migratory and proliferative cells give rise to diverse cell types and organs in the vertebrate body.

In summary, using an inducible Cre/loxP system for genetic lineage tracing, we demonstrate a NC contribution to various structures in metamorphic and adult zebrafish, an important model teleost. In particular, our analysis reveals a direct involvement of NC in the development of gill pillar cells, an atypical cell type found in vertebrates and hagfishes. A switch from ciliary ventilation to respiratory muscular ventilation with gills was an early event during the evolutionary history of modern vertebrates, followed by skull reorganization and the emergence of a jaw. A role for the NC in remodeling the respiratory system of early crest animals is underappreciated, in part owing to the lack of such analyses in non-tetrapod vertebrates. Respiratory systems underwent a profound transformation and pillar cells were lost along the tetrapod lineage. We propose that the evolution of the gills, with their highly expanded respiratory surface, was driven by the NC, and thus confirm the fundamental role played by this embryonic tissue in vertebrate radiation.

Acknowledgements
We thank F. Argenton, C. Baker, R. Kelsh and all our colleagues for insightful discussion and helpful comments on the manuscript; F. S. Rodrigues (R. Kelsh laboratory) for sharing unpublished data; and C. Dooley for valuable support in the early phases of this work.

Funding
This work was funded by the Max-Planck Society for the Advancement of Science and the European Molecular Biology Organization to A.P.S.

Competing interests statement
The authors declare no competing financial interests.

Supplementary material
Supplementary material available online at
http://dev.biologists.org/lookup/suppl/doi:10.1242/dev.091066/-/DC1

References

Abitua, P. B., Wagner, E., Navarrete, I. A. and Levine, M. (2012). Identification of a rudimentary neural crest in a non-vertebrate chordate. *Nature* **492**, 104-107.
Baskin, D. G. and Detmers, P. A. (1976). Electron microscopic study on the gill bars of amphioxus (Branchiostoma californiense) with special reference to neurociliary control. *Cell Tissue Res.* **166**, 167-178.
Bertrand, J. Y., Chi, N. C., Santoso, B., Teng, S., Stainier, D. Y. and Traver, D. (2010). Haematopoietic stem cells derive directly from aortic endothelium during development. *Nature* **464**, 108-111.
Bettex-Galland, M. and Hughes, G. M. (1973). Contractile filamentous material in the pillar cells of fish gills. *J. Cell Sci.* **13**, 359-370.
Bietrix, E. (1895). Quelques considerations sur les notions de lacune et d'endothelium en anatomie generale, a propos du rescau vasculaire branchial des Poissons. *C. R. Somm. Seanc. Soc. Philomath.* **189**, 26-28.
Bronner-Fraser, M. and Fraser, S. E. (1988). Cell lineage analysis reveals multipotency of some avian neural crest cells. *Nature* **335**, 161-164.
Carney, T. J., Dutton, K. A., Greenhill, E., Delfino-Machín, M., Dufourcq, P., Blader, P. and Kelsh, R. N. (2006). A direct role for Sox10 in specification of neural crest-derived sensory neurons. *Development* **133**, 4619-4630.
Chai, Y., Jiang, X. B., Ito, Y., Bringas, P., Jr, Han, J., Rowitch, D. H., Soriano, P., McMahon, A. P. and Sucov, H. M. (2000). Fate of the mammalian cranial neural crest during tooth and mandibular morphogenesis. *Development* **127**, 1671-1679.
Chen, J. Y. (2008). Early crest animals and the insight they provide into the evolutionary origin of craniates. *Genesis* **46**, 623-639.
Chen, J. Y., Huang, D. Y. and Li, C. W. (1999). An early Cambrian craniate-like chordate. *Nature* **402**, 518-522.
Collazo, A., Bronner-Fraser, M. and Fraser, S. E. (1993). Vital dye labelling of Xenopus laevis trunk neural crest reveals multipotency and novel pathways of migration. *Development* **118**, 363-376.
Couly, G. F., Coltey, P. M. and Le Douarin, N. M. (1993). The triple origin of skull in higher vertebrates: a study in quail-chick chimeras. *Development* **117**, 409-429.
Cubbage, C. C. and Mabee, P. M. (1996). Development of the cranium and paired fins in the zebrafish Danio rerio (Ostariophysi, cyprinidae). *J. Morphol.* **229**, 121-160.
Datta Munshi, J. S. and Singh, B. N. (1968). On the micro-circulatory system of the gills of certain freshwater teleostean fishes. *J. Zool.* **154**, 365-376.
Dutton, K. A., Pauliny, A., Lopes, S. S., Elworthy, S., Carney, T. J., Rauch, J., Geisler, R., Haffter, P. and Kelsh, R. N. (2001). Zebrafish colourless encodes sox10 and specifies non-ectomesenchymal neural crest fates. *Development* **128**, 4113-4125.
Elger, M. (1987). The branchial circulation and the gill epithelia in the Atlantic hagfish, Myxine glutinosa L. *Anat. Embryol. (Berl.)* **175**, 489-504.
Etchevers, H. C., Couly, G., Vincent, C. and Le Douarin, N. M. (1999). Anterior cephalic neural crest is required for forebrain viability. *Development* **126**, 3533-3543.
Etchevers, H. C., Vincent, C., Le Douarin, N. M. and Couly, G. F. (2001). The cephalic neural crest provides pericytes and smooth muscle cells to all blood vessels of the face and forebrain. *Development* **128**, 1059-1068.
Evans, D. J. and Noden, D. M. (2006). Spatial relations between avian craniofacial neural crest and paraxial mesoderm cells. *Dev. Dyn.* **235**, 1310-1325.
Evans, D. H., Piermarini, P. M. and Choe, K. P. (2005). The multifunctional fish gill: dominant site of gas exchange, osmoregulation, acid-base regulation, and excretion of nitrogenous waste. *Physiol. Rev.* **85**, 97-177.
Fox, H. (1999). Barbels and barbel-like tentacular structures in sub-mammalian vertebrates: a review. *Hydrobiologia* **403**, 153-193.
Gai, Z., Donoghue, P. C., Zhu, M., Janvier, P. and Stampanoni, M. (2011). Fossil jawless fish from China foreshadows early jawed vertebrate anatomy. *Nature* **476**, 324-327.
Gans, C. and Northcutt, R. G. (1983). Neural crest and the origin of vertebrates: a new head. *Science* **220**, 268-273.
Gross, J. B. and Hanken, J. (2005). Cranial neural crest contributes to the bony skull vault in adult Xenopus laevis: insights from cell labeling studies. *J. Exp. Zool.* **304B**, 169-176.
Gross, J. B. and Hanken, J. (2008a). Review of fate-mapping studies of osteogenic cranial neural crest in vertebrates. *Dev. Biol.* **317**, 389-400.
Gross, J. B. and Hanken, J. (2008b). Segmentation of the vertebrate skull: neural-crest derivation of adult cartilages in the clawed frog, Xenopus laevis. *Integr. Comp. Biol.* **48**, 681-696.
Hans, S., Kaslin, J., Freudenreich, D. and Brand, M. (2009). Temporally-controlled site-specific recombination in zebrafish. *PLoS ONE* **4**, e4640.
Holland, N. D. and Chen, J. (2001). Origin and early evolution of the vertebrates: new insights from advances in molecular biology, anatomy, and palaeontology. *BioEssays* **23**, 142-151.
Hörstadius, S. (1950). *The Neural Crest: Its Properties and Derivatives in the Light of Experimental Research*. London: Oxford University Press.
Hughes, G. M. and Morgan, M. (1973). The structure of fish gills in relation to their respiratory function. *Biol. Rev. Camb. Philos. Soc.* **48**, 419-475.
Jiang, X., Iseki, S., Maxson, R. E., Sucov, H. M. and Morriss-Kay, G. M. (2002). Tissue origins and interactions in the mammalian skull vault. *Dev. Biol.* **241**, 106-116.
Kelsh, R. N., Brand, M., Jiang, Y. J., Heisenberg, C. P., Lin, S., Haffter, P., Odenthal, J., Mullins, M. C., van Eeden, F. J. M., Furutani-Seiki, M. et al. (1996). Zebrafish pigmentation mutations and the processes of neural crest development. *Development* **123**, 369-389.
Kimmel, C. B., DeLaurier, A., Ullmann, B., Dowd, J. and McFadden, M. (2010). Modes of developmental outgrowth and shaping of a craniofacial bone in zebrafish. *PLoS ONE* **5**, e9475.
Knopf, F., Hammond, C., Chekuru, A., Kurth, T., Hans, S., Weber, C. W., Mahatma, G., Fisher, S., Brand, M., Schulte-Merker, S. et al. (2011). Bone regenerates via dedifferentiation of osteoblasts in the zebrafish fin. *Dev. Cell* **20**, 713-724.
Kwan, K. M., Fujimoto, E., Grabher, C., Mangum, B. D., Hardy, M. E., Campbell, D. S., Parant, J. M., Yost, H. J., Kanki, J. P. and Chien, C. B. (2007). The Tol2kit: a multisite gateway-based construction kit for Tol2 transposon transgenesis constructs. *Dev. Dyn.* **236**, 3088-3099.
Landacre, F. L. (1921). The fate of the NC in the head of the Urodeles. *J. Comp. Neurol.* **33**, 1-43.
Langille, R. M. and Hall, B. K. (1988a). Role of the neural crest in development of the cartilaginous cranial and visceral skeleton of the medaka, Oryzias latipes (Teleostei). *Anat. Embryol. (Berl.)* **177**, 297-305.
Langille, R. M. and Hall, B. K. (1988b). Role of the neural crest in development of the trabeculae and branchial arches in embryonic sea lamprey, Petromyzon-Marinus (L). *Development* **102**, 301-310.
Lauder, G. V. (1980a). Evolution of the feeding mechanism in primitive actinopterygian fishes – a functional anatomical analysis of Polypterus, Lepisosteus, and Amia. *J. Morphol.* **163**, 283-317.
Lauder, G. V. (1980b). On the evolution of the jaw adductor musculature in primitive gnathostome fishes. *Breviora* **460**, 1-10.
Lauder, G. V. (1982). Patterns of evolution in the feeding mechanism of actinopterygian fishes. *Am. Zool.* **22**, 275-285.
Lawson, N. D. and Weinstein, B. M. (2002). In vivo imaging of embryonic vascular development using transgenic zebrafish. *Dev. Biol.* **248**, 307-318.
Le Douarin, N. M. (1986). Cell line segregation during peripheral nervous system ontogeny. *Science* **231**, 1515-1522.
Le Douarin, N. M. and Dupin, E. (2012). The neural crest in vertebrate evolution. *Curr. Opin. Genet. Dev.* **22**, 381-389.
Le Douarin, N. M. and Kalcheim, C. (1999). *The Neural Crest*. Cambridge: Cambridge University Press.
Le Lièvre, C. S. (1978). Participation of neural crest-derived cells in the genesis of the skull in birds. *J. Embryol. Exp. Morphol.* **47**, 17-37.
Le Lièvre, C. S. and Le Douarin, N. M. (1975). Mesenchymal derivatives of the neural crest: analysis of chimaeric quail and chick embryos. *J. Embryol. Exp. Morphol.* **34**, 125-154.
LeClair, E. E. and Topczewski, J. (2010). Development and regeneration of the zebrafish maxillary barbel: a novel study system for vertebrate tissue growth and repair. *PLoS ONE* **5**, e8737.
Li, Y. X., Zdanowicz, M., Young, L., Kumiski, D., Leatherbury, L. and Kirby, M. L. (2003). Cardiac neural crest in zebrafish embryos contributes to myocardial cell lineage and early heart function. *Dev. Dyn.* **226**, 540-550.
Luo, R., An, M., Arduini, B. L. and Henion, P. D. (2001). Specific pan-neural crest expression of zebrafish Crestin throughout embryonic development. *Dev. Dyn.* **220**, 169-174.
Mallatt, J. and Paulsen, C. (1986). Gill ultrastructure of the Pacific hagfish Eptatretus stouti. *Am. J. Anat.* **177**, 243-269.
Mallatt, J. and Chen, J. Y. (2003). Fossil sister group of craniates: predicted and found. *J. Morphol.* **258**, 1-31.
Metzger, D., Clifford, J., Chiba, H. and Chambon, P. (1995). Conditional site-specific recombination in mammalian cells using a ligand-dependent chimeric Cre recombinase. *Proc. Natl. Acad. Sci. USA* **92**, 6991-6995.
Mosimann, C., Kaufman, C. K., Li, P., Pugach, E. K., Tamplin, O. J. and Zon, L. I. (2011). Ubiquitous transgene expression and Cre-based recombination driven by the ubiquitin promoter in zebrafish. *Development* **138**, 169-177.

Ni, T. T., Lu, J., Zhu, M., Maddison, L. A., Boyd, K. L., Huskey, L., Ju, B., Hesselson, D., Zhong, T. P., Page-McCaw, P. S. et al. (2012). Conditional control of gene function by an invertible gene trap in zebrafish. *Proc. Natl. Acad. Sci. USA* **109**, 15389-15394.
Noden, D. M. (1978). The control of avian cephalic neural crest cytodifferentiation. I. Skeletal and connective tissues. *Dev. Biol.* **67**, 296-312.
Noden, D. M. (1983). The role of the neural crest in patterning of avian cranial skeletal, connective, and muscle tissues. *Dev. Biol.* **96**, 144-165.
Noden, D. M. and Trainor, P. A. (2005). Relations and interactions between cranial mesoderm and neural crest populations. *J. Anat.* **207**, 575-601.
Northcutt, R. G. (2005). The new head hypothesis revisited. *J. Exp. Zool.* **304B**, 274-297.
Northcutt, R. G. and Gans, C. (1983). The genesis of neural crest and epidermal placodes: a reinterpretation of vertebrate origins. *Q. Rev. Biol.* **58**, 1-28.
O'Gorman, S. (2005). Second branchial arch lineages of the middle ear of wild-type and Hoxa2 mutant mice. *Dev. Dyn.* **234**, 124-131.
Olsson, L. and Hanken, J. (1996). Cranial neural-crest migration and chondrogenic fate in the oriental fire-bellied toad Bombina orientalis: Defining the ancestral pattern of head development in anuran amphibians. *J. Morphol.* **229**, 105-120.
Piotrowski, T., Schilling, T. F., Brand, M., Jiang, Y. J., Heisenberg, C. P., Beuchle, D., Grandel, H., van Eeden, F. J., Furutani-Seiki, M., Granato, M. et al. (1996). Jaw and branchial arch mutants in zebrafish II: anterior arches and cartilage differentiation. *Development* **123**, 345-356.
Quarto, N. and Longaker, M. T. (2005). The zebrafish (Danio rerio): a model system for cranial suture patterning. *Cells Tissues Organs* **181**, 109-118.
Richardson, J., Shono, T., Okabe, M. and Graham, A. (2012). The presence of an embryonic opercular flap in amniotes. *Proc. Biol. Sci.* **279**, 224-229.
Rodrigues, F. S., Doughton, G., Yang, B. and Kelsh, R. N. (2012). A novel transgenic line using the Cre-lox system to allow permanent lineage-labeling of the zebrafish neural crest. *Genesis* **50**, 750-757.
Sato, M. and Yost, H. J. (2003). Cardiac neural crest contributes to cardiomyogenesis in zebrafish. *Dev. Biol.* **257**, 127-139.
Schilling, T. F. and Kimmel, C. B. (1994). Segment and cell type lineage restrictions during pharyngeal arch development in the zebrafish embryo. *Development* **120**, 483-494.
Schilling, T. F., Piotrowski, T., Grandel, H., Brand, M., Heisenberg, C. P, Jiang, Y. J., Beuchle, D., Hammerschmidt, M., Kane, D. A., Mullins, M. C. et al. (1996). Jaw and branchial arch mutants in zebrafish I: branchial arches. *Development* **123**, 329-344.
Shigetani, Y., Sugahara, F., Kawakami, Y., Murakami, Y., Hirano, S. and Kuratani, S. (2002). Heterotopic shift of epithelial-mesenchymal interactions in vertebrate jaw evolution. *Science* **296**, 1316-1319.
Simon, C., Lickert, H., Götz, M. and Dimou, L. (2012). Sox10-iCreERT2 : a mouse line to inducibly trace the neural crest and oligodendrocyte lineage. *Genesis* **50**, 506-515.
Smith, D. G. and Chamley-Campbell, J. (1981). Localization of smooth-muscle myosin in branchial pillar cells of snapper (Chrysophys auratus) by immunofluorescence histochemistry. *J. Exp. Zool.* **215**, 121-124.
Trinh, A., Hochgreb, T., Graham, M., Wu, D., Ruf-Zamojski, F., Jayasena, C. S., Saxena, A., Hawk, R., Gonzalez-Serricchio, A., Dixson, A. et al. (2011). A versatile gene trap to visualize and interrogate the function of the vertebrate proteome. *Genes Dev.* **25**, 2306-2320.
Wada, N., Javidan, Y., Nelson, S., Carney, T. J., Kelsh, R. N. and Schilling, T. F. (2005). Hedgehog signaling is required for cranial neural crest morphogenesis and chondrogenesis at the midline in the zebrafish skull. *Development* **132**, 3977-3988.
Welsch, U. (1975). The fine structure of the pharynx, cyrtopodocytes and digestive caecum of amphioxus (Branchiostoma lanceolatum). *Symp. Zool. Soc. Lond.* **36**, 17-41.
Whitfield, T. T., Granato, M., van Eeden, F. J. M., Schach, U., Brand, M., Furutani-Seiki, M., Haffter, P., Hammerschmidt, M., Heisenberg, C. P., Jiang, Y. J. et al. (1996). Mutations affecting development of the zebrafish inner ear and lateral line. *Development* **123**, 241-254.
Yoshida, T., Vivatbutsiri, P., Morriss-Kay, G., Saga, Y. and Iseki, S. (2008). Cell lineage in mammalian craniofacial mesenchyme. *Mech. Dev.* **125**, 797-808.
Youson, J. H. and Freeman, P. A. (1976). Morphology of the gills of larval and parasitic adult sea lamprey, Petromyzon marinus L. *J. Morphol.* **149**, 73-103.
Yu, J. K., Meulemans, D., McKeown, S. J. and Bronner-Fraser, M. (2008). Insights from the amphioxus genome on the origin of vertebrate neural crest. *Genome Res.* **18**, 1127-1132.

Publication 2:

Mongera A. and Nüsslein-Volhard C. (2013).
Scales of fish arise from mesoderm.
Current Biology 23:338-9.

The embryonic origin of the post-cranial integumentary skeleton, which in fish is formed by scales and fin-rays, is debated. However, the common view is that these elements have a NC origin. As these dermoskeletal structures arise during late developmental stages, discovering their ontogenetic source is complicated and can not be achieved by short-term labeling techniques. To overcome this limitation and test a possible NC contribution to the scales of zebrafish, I made use of stable genetic lineage tracing, transplantation experiments and transposon-based clonal analysis.
First, I used Cre/loxP genetic labeling based on sox10:ER^{T2}-Cre-dependent recombination. Cre induction led to robust marking of cranial skeletogenic tissues that are established NC derivatives. In contrast, I failed to get substantial labeling of post-cranial skeletal elements in adults (n=150), with the exception of a small number of scale clones (n=31). Within these scales, different populations of osteoblasts were labeled: in particular, I found labeled osteoblasts at the scale margin, along the grooves of the posterior field, and, on the outer surface, along the growth ridges of the anterior field. Based on the observations that: *i)* in rare cases the *sox10* promoter used drives ectopic transgene expression in cells that eventually give rise to larval and adult somatic muscle fibers; and *ii)* the frequency of labeled scale clones (1 every 5 fish, f=0,2) is much

lower than the frequency of labeled clones within most NC-derived cell lineages (in case of pigment cells, for example, 5 per fish, f=5); I sought to verify whether these scale-forming osteoblast clones were associated with marker expression in other tissues, in particular with mesoderm-derived skeletal muscles. As in 84% of these clones the rare, labeled scales have been found spatially associated with muscle clones, I concluded that scale-forming osteoblasts do not derive from NC, but from sox10:ERT2-Cre expressing progenitor cells that also give rise to somatic muscles and are thus of mesodermal origin.

Next, in order to validate this finding, I took advantage of an additional transgenic line driving ER^{T2}-Cre expression in the embryonic paraxial mesoderm [Jungke et al., 2013]. After embryonic induction, while I did not observe labeled cells in any of the well-established NC-derived structures, I detected numerous labeled scales (n=30). These scales were clonally associated with labeled, mesoderm-derived muscles and blood vessels in adult fish (n=50). Association analysis revealed that labeled scales were often exclusively associated with muscle clones (60%) and in few cases also with blood vessels (7%). In 33% of the cases, labeled scales were not associated with other recombined tissues. Remarkably, the same populations of osteoblasts that have been detected after sox10-mediated induction were labeled. In particular, within the scales, I found marked cells in the dermis at the anterior margin site and osteoblasts along the serrations, on the scale surface, in the grooves and at the scale rim. *i)* The spatial association of labeled scales and muscles/blood vessels and *ii)* the absence of labeled NC-derived tissues strongly support a shared, mesodermal origin for these structures.

In order to further validate these findings, I conducted trans-

plantation experiments with cells that ubiquitously express GFP under the control of the *b-actin* promoter. By transplanting these cells into wt donor blastula stage embryos and screening the adult fish for scale clones, I found a total of 9 scales with *b-actin*-driven GFP expression. Of these, 7 (77%) were associated with muscle clones. The transplanted scale clones presented in a similar ridged pattern on the anterior half of the scales, as did the floxed clones and are consistent with an osteoblast-like function.

Last, I injected plasmid DNA encoding ubiquitously driven DsRed (under the *ef1a* promoter) into single-cell zebrafish embryos and screened for random integration events in the adult. I identified mosaic fish expressing DsRed in scales, and out of 50 scales with osteoblast-like expression, 45 (89%) had corresponding expression in muscle tissues (Figure 4 C, D). Also in this case the positive cells had a osteoblast-like ridged pattern.

Scales of fish arise from mesoderm

Alessandro Mongera and Christiane Nüsslein-Volhard

The trunk of fish is covered by a large variety of morphologically and structurally diverse skeletal elements, such as scales, scutes and bony plates [1]. These elements are formed from intramembraneous ossifications and are part of the integumentary skeleton [2]. Histological and developmental similarities with neural crest-derived teeth in fossil and extant vertebrates, have led to the widely accepted notion that scales and fin rays, which are thought to be a scale modification, primarily derive from neural crest and not from mesodermal sources as the majority of the post-cranial skeleton [2]. Although short- and long-term labeling experiments in zebrafish have suggested a neural crest origin of fin rays [3,4], the contribution of neural crest to the post-cranial integumentary skeleton, and in particular to the scales, has not been thoroughly analyzed. By Cre/loxP-based genetic labeling, transplantation experiments and transposon-mediated clonal analysis, we demonstrate a mesodermal origin of scale-forming osteoblasts. Furthermore, our data do not support an extensive, if any, neural crest contribution to the post-cranial integumentary skeleton.

Zebrafish (*Danio rerio*) possess an integumentary skeleton in the form of elasmoid scales — a highly derived scale type that protects the bodies of most teleost fish [1,5]. To investigate a possible neural crest origin for scale osteoblasts, we used a recently developed sox10:ER^{T2}-Cre driver line that allows permanent labeling of neural crest-derived cells in zebrafish [6]. In particular, induction of Cre-mediated recombination in *Tg(sox10:ER^{T2}-CRE;bactin:switch)* embryos leads to robust marking of cranial skeletogenic tissues that are known to be derived from neural crest. By contrast, we failed to obtain substantial labeling of post-cranial skeletal elements in adults (n = 150), with the exception of a small number of scale clones (n = 31) (Figure 1A–J). Within these scales, we found labeled osteoblasts at the margin, along the grooves of the posterior field (Figure 1A), and on the outer surface, along the growth ridges of the anterior field (Figure 1A,B) and in the posterior field (Figure 1C; Supplemental data). In rare cases, the *sox10* promoter used drives transgene expression in future larval and adult somatic muscle fibers (Figure 1D,E). Moreover, the frequency of labeled scale clones (one in every five fish; f = 0,2) is much lower than the frequency of labeled clones within most neural crest-derived cell lineages (for example, there are five pigment cell clones per fish, f = 5). We thus sought to verify whether labeled scale osteoblasts were clonally associated with other labeled tissues, in particular with mesoderm-derived skeletal muscles (Figure 1F–J). Three scale clones (10%) were not associated with other labeled tissues (Figure 1F), 19 (61%) presented exclusive association with labeled muscles (Figure 1G), 7 (23%) were spatially related with both labeled neural crest derivatives and muscles (Figure 1H), and two (6%) were associated exclusively with neural crest derivatives, such as pigment cells (Figure 1I). As in 84% of our clones labeled scales have been found spatially associated with labeled muscles, we conclude that scale-forming osteoblasts do not derive from neural crest, but from sox10:ERT2-Cre expressing cells that are also the progenitors of somatic muscles and have thus a mesodermal origin.

In order to independently validate our finding, we used an additional transgenic line driving ERT2-Cre expression in the early paraxial mesoderm [Tg(*SA1-mCT2aC#HB*)] [7]. After embryonic induction (16–48 hpf), we did not observe labeled cells in any of the well-established neural crest-derived structures. By contrast, we detected numerous labeled scales (n = 30) clonally associated with labeled, mesoderm-derived muscles and blood vessels in adult fish (n = 50) (Figure 1K–N; Supplemental Information). Remarkably, we found the same cell populations that have been detected after *sox10*-mediated induction. Within the scales, we found marked cells in the dermis at the anterior margin and osteoblasts along the serrations, on the scale surface, in the grooves and at the scale rim (Figure 1K–L). The spatial association of labeled scales and somatic muscles (Figure 1M–N) and the absence of labeled neural crest-derived tissues as expected from the expression profile of the driver line, strongly support a shared, mesodermal origin for these structures. Further cross-validation has been carried out by means of blastula transplantations of *ß*-actin:GFP labeled cells into wild-type embryos (Figure 1O,O') and transposon-based clonal insertion of a vector expressing ubiquitously the DsRed reporter gene (Figure 1P,P'; Supplemental Information), which permits a finer control of clone size. In both cases, the scale–muscle association was confirmed (77% and 89%, respectively).

In the light of the 'new head' theory, which views neural crest as the source for many vertebrate-specific traits, and on the basis of similarities between dental elements and the ancestral scale type, the entire set of post-cranial integumentary skeletal elements was thought to be neural crest-derived [2]. Recent work supported this view with respect to fin rays [4]. However, we here show that teleost scales are predominantly derived from mesoderm. Despite their diversity, the multiple types of scales and skeletal components of the integument are considered to share an evolutionary origin, the odontode, and use similar developmental mechanisms [1,8,9]. However, a general lack of structural details at the tissue level impedes confirmation of homologies between different integumentary skeletal elements. Elasmoid scales are quite divergent from the ancestral condition, which has persisted almost unchanged in placoid scales of cartilaginous fish [8]. Although it is generally accepted that a reduction led to the loss of some components, the precise identity of the mineralized layers that persisted in the elasmoid scales is debated. In particular, the presence of true dentine, which in the teeth is a product of neural crest-derived odontoblasts, is not widely accepted [5,8]. Our data point to a mesodermal origin of scale-forming osteoblasts in zebrafish and do not support a neural crest contribution to scales in teleosts. However, our analysis does not exclude that more ancestral types of scales with a structure closer to teeth such as placoid scales of cartilaginous fish may include neural crest-derived tissues.

Supplemental Information

Supplemental Information including experimental procedures and two figures can be found online at http://dx.doi.org/10.1016/j.cub.2013.02.056.

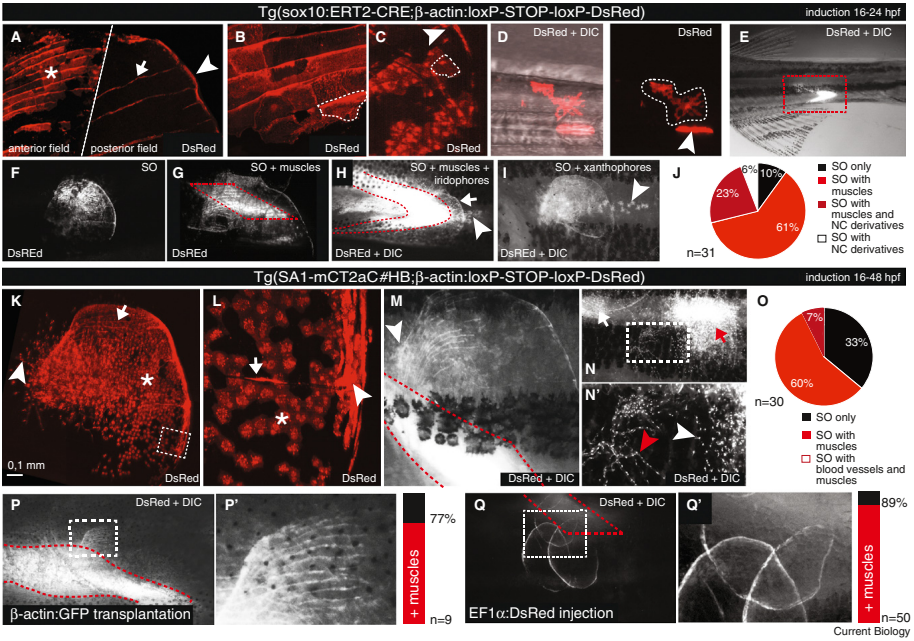

Figure 1. Mesoderm-derived scale osteoblasts.
(A–J) *sox10:ERT2-Cre*-mediated cell labeling. (A) Labeled SOs along the serrations (asterisk), the radii (arrow) and at the margin (arrowhead). (B) Labeled SOs covering the scale outer surface in the anterior field and (C) in the posterior field. Representative cell shapes are highlighted by dashed insets. The arrowhead in (C) highlights SOs at the posterior scale margin. (D) Labeled neural crest-derived cell types (dashed inset) and mesodermal derivatives (muscle fiber, arrowhead) in the trunk of 5 days post-fertilisation larvae. (E) Somitic muscle clone in adult fish. (F) SO clone. (G) SOs and somatic muscles (dashed inset). (H) SOs, somatic muscles (red dashed inset), and iridophores (arrowhead). (I) SOs and xanthophores (arrowhead). (J) Analysis of clonal association between labeled scales (n = 31) and neural crest-/mesoderm-derived tissues. (K–O) *SA1-mCT2aC#HB*-mediated cell labeling. (K) Scale clone with labeled fibroblast-like cells (arrowhead) and scale osteoblasts (SOs) along the serrations (arrow) and on the outer surface of the posterior field (asterisk). (L) Magnification of the inset in (K) showing labeled SOs along the radii (arrow), covering the scale surface (asterisk), and at the scale margin (arrowhead). (M) Recombined SOs associated with recombined muscles. (N,N') Recombined SOs associated with recombined blood vessels. (N) Labeled SOs along the serrations (white arrow) and on the scale surface (red arrow). (N') Magnification of the inset in (N) showing recombined blood vessels (red arrowhead) and fibroblast-like cells (white arrowhead). (O) Analysis of clonal association between labeled scales (n = 30), muscles and blood vessels. (P,P') Independent validation of SO/muscle clonal association by blastula transplantation (77%; n = 9) and (Q,Q') transposon-based clonal insertion (89%; n = 50). (P',Q') are magnifications of the insets in (P) and (Q), respectively.

Acknowledgements
We would like to thank M. Almuedo-Castillo, O. Campas and M.P. Harris for critically reading the manuscript; Michael Brand and the CreZoo Consortium for sharing the Tg(SA1-mCT2aC#HB) line; C. Liebig for technical assistance; A.P. Singh, S. Perathoner, J. Krauss, M.P. Levesque and S. Alsheimer for stimulating discussions.

References

1. Sire, J.Y., Donoghue, P.C., Vickaryous, M.K. (2009). Origin and evolution of the integumentary skeleton in non-tetrapod vertebrates. J. Anat. *214*, 409–440.
2. Smith, M.M., and Hall, B.K. (1990). Development and evolutionary origins of vertebrate skeletogenic and odontogenic tissues. Biol. Rev. Camb. Philos. Soc. *65*, 277–373.
3. Smith, M., Hickman, A., Amanze, D., Lumsden, A. and Thorogood, P. (1994). Trunk neural crest origin of caudal fin mesenchyme in the zebrafish *Brachydanio rerio*. Proc. R. Soc. Lond. B *256*, 137–145.
4. Kague, E., Gallagher, M., Burke, S., Parsons, M., Franz-Odendaal, T., Fisher, S. (2012). Skeletogenic fate of zebrafish cranial and trunk neural crest. PLoS One *7*, e47394.
5. Sire, J.Y., Akimenko, M.A. (2004). Scale development in fish: a review, with description of sonic hedgehog (shh) expression in the zebrafish (*Danio rerio*). Int. J. Dev. Biol. *48*, 233–247.
6. Mongera, A., Singh, A.P., Levesque, M.P., Chen, Y.Y., Konstantinidis, P., and Nüsslein-Volhard, C. (2013). Genetic lineage labeling uncovers novel neural crest contributions to the head including gill pillar cells. Development *140*, 916–925.
7. http://crezoo.crt-dresden.de/crezoo/transgenicLine/detail/22#
8. Reif, W.E. (1982). Evolution of dermal skeleton and dentition in Vertebrates. The odontode regulation theory. Evol. Biol. 287–368.
9. Harris, M.P., Rohner, N., Schwarz, H., Perathoner, S., Konstantinidis, P., Nüsslein-Volhard. (2008). Zebrafish eda and edar mutants reveal conserved and ancestral roles of ectodysplasin signaling in vertebrates. PLoS Genet. *4*, e1000206.

Max-Planck-Institut für Entwicklungsbiologie, Spemannstrasse 35, 72076 Tübingen, Germany.
E-mail: alessandro.mongera@tuebingen.mpg.de, christiane.nuesslein-volhard@tuebingen.mpg.de

CHAPTER 3

Discussion

3.1 NC-driven expansion of the respiratory surface

The appearance of NC was a fundamental step in vertebrate evolution, since its derivatives have tremendously accelerated the transition between a sessile and a more active lifestyle. Furthermore, they have led to the emergence of predation, the acquisition of bigger body sizes, and the exploitation of unexplored ecological niches. Although NC contribution to multiple cell types is well documented in different model organisms [Gross and Hanken, 2008], the lack of a comprehensive analysis of NC-derived adult structures in vertebrate groups other than amphibians, avians, and mammals, leaves a gap in our understanding of important evolutionary transitions. Key innovations that endowed vertebrates with predatory capacity were: *i)* the emergence of a skull vault and a dorsoventrally articulated jaw and *ii)* the acquisition of muscular ventilation

coupled with respiratory surface expansion. During my doctoral studies I have developed and employed a genetic long-term labeling method to uncover a potential NC origin of evolutionarily important cell-types and tissues of previously unrecognized or debated origin in zebrafish, a model teleost. In particular, I focused on the respiratory system and showed that, by giving rise to pillar cells of the gills, NC might have expedited respiratory surface expansion and muscular ventilation.
At the protochordate-vertebrate transition, the expansion of the respiratory surface of the gills accompanied the switch from ciliary to muscular ventilation [Gans and Northcutt, 1983]. Moreover, recent paleontological analysis of Cristozoan fossils, such as *Haikouella lanceolata* and *Yunnanozoon lividum*, suggests a pre-craniate history of 'crest animals'. These fossils are indeed characterized by paired gill rays and jointed branchial arches but do not possess a skull [Chen, 2008; Holland and Chen, 2001; Mallatt and Chen, 2003; Mallatt et al., 2003]. Although many structures directly involved in prey capture have been shown to derive from NC, the embryonic origin of the new, expanded respiratory organ, which according to the recent paleontological interpretation seems to predate the appearance of the skull, has not been investigated. Our demonstration of a NC origin for gill pillar cells reinforces the importance of this embryonic tissue in the evolution of respiratory systems and, possibly, in the radiation of pre-craniate, 'crest animals' without skull at the protochordate-vertebrate transition.
Pillar cells are found in the gills of hagfishes [Mallatt and Paulsen, 1986; Elger, 1987], lampreys [Youson and Freeman, 1976], chondrichthyans and osteognathostomes [Evans et al., 2005]. However, cephalochordates lack specialized gill cells that increase the respiratory surface area. Instead, this group has

rather simple collagen bars located in the pharynx atrium, and gas exchange occurs through ciliated epithelial cells [Baskin and Detmers, 1976]. Thus, pillar cells are a craniate synapomorphy and, as they provide the structural basis for the new expanded gill organ, represent a key innovation in vertebrate evolution. Pillar cells form small channels to conduct blood through the gills and possess the ability to expand or contract their cytoplasmic processes to control blood flow [Bettex-Galland and Hughes, 1973]. This 'contraction/expansion' activity regulates also the distance between neighboring secondary lamellae, thereby modulating water flow through the gills. The development of this unique vertebrate-specific cell type is still poorly understood. Observations of cellular microanatomy and tissue ontogeny [Datta Munshi and Singh, 1968], supported by expression of smooth muscle myosin [Smith and Chamley-Campbell, 1981], suggest a derivation of pillar cells from the smooth muscles forming the blood vessels of the primary lamellae. Cephalic NC is known to give rise to avian and mammalian smooth muscle cells of blood vessels of the face and forebrain but not to the endothelium [Etchevers et al., 2001; Le Lièvre and Le Douarin, 1975; Yoshida et al., 2008]. Our finding that, in addition to the smooth muscles of the pharyngeal arches, also those forming the primary lamellae have a NC origin, supports the hypothesis that pillar cells evolved from this tissue rather than from endothelial cells, as originally proposed [Bietrix, 1895].

In summary, using an inducible Cre/loxP system for genetic lineage tracing, we demonstrate NC contribution to various structures in metamorphic and adult zebrafish, an important model teleost. In particular, our analysis reveals a direct involvement of NC in the development of gill pillar cells, a unique

cell type found in vertebrates and hagfishes. A switch from ciliary ventilation to respiratory muscular ventilation with gills was an early event during the evolutionary history of modern vertebrates followed by skull reorganization and the emergence of a jaw. A role for the NC in remodeling the respiratory system of early crest animals is underappreciated, in part due to the lack of such analysis in non-tetrapod vertebrates. Respiratory systems underwent a profound transformation and pillar cells were lost along the tetrapod lineage. We propose that the evolution of the gills with their highly expanded respiratory surface was driven by NC, and thus confirm the fundamental role of this embryonic tissue in vertebrate radiation.

3.2 Mesoderm, and not NC, contributes to fish scales

In the light of the 'new head' theory, that regards NC as the *bona fide* ontogenetic source for a large set of vertebrate-specific traits, and on the basis of structural and ontogenetic similarities between dental elements and the ancestral scale type, it has been believed that the entire set of post-cranial integumentary skeletal elements represents a NC derivative [Smith and Hall, 1990]. Short-term labeling experiments support this view with respect to fin rays [Smith, 1994], which are considered to be a scale modification. Notably, this study neither makes use of proper markers nor shows labeling of osteoblasts, but only of fibroblast-like cells that are assumed to be progenitors of fin osteoblasts. Also recent work taking advantage of long-term labeling techniques based on the Cre/loxP sys-

tem has supported a NC origin for fin ray-forming cells of the zebrafish caudal fin [Kague et al., 2012]. However, some experimental weaknesses can be highlighted: *i)* a NC-specific enhancer from mouse has been used without carefully characterizing its activity in zebrafish; *ii)* to enhance transgene expression a minimal promoter has been added, but its autonomous activity in the absence of the enhancer has not been controlled; *iii)* a possible association of labeled osteoblasts and non-NC-derived tissues has not been analyzed.

By Cre/loxP-based genetic labeling, transplantation experiments and transposon-based clonal analysis, I demonstrated conclusively that teleost scales arise from mesoderm-derived cell lineages, excluding an extensive, if any, NC contribution to these skeletal elements. The same result has been recently obtained in independent studies [Ho Lee et al., 2013; Shimada et al., 2013]. Moreover, it has been shown that fin mesenchyme derives exclusively from mesoderm and thus that trunk NC does not generate ectomesenchyme [Lee et al., 2013]. Together, these works show how powerful and informative long-term genetic labeling based on the Cre/loxP system can be when applied also to non-mammal models.

Despite their diversity, the multiple types of scales and skeletal components of the integumentum are considered homologous structures: they are thought to share a common evolutionary predecessor, the odontode, and are induced by similar molecular programs [Sire et al., 2009; Reif, 1982; Harris et al., 2008]. However, a general lack of structural and histological details and a substantial phenotypic divergence impede confirmation of homologies between different integumentary skeletal elements [Sire et al., 2009]. The elasmoid scale, a common structure in teleost species, is a highly derived structure that

hardly resembles the original tissue and morphological organization of odontodes [Sire and Akimenko, 2004]. Although it is generally accepted that a reduction process took place, leading to the loss of some components, the precise identity of the mineralized layers that persisted in the elasmoid scales is debated. In particular, the presence of enamel and true dentine, which in the teeth is a product of NC-derived odontoblasts, is not widely accepted [Sire et al., 2009; Reif, 1982]. Some work suggests that, depending on the species and the tissue at the scale/epidermis interface, a *limiting layer* of ultra-mineralized tissue similar to enamel may be localized superficially, covering the external layer in the posterior field of the zebrafish scale [Sire et al., 2009].

Generally, elasmoid scales share a common multi-layered architecture characterized by: a superficial cellular layer called *episquama*; a thin mineralized 'osseus plate' with regular elevations in form of circular ridges referred to as *external layer*; the *isopedine*, a thick non-mineralized *fibrillary plate* with plywood-like fiber orientation; and the *hyposquama*, representing the basal cell layer [Sire and Akimenko, 2004; Waterman, 1970]. It has been proposed that the episquama is formed by osteoblast-like cells responsible for the deposition of the external layer, whereas cells of the hyposquama would be involved in the formation of the isopedine layer [Pevsner, 1926; Pasqualetti et al., 2012b,a]. Notably, elasmoid scales are thought to derive from the ganoid type after complete disappearance of dentine and ganoine (enamel-like mineral layer) as well as after modifications of its osseous basal plate into the isopedine and the external layer [Schultze, 1977; Goodrich, 1907].

Among the different types of scales found in extant fish, placoid scales of cartilaginous fish such as sharks and rays feature an

ancestral organization similar to odontodes of agnathan fossils. My result of a mesodermal origin for scale-forming osteoblasts in zebrafish does not exclude that this type of scales with a structure closer to teeth may include NC-derived tissues. To address the possible contribution of NC to more ancient integumentary skeletal elements such as placoid scales, tools for long-term labeling need to be developed in a cartilaginous fish. Although standard techniques of molecular biology and vital dye injections have been recently applied successfully in Chondrichthyans [Gillis et al., 2009, 2012], genetic manipulation is not yet possible in any of these species.

3.3 *Tg(sox10:ERT2-Cre)* line as a tool to understand vertebrate evolution

Little is known about the cellular and molecular events underlying NC-driven diversification of the vertebrate body plan. This is due, in part, to a dearth of tools allowing consistent and long-term labeling of NC-derivatives. Inducible sox10:ER^{T2}-Cre recombination allows NC long-term labeling in a spatiotemporal manner: the spatial domain of Cre-mediated recombination is restricted by the *sox10* promoter and the temporal domain is under tamoxifen control. In the future, the sox10:ER^{T2}-Cre line will also enable the genetic manipulation of NC and its derivatives. For example, taking advantage of the new 'FlipTrap' and 'FlEx' technologies [Ni et al., 2012; Trinh et al., 2011], it will be possible to specifically manipulate particular genes in cell lineages that fall into the spatial and temporal domain of the sox10:ER^{T2}-Cre transgene. This

will greatly improve our understanding of how these populations of migratory and proliferative cells give rise to diverse cell types and organs in the vertebrate body.

Bibliography

Abitua, P. B., Wagner, E., Navarrete, I. A., and Levine, M. (2012). Identification of a rudimentary neural crest in a non-vertebrate chordate. *Nature*, 492(7427):104–7.

Baskin, D. G. and Detmers, P. A. (1976). Electron microscopic study on the gill bars of amphioxus (branchiostoma californiense) with special reference to neurociliary control. *Cell Tissue Res*, 166(2):167–78.

Bertrand, J. Y., Chi, N. C., Santoso, B., Teng, S., Stainier, D. Y. R., and Traver, D. (2010). Haematopoietic stem cells derive directly from aortic endothelium during development. *Nature*, 464(7285):108–11.

Bettex-Galland, M. and Hughes, G. M. (1973). Contractile filamentous material in the pillar cells of fish gills. *J Cell Sci*, 13(2):359–70.

Bietrix, E. (1895). Quelques considerations sur les notions de lacune et d'endothelium en anatomie generale, a propos du rescau vasculaire branchial des poissons. *C. r. somm. Seanc. Soc. Philomath*, (8):26–28.

Bronner-Fraser, M. and Fraser, S. E. (1988). Cell lineage analysis reveals multipotency of some avian neural crest cells. *Nature*, 335(6186):161–4.

Carney, T. J., Dutton, K. A., Greenhill, E., Delfino-Machín, M., Dufourcq, P., Blader, P., and Kelsh, R. N. (2006). A direct role for sox10 in specification of neural crest-derived sensory neurons. *Development*, 133(23):4619–30.

Chai, Y., Jiang, X., Ito, Y., Bringas, Jr, P., Han, J., Rowitch, D. H., Soriano, P., McMahon, A. P., and Sucov, H. M. (2000). Fate of the mammalian cranial neural crest during tooth and mandibular morphogenesis. *Development*, 127(8):1671–9.

Chen, J.-Y. (2008). Early crest animals and the insight they provide into the evolutionary origin of craniates. *Genesis*, 46(11):623–39.

Chen, Y.-Y. (2011). PhD thesis, Eberhard Karls Universität Tübingen.

Collazo, A., Bronner-Fraser, M., and Fraser, S. E. (1993). Vital dye labelling of xenopus laevis trunk neural crest reveals multipotency and novel pathways of migration. *Development*, 118(2):363–76.

Datta Munshi, J. S. and Singh, B. N. (1968). On the microcirculatory system of the gills of certain freshwater teleostean fishes. *J. Zool.*, (154):365–376.

de Beer, G. R. (1947). The differentiation of neural crest cells into visceral cartilages and odontoblasts in amblystoma, and a re-examination of the germ-layer theory. *Proc R Soc*, B134:377–398.

Elger, M. (1987). The branchial circulation and the gill epithelia in the atlantic hagfish, myxine glutinosa l. *Anat Embryol (Berl)*, 175(4):489–504.

Etchevers, H. C., Vincent, C., Le Douarin, N. M., and Couly, G. F. (2001). The cephalic neural crest provides pericytes and smooth muscle cells to all blood vessels of the face and forebrain. *Development*, 128(7):1059–68.

Evans, D. H., Piermarini, P. M., and Choe, K. P. (2005). The multifunctional fish gill: dominant site of gas exchange, osmoregulation, acid-base regulation, and excretion of nitrogenous waste. *Physiol Rev*, 85(1):97–177.

Gans, C. and Northcutt, R. G. (1983). Neural crest and the origin of vertebrates: a new head. *Science*, 220(4594):268–73.

Gillis, J. A., Dahn, R. D., and Shubin, N. H. (2009). Chondrogenesis and homology of the visceral skeleton in the little skate, leucoraja erinacea (chondrichthyes: Batoidea). *J Morphol*, 270(5):628–43.

Gillis, J. A., Modrell, M. S., Northcutt, R. G., Catania, K. C., Luer, C. A., and Baker, C. V. H. (2012). Electrosensory ampullary organs are derived from lateral line placodes in cartilaginous fishes. *Development*, 139(17):3142–6.

Goodrich, E. S. (1907). On the scales of fish, living and extinct, and their importance in classification. *Proceedings of the Zoological Society of London*, 77(4):751–773.

Gross, J. B. and Hanken, J. (2008). Review of fate-mapping studies of osteogenic cranial neural crest in vertebrates. *Dev Biol*, 317(2):389–400.

Hall, B. K. (2000). The neural crest as a fourth germ layer and vertebrates as quadroblastic not triploblastic. *Evol Dev*, 2(1):3–5.

Hall, B. K. (2009). *The Neural Crest and Neural Crest Cells in Vertebrate Development and Evolution.* Springer.

Hans, S., Freudenreich, D., Geffarth, M., Kaslin, J., Machate, A., and Brand, M. (2011). Generation of a non-leaky heat shock-inducible cre line for conditional cre/lox strategies in zebrafish. *Dev Dyn*, 240(1):108–15.

Hans, S., Kaslin, J., Freudenreich, D., and Brand, M. (2009). Temporally-controlled site-specific recombination in zebrafish. *PLoS One*, 4(2):e4640.

Harris, M. P., Rohner, N., Schwarz, H., Perathoner, S., Konstantinidis, P., and Nüsslein-Volhard, C. (2008). Zebrafish eda and edar mutants reveal conserved and ancestral roles of ectodysplasin signaling in vertebrates. *PLoS Genet*, 4(10):e1000206.

His, W. (1868). Untersuchungen über die ersten anlagen des wirbeltierleibes. die erste entwicklung des hühnchens im ei. *Verlag von FCW Vogel*, pages 164–166.

Ho Lee, R. T., Thiery, J. P., and Carney, T. J. (2013). Dermal fin rays and scales derive from mesoderm, not neural crest. *Curr Biol*, 23(9):R336–7.

Holland, N. D. and Chen, J. (2001). Origin and early evolution of the vertebrates: new insights from advances in molecular biology, anatomy, and palaeontology. *Bioessays*, 23(2):142–51.

Hörstadius, S. (1950). *The Neural Crest: Its Properties and Derivatives in the Light of Experimental Research.* Oxford Univesrity Press.

Hughes, G. M. and Morgan, M. (1973). The structure of fish gills in relation to their respiratory function. *Biological Reviews*, 48(3):419–475.

Huxley, T. H. (1849). On the anatomy and affinities of the family of the medusae. *Phil Trans R Soc*, (139):413–434.

Huysseune, A. and Sire, J. Y. (1998). Evolution of patterns and processes in teeth and tooth-related tissues in non-mammalian vertebrates. *Eur J Oral Sci*, 106 Suppl 1:437–81.

Jungke, P., Hans, S., and Brand, M. (2013). The zebrafish crezoo: An easy-to-handle database for novel creer(t2)-driver lines. *Zebrafish*.

Kague, E., Gallagher, M., Burke, S., Parsons, M., Franz-Odendaal, T., and Fisher, S. (2012). Skeletogenic fate of zebrafish cranial and trunk neural crest. *PLoS One*, 7(11):e47394.

Landacre, F. L. (1921). The fate of the neural crest in the head of the urodeles. *J Comp Neurol*, 33:1–43.

Langille, R. M. and Hall, B. K. (1986). Evidence of cranial neural crest contribution to the skeleton of the sea lamprey, petromyzon marinus. *Prog Clin Biol Res*, 217B:263–6.

Langille, R. M. and Hall, B. K. (1988). Role of the neural crest in development of the cartilaginous cranial and visceral skel-

eton of the medaka, oryzias latipes (teleostei). *Anat Embryol (Berl)*, 177(4):297–305.

Lankester, E. R. (1873). On the primitive cell-layers of the embryo as the basis of genealogical classification of animals, and on the origin of vascular and lymph systems. 4(11):321–338.

Le Douarin, N. M. (1974). Cell recognition based on natural morphological nuclear markers. *Med Biol*, 52(5):281–319.

Le Douarin, N. M. (1986). Cell line segregation during peripheral nervous system ontogeny. *Science*, 231(4745):1515–22.

Le Douarin, N. M. and Kalcheim, C. (1999). *The neural crest*. Cambridge University Press.

Le Lievre, C. S. and Le Douarin, N. M. (1975). Mesenchymal derivatives of the neural crest: analysis of chimaeric quail and chick embryos. *J Embryol Exp Morphol*, (34):125–154.

Le Lièvre, C. S. and Le Douarin, N. M. (1975). Mesenchymal derivatives of the neural crest: analysis of chimaeric quail and chick embryos. *J Embryol Exp Morphol*, 34(1):125–54.

Lee, R. T. H., Knapik, E. W., Thiery, J. P., and Carney, T. J. (2013). An exclusively mesodermal origin of fin mesenchyme demonstrates that zebrafish trunk neural crest does not generate ectomesenchyme. *Development*, 140(14):2923–32.

Li, Y.-X., Zdanowicz, M., Young, L., Kumiski, D., Leatherbury, L., and Kirby, M. L. (2003). Cardiac neural crest in zebrafish

embryos contributes to myocardial cell lineage and early heart function. *Dev Dyn*, 226(3):540–50.

Lumsden, A. (1991). Cell lineage restrictions in the chick embryo hindbrain. *Philos Trans R Soc Lond B Biol Sci*, 331(1261):281–6.

Luo, R., An, M., Arduini, B. L., and Henion, P. D. (2001). Specific pan-neural crest expression of zebrafish crestin throughout embryonic development. *Dev Dyn*, 220(2):169–74.

Mallatt, J., Chen, J., and Holland, N. D. (2003). Comment on "a new species of yunnanozoan with implications for deuterostome evolution". *Science*, 300(5624):1372; author reply 1372.

Mallatt, J. and Chen, J.-y. (2003). Fossil sister group of craniates: predicted and found. *J Morphol*, 258(1):1–31.

Mallatt, J. and Paulsen, C. (1986). Gill ultrastructure of the pacific hagfish eptatretus stouti. *Am J Anat*, 177(2):243–69.

Metzger, D., Clifford, J., Chiba, H., and Chambon, P. (1995). Conditional site-specific recombination in mammalian cells using a ligand-dependent chimeric cre recombinase. *Proc Natl Acad Sci U S A*, 92(15):6991–5.

Nakamura, H. and Ayer-le Lievre, C. S. (1982). Mesectodermal capabilities of the trunk neural crest of birds. *J Embryol Exp Morphol*, 70:1–18.

Ni, T. T., Lu, J., Zhu, M., Maddison, L. A., Boyd, K. L., Huskey, L., Ju, B., Hesselson, D., Zhong, T. P., Page-McCaw,

P. S., Stainier, D. Y., and Chen, W. (2012). Conditional control of gene function by an invertible gene trap in zebrafish. *Proc Natl Acad Sci U S A*, 109(38):15389–94.

Orban, P. C., Chui, D., and Marth, J. D. (1992). Tissue- and site-specific dna recombination in transgenic mice. *Proc Natl Acad Sci U S A*, 89(15):6861–5.

Pander, C. (1817). Dissertation inauguralis, sistens historiam metamorphoseos quam ovum incubatum prioribus quinque diebus subit.

Pasqualetti, S., Banfi, G., and Mariotti, M. (2012a). Osteoblast and osteoclast behavior in zebrafish cultured scales. *Cell Tissue Res*, 350(1):69–75.

Pasqualetti, S., Banfi, G., and Mariotti, M. (2012b). The zebrafish scale as model to study the bone mineralization process. *J Mol Histol*, 43(5):589–95.

Pevsner, V. V. (1926). Zur frage uber die struktur und die entwicklung der schuppen einiger knochenfische. *Zool. Anz.*, (68):303–313.

Platt, J. B. (1893). Ectodermic origin of the cartilages of the head. *Anat Anz*, (8):506–509.

Platt, J. B. (1894). Ontogenetic differentiation of the ectoderm in necturus. second preliminary note. *Arch Mikrosk Anat EntwMech*, (43):911–966.

Reif, W. E. (1982). Evolution of dermal skeleton and dentition in vertebrates. *Evol. Biol.*, pages 287–368.

Sauer, B. and Henderson, N. (1988). Site-specific dna recombination in mammalian cells by the cre recombinase of bacteriophage p1. *Proc Natl Acad Sci U S A*, 85(14):5166–70.

Schilling, T. F. and Kimmel, C. B. (1994). Segment and cell type lineage restrictions during pharyngeal arch development in the zebrafish embryo. *Development*, 120(3):483–94.

Schultze, H. P. (1977). Ausgangsform und entwicklung der rhombischen schuppen der osteichthyes (pisces). *Palaontol. Z.*, (51):152–168.

Selleck, M. A. and Stern, C. D. (1991). Fate mapping and cell lineage analysis of hensen's node in the chick embryo. *Development*, 112(2):615–26.

Shimada, A., Kawanishi, T., Kaneko, T., Yoshihara, H., Yano, T., Inohaya, K., Kinoshita, M., Kamei, Y., Tamura, K., and Takeda, H. (2013). Trunk exoskeleton in teleosts is mesodermal in origin. *Nat Commun*, 4:1639.

Sire, J.-Y. and Akimenko, M.-A. (2004). Scale development in fish: a review, with description of sonic hedgehog (shh) expression in the zebrafish (danio rerio). *Int J Dev Biol*, 48(2-3):233–47.

Sire, J.-Y., Donoghue, P. C. J., and Vickaryous, M. K. (2009). Origin and evolution of the integumentary skeleton in non-tetrapod vertebrates. *J Anat*, 214(4):409–40.

Sire, J.-Y. and Huysseune, A. (2003). Formation of dermal skeletal and dental tissues in fish: a comparative and evolutionary approach. *Biol Rev Camb Philos Soc*, 78(2):219–49.

Smith, D. G. and Chamley-Campbell, J. (1981). Localization of smooth-muscle myosin in branchial pillar cells of snapper (chrysophys auratus) by immunofluorescence histochemistry. *J Exp Zool*, 215(1):121–4.

Smith, M, H. A. A. D. L. A. T. P. (1994). Trunk neural crest origin of caudal fin mesenchyme in the zebrafish brachydanio rerio. *Proc. R. Soc. Lond. B*, (256):137–145.

Smith, M. M. and Hall, B. K. (1990). Development and evolutionary origins of vertebrate skeletogenic and odontogenic tissues. *Biol. Rev. Camb. Philos. Soc.*, (65):277–373.

Stone, L. S. (1929). Experiments showing the role of migrating neural crest (mesectoderm) in the formation of head skeleton and loose connective tissue in rana palustris. *Wilhelm Roux Arch EntwMech Org*, 118:40–77.

Trinh, L. A., Hochgreb, T., Graham, M., Wu, D., Ruf-Zamojski, F., Jayasena, C. S., Saxena, A., Hawk, R., Gonzalez-Serricchio, A., Dixson, A., Chow, E., Gonzales, C., Leung, H.-Y., Solomon, I., Bronner-Fraser, M., Megason, S. G., and Fraser, S. E. (2011). A versatile gene trap to visualize and interrogate the function of the vertebrate proteome. *Genes Dev*, 25(21):2306–20.

Wada, N., Javidan, Y., Nelson, S., Carney, T. J., Kelsh, R. N., and Schilling, T. F. (2005). Hedgehog signaling is required for cranial neural crest morphogenesis and chondrogenesis at the midline in the zebrafish skull. *Development*, 132(17):3977–88.

Warga, R. M. and Kimmel, C. B. (1990). Cell movements during epiboly and gastrulation in zebrafish. *Development*, 108(4):569–80.

Waterman, R. E. (1970). Fine structure of scale development in the teleost, brachydanio rerio. *Anat Rec*, 168(3):361–79.

Yokota, Y., Saito, D., Tadokoro, R., and Takahashi, Y. (2011). Genomically integrated transgenes are stably and conditionally expressed in neural crest cell-specific lineages. *Dev Biol*, 353(2):382–95.

Yoshida, T., Vivatbutsiri, P., Morriss-Kay, G., Saga, Y., and Iseki, S. (2008). Cell lineage in mammalian craniofacial mesenchyme. *Mech Dev*, 125(9-10):797–808.

Youson, J. H. and Freeman, P. A. (1976). Morphology of the gills of larval and parasitic adult sea lamprey, petromyzon marinus l. *J Morphol*, 149(1):73–103.

Own contribution to the manuscripts

Both lead-author manuscripts were primarily written by myself with the help of all the coauthors. The project leading to 'Publication 1' has been initially designed with the help of Dr. Mitch Levesque. The experiments were designed by myself and mostly done by myself. Dr. Peter Konstantinidis helped with the interpretation of the data, Dr. Yi-Yen Chen generated the *crestin* transgenic line, and Dr. Ajeet Singh contributed with some confocal pictures of adult fish. The mesoderm-specific Cre-driver line used in 'Publication 2' was generated in the Brand Lab by Peggy Jungke. My contribution to publication 3 and 4 is stated in the 'Appendix' section.

Curriculum vitae

Alessandro Mongera

born: March 3rd, 1982 in Trento (IT)

01/2009-10/2013	PhD student at the Max Planck Institute for Developmental Biology in Tübingen, Germany *Supervisor*: Prof. Dr. Christiane Nüsslein-Volhard *Project*: Long-term fate mapping of neural crest in zebrafish
09/2007-10/2008	Master thesis at the Unit for Developmental Genetics and Dynamics, University of Padua, Italy *Supervisors*: Prof. Dr. Francesco Argenton and Dr. Enrico Moro *Project*: Wnt signaling in zebrafish early development and pancreatic regeneration
10/2006-10/2008	MSc in Evolutionary Biology, University of Padua, Italy
10/2004-09/2006	BSc in Biology, University of Padua, Italy
01/2004-07/2004	Bachelor thesis at the Department of Philosophy, University of Padua, Italy *Supervisor*: Prof. Dr. Giovanni Boniolo *Project*: Biological Fitness: a philosophical analysis
09/2003-03/2004	International exchange student at LMU, Munich, Germany
10/2001-07/2004	BA in Philosophy, University of Padua, Italy
1996-2001	Galileo Galilei Scientific Lyceum, Trento, Italy

Full publication list

Wang, L., **Mongera, A.**, Bonanomi, D., Cyganek, L., Pfaff, S.L., Nüsslein-Volhard, C., and Marquardt, T. (2013). A conserved axon type hierarchy governing peripheral nerve assembly. *submitted*

Mongera, A.[#] and Dooley, C.M. (2013). Of white tigers and solute carriers. *PCMR* doi: 10.1111/pcmr.12163.

Mongera, A.[#] and Nüsslein-Volhard, C[#]. (2013). Scales of fish arise from mesoderm. *Current Biology* 23:338-9

Dooley, C.M., **Mongera, A.**, Walderich, B., and Nüsslein-Volhard, C. (2013). The role of ErbB and Kit signalling in establishing melanophore stem cells in zebrafish. *Development* 140(5):1003-13.

Mongera, A.[#], Singh, A.P., Levesque, M.P., Chen, Y.Y., Konstantinidis, P., and Nüsslein-Volhard, C.[#] . (2013). Genetic lineage labeling in zebrafish uncovers novel neural crest contributions to the head, including gill pillar cells. *Development* 140(4):916-25.

Dooley, C., Schwarz, H., Müller, K.P., **Mongera, A.**, Konantz, M., Neuhauss, S.C.F., Nüsslein-Volhard, C., and Geisler, R. (2012). Slc45a2 and V-ATPase are regulators of melanosomal pH homeostasis in zebrafish, providing a mechanism for human pigment evolution and disease. *PCMR* 26:205-17.

Dodge, M.E., Moon, J., Tuladhar, R., Lu, J., Jacob, L.S., Zhang, L.S., Shi, H., Wang, X., Moro, E., **Mongera, A.**, Argenton, F., Karner, C.M., Carroll, T.J., Chen, C., Amatruda, J.F., and Lum, L. (2012). Diverse chemical scaffolds support direct inhibition of the membrane bound O-acyltransferase Porcupine. *J Biol Chem.* 287(27):23246-54.

Moro, E., Ozhan-Kizil, G.*, **Mongera, A.***, Beis, D.*, Wierzbicki, C., Young, R.M., Bournele, D., Domenichini, A., Valdivia, L.E., Lum, L., Chen, C., Amatruda, J.F., Tiso, N., Weidinger, G., and Argenton, F. (2012). In vivo Wnt signaling tracing through a transgenic biosensor fish reveals novel activity domains. *Dev Biol* 366(2):327-40.

corrisponding author(s)
* equal contributions

Acknowledgments

I thank Janni for giving me the opportunity to develop this project without any constraint, neither in resources nor in timing. Freedom was very much appreciated.

I thank Simon for his friendship, for every happy and sad moment we experienced together in the last 5 years. Patience was very much appreciated. Grazie.

I thank Davide for being a perfect flatmate. Sharing the kitchen became soon a means to share our lives. Organizational skills were very much appreciated. Grazie.

I thank all the colleagues, the ones who are still in the lab and the ones who left. In particular, I'm thankful to Chris, Yi-Yen, Sören, and Mitch for showing me the good aspects of being a scientist.

I thank HMM for cheering me up whenever it was needed and for sharing few small secrets about life. I thank also Christian W. for showing me that good cycling in Germany is possible. I thank Iris for Pranzo.

I'm also grateful to Dr. Brigitte Walderich, the animal caretakers and the non-scientific staff.

Bea, thanks for patience and happiness. Lorenzo, thanks for sharing ideas about possible projects at the interface between astrophysics and developmental biology.

I would also like to thank Sophie, Cosimo, Giovanna, and Michaela, who helped me, in different ways, to make it through.

I thank the old friends and the new ones, lost around the world: Marco A, Marco D, Pippo, Giulia, Madda, Matteo, Kuba, Maria, Mary, Pian di Stantino... your long-distance support has been always important!

Finally, I thank my family for giving me always unconditioned freedom.

Appendix

Publication 3:

Dooley, C.M., Schwarz, H., Mueller, K.P., Mongera, A., Konantz, M., Neuhauss, S.C.F., Nüsslein-Volhard, C., and Geisler, R. (2013). **Slc45a2 and V-ATPase are regulators of melanosomal pH homeostasis in zebrafish, providing a mechanism for human pigment evolution and disease.** *Pigment Cell Melanoma Res* 26(2):205-17.

For this paper, which presents the positional cloning of the *Danio rerio albino* mutant, I first cloned the zebrafish *slc45a2* and the human *SLC45A2* coding sequence; next, I subcloned them in a vector for RNA expression and performed rescue experiments that confirmed the causative role of the identified mutations.

Pigment Cell Melanoma Res. **26**; 205–217

ORIGINAL ARTICLE

Slc45a2 and V-ATPase are regulators of melanosomal pH homeostasis in zebrafish, providing a mechanism for human pigment evolution and disease

Christopher M. Dooley[1]*, Heinz Schwarz[1], Kaspar P. Mueller[2], Alessandro Mongera[1], Martina Konantz[1,†], Stephan C. F. Neuhauss[2], Christiane Nüsslein-Volhard[1] and Robert Geisler[1,‡]

1 Max Planck Institute for Developmental Biology, Tübingen, Germany **2** Institute of Molecular Life Sciences, University of Zurich, Zürich, Switzerland *Current address: The Wellcome Trust Sanger Institute, The Wellcome Trust Genome Campus, Hinxton, UK †Current address: Department of Hematology, Oncology, Immunology, Rheumatology and Pneumology, University of Tübingen Medical Center II, Tübingen, Germany ‡Current address: Institute of Toxicology and Genetics, Karlsruhe Institute of Technology, Eggenstein-Leopoldshafen, Germany

CORRESPONDENCE Christopher M. Dooley, e-mail: chris.dooley@sanger.ac.uk and Robert Geisler, e-mail: robert.geisler@kit.edu

KEYWORDS slc45a2/albinism/V-ATPase/melanosome/melanocyte/retinal pigment epithelium/skin color variation

PUBLICATION DATA Received 11 September 2012, revised and accepted for publication 22 November 2012, published online 3 December 2012

doi: 10.1111/pcmr.12053

Summary

We present here the positional cloning of the *Danio rerio albino* mutant and show that the affected gene encodes Slc45a2. The human orthologous gene has previously been shown to be involved in human skin color variation, and mutations therein have been implicated in the disease OCA4. Through ultrastructural analysis of the melanosomes in *albino* alleles as well as the tyrosinase-deficient mutant *sandy,* we add new insights into the role of *Slc45a2* in the production of melanin. To gain further understanding of the role of *Slc45a2* and its possible interactions with other proteins involved in melanization, we further analyzed the role of the V-ATPase as a melanosomal acidifier. We show that it is possible to rescue the melanization potential of the *albino* melanosomes through genetic and chemical inhibition of V-ATPase, thereby increasing internal melanosome pH.

Introduction

Body pigmentation in vertebrates has an important function in camouflage, kin recognition, and sexual selection as well as shielding the skin from sunlight. Large-scale genetic screens in mouse and zebra fish have identified a great number of genes that affect melanin-dependent body pigmentation. Pigmentation of the skin results from melanocytes originating in the neural crest (NC), while pigmented retinal epithelium (RPE) arises from the neuroectoderm of the developing optic cup. In zebra fish, a mutation in the *nacre*/*mitfa* gene eliminates all NC–derived melanophores causing the body of the mutant to appear yellow due to a lack of the black stripes, while the RPE is normally pigmented (Lister et al., 1999). In contrast, other genes specifically affect the pigmentation of the melanocytes of the body as well as the RPE, suggesting that they are involved in the production and

Significance

Our findings show that Slc45a2 and V-ATPase along with Slc24a5 control pH and ionic homeostasis within melanosomes. In our model, a reduction in the efficiency of Slc45a2 has a quenching effect on the activity of tyrosinase by lowering the melanosomal pH while still maintaining the integrity of the melanosomes avoiding the toxic effects seen in tyrosinase mutants. These findings offer new clues to the molecular basis of melanin biosynthesis as well as providing a potential mechanism for human skin color variation.

distribution of the dark pigment melanin within these cells. In zebra fish, mutations in the *sandy*, *golden*, *mustard*, and *albino* genes result in absent or pale body and eye pigmentation. With the exception of *sandy*, these mutants retain tyrosinase activity when supplied with L-DOPA (Haffter et al., 1996).

Melanin is synthesized within subcellular lysosome-related vesicles called melanosomes in a stepwise process. The key enzymes involved in melanin synthesis tyrosinase, tyrosinase-related protein 1 (TYRP1), and dopachrome tautomerase (DCT) convert tyrosine to L-DOPA and then dopaquinone, which is then further processed to eumelanin (Braasch et al., 2007). Melanosomes are classified into four types according to their structural architecture and maturation. The exact origin of premelanosomes (types I and II) appears to be complex as both a direct endoplasmic reticulum origin and premelanosomes arising from compartments of late secretory and endocytic pathways have been described (Dell'Angelica, 2003). Nevertheless, enzymes such as tyrosinase and TYRP1 are trafficked through the Golgi and join type II melanosomes, which have been progressively filled with PMEL17 fibrils. The addition of these enzymes promotes the deposition of melanin along internal melanosome fibrils and eventually leads to a mature melanosome (type IV; Raposo and Marks, 2007).

Mammalian melanocytes export their melanosomes to other tissues, for example to keratinocytes of the epidermis and hair, while in fishes and amphibians, melanophores retain melanosomes within their cell bodies and traffic them dynamically throughout the cell in response to stimuli such as light or kin communication. Nevertheless, melanosome biosynthesis is similar in all melanosome containing cells. The melanophores, together with other chromophores such as the yellow xanthophores and silvery iridophores distributed in the hypodermis, serve to generate a multitude of elaborate pigmentation patterns that are characteristic for each species of fish or amphibian (Hirata et al., 2003).

The role of SLC45A2 in pigmentation was initially brought to light through its description as the causative gene of oculocutaneous albinism type 4 (OCA4; Newton et al., 2001). OCA4 is a tyrosinase-positive form of OCA and is the leading form of albinism in Japan with patients presenting yellowish-blonde to white hair with varying loss of RPE melanization. In the most debilitating manifestations of OCA, the patients present with a reduced visual acuity that still leaves them disabled after attempts at optical correction. Visual acuity in adults has been proposed to be related to the amount of melanin that is produced in the RPE over time (Summers, 1996). Slc45a2 is also affected in the medaka *b* mutant (Fukamachi et al., 2001) and in the *underwhite* coat color mutant of the mouse (Du and Fisher, 2002). Variants of SLC45A2 have been implicated in skin color variation and also in protection against melanoma (He et al., 2009). Others have speculated on its role as a Na^+/H^+ exchanger in melanocytes (Smith et al., 2004).

Many other genes have been identified as being involved in body pigmentation in vertebrates including humans (Sturm et al., 2001). Even though this collection of genes has been studied in detail, very few have been shown to play a causative role in the variation of human pigmentation. A casual association between genetic polymorphisms in the melanocortin receptor 1 (MC1R) and specific variants of freckling, fair skin and red hair has been shown but this is a phenotype typically only seen in people of European descent (Rees, 2003; Sturm et al., 2001). SLC24A5, a transmembrane cation exchanger localized to intracellular structures consistent with the membranes of melanosomes, was also shown to play a role in human skin color variation. Its zebra fish, ortholog is affected in the zebra fish mutant *golden* (Lamason et al., 2005). Furthermore, Sabeti et al. (2007) undertook a selective sweep analysis of the human genome, which suggested that SCL45A2 and SLC24A5 together play a role in the variation of human skin color (Lamason et al., 2005). Polymorphisms in the SLC45A2 locus had previously been noted to be in linkage disequilibrium when compared between Asian, African, and European populations (Graf et al., 2005, 2007). On the other hand, well-established polymorphisms in the transmembrane enzyme tyrosinase, which has long been known to play a key role in melanin biosynthesis, have failed to show a strong linkage to the natural variation of skin color (Fernandez et al., 2008). To date, the actual cellular mechanisms involved in melanization variation remain largely elusive.

Here, we describe the analysis of the *albino* (*alb*) gene and show that *albino* encodes the 12 transmembrane domain solute carrier Slc45a2. Strong *albino* alleles result from premature stop codons, while several alleles containing missense mutations result in intermediate phenotypes. *albino* melanophores contain normally sized melanosomes that are almost devoid of pigment, while more pigment is present in hypomorphic alleles. In this respect, *albino* resembles the *golden* mutation that has also been previously described to affect melanosome pigment content, while we have found that *sandy*/*tyrosinase* mutants at 3–4 dpf fail to produce melanosomes altogether. We present evidence that *slc45a2*, the V-ATPase complex and *slc24a5* are involved in melanosomal pH homeostasis required for the normal enzymatic activity of tyrosinase while also playing a role in the exchange of cations through Slc24a5.

Results

albino Melanophores fail to pigment properly

Zebra fish *albino* mutants present defects in the pigmentation of both NC–derived melanophores and the RPE. In wild-type fish, the RPE begins melanization at 24 hpf

while at the same time NC-derived body melanophores also start to become visible, and both are completely dark by 48 hpf (Figure 1A). The first described zebra fish *albino* mutant, *alb*^{b4}, which was described by Streisinger more than 25 yr ago (Streisinger et al., 1986), fails to melanize by 48 hpf and appears to lack melanin in both RPE- and NC-derived melanophores (Figure 1B). Although multiple *albino* alleles have been generated in previous screens (Kelsh et al., 1996), we decided to isolate additional alleles to generate a more complete series. For example, *alb*^{ti225} (Figure 1E, H), *alb*^{ti20e} (data not shown) from the Tübingen 1996 screen (Kelsh et al., 1996). and the newly identified *alb*^{tnr52} (Figure S1E) show the same strong larval phenotype as *alb*^{b4} (Figure 1G) but *alb*^{ti225} shows a slightly weaker phenotype than *alb*^{b4} as an adult (Figure 1E). An allele of particular interest, *alb*^{tnr39}, was identified in our screen in which the melanophores of both the body and the RPE of transheterozygous *alb*^{tnr39}/*alb*^{b4} larvae have greatly reduced melanin, but the cells are still readily visible (Figure 1F, I). This suggests that both cell types are capable of producing at least small amounts of melanin by 78 hpf. As adults, the body melanophores of *alb*^{tnr39}/*alb*^{b4} seem to contain almost no melanin, but the dark eyes of the RPE are an obvious contrast to the stronger *alb*^{b4} allele (Figure 1F). Finally, transheterozygous larval fish *alb*^{b4}/*alb*^{tm83a} (Figure 1J) have melanophores with slightly reduced melanin, but as an adult, the homozygous *alb*^{tm83a} allele is practically indiscernible from wild type. Figure 1 shows the pigmentation phenotype of representative alleles. Table 1 presents a summary of the *alb* alleles investigated in this study and their corresponding sequences (Figure S2A–F).

Table 1. Overview of *albino* alleles characterized in this study

Allele	Mutation type	Change	Source
alb^{b4}	Nonsense	[c.1386G>T; p. G461X]	Streisinger
alb^{ti20e}	Nonsense	[c.1270T>A; p. Y423X]	Tübingen 1996 screen
alb^{ti225}	Missense	[c.182G>A; p.G61R]	Tübingen 1996 screen
alb^{tm83a}	In-frame deletion	[c.184_186del; p. S62del]	Tübingen 1996 screen
alb^{tnr39}	Missense	[c.1545A>G; p. Q516R]	New allele
alb^{tnr52}	Deletion	[c.1244_1451del; p. Y415X]	New allele

albino Fish present reduced visual acuity

Visual acuity is highly reduced in humans afflicted with different forms of albinism, so we asked whether the visual resolution of adult *alb*^{b4}, *alb*^{tnr52}, and *alb*^{tnr39} alleles was affected when compared to a collection of different wild-type and pigment mutant fish. Previous studies have shown that the *sandy* mutant presents a specific visual phenotype with impaired light adaption ability that is fundamentally different from that of *albino*, but *sandy* also displays an erratic optokinetic response (OKR; Page-McCaw et al., 2004). The OKR is a series of stereotypic eye movements evoked by movements in the surrounding, such as a moving grate of black and white stripes (Brockerhoff et al., 1995; Mueller and Neuhauss, 2010). Visual acuity can be assessed by determining the minimal

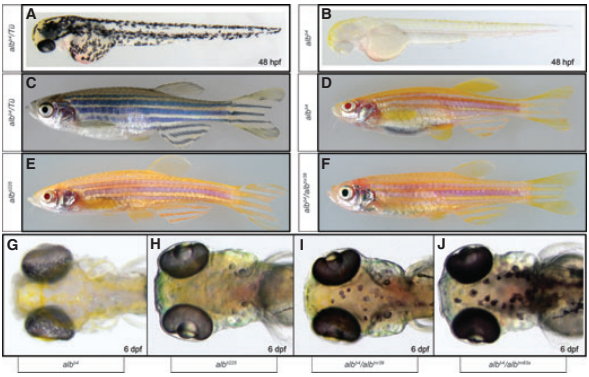

Figure 1. Neural crest–derived and retina pigment melanophores fail to pigment properly in *alb* mutants. At 48 hpf, the melanophores of the neural crest (NC) and retinal epithelium (RPE) are completely melanized in heterozygous siblings (A), whereas *alb*^{b4} fails to produce any visible melanin but developing iridophores become more obvious on the dorsal aspect of the trunk (B). The lack of melanization persists to adulthood in the mutant as compared to heterozygous siblings (C–D). *alb*^{ti225} presents as an adult an almost complete, but pale melanization (E), while the *alb*^{tnr39}/*alb*^{b4} transheterozygous adult lacks visible melanin in the body but retains noticeable amounts in the RPE (F). As a larva, *alb*^{ti225} (H) is indistinguishable from *alb*^{b4}, (G) but *alb*^{tnr39}/*alb*^{b4} larvae display lightly melanized melanophores (I). *alb*^{b4}/*alb*^{tm83a} present an almost wild-type amount of melanin (J).

spatial frequency of the stimulus that is able to evoke the OKR (Haug et al., 2010). We measured in an automated fashion the temporal-to-nasal OKR slow-phase velocity of the right eye of *alb*^{b4} (n = 12), *alb*^{tnr52} (n = 13), and *alb*^{tnr39} (n = 9) fish along with a collection of wild-type fish as well as the *golden* and *nacre* mutants in response to changing contrast or spatial frequency of the optokinetic stimulation (Figure 2A, D). We could not detect any difference in contrast sensitivity of *alb*^{b4}, *alb*^{tnr52}, *alb*^{tnr39}, and other fish (Figure 2E) showing that all fish are fully capable of seeing and responding to the stripe pattern (see methods). However, we were able to establish a significant difference in spatial resolution (Figure 2F) in the range from 0.2 to 0.35 cycles/degree. The average gain of *alb*^{b4} *and alb*^{tnr52} is significantly lower than that of the wild-type control group but not for *alb*^{tnr39} fish (*alb*^{b4}: $P < 0.001$). Therefore, we conclude that similar to *sandy*, visual acuity of both *alb*^{b4} and *alb*^{tnr52} fish is reduced compared to wild-type fish. While, unlike in *albino* mutants, the light adaptation phenotype of *sandy* may involve a defect in network adaptation (Page-McCaw et al., 2004), the similar OKR phenotypes of *sandy* and *albino* strengthen the case for a common root cause of the visual phenotypes of both mutants and further point to a direct link between RPE melanization and visual acuity.

albino Encodes the 12-transmembrane domain transporter SLC45A2

Through genome scanning with a set of SSLP markers (Geisler et al., 2007), we rough mapped the *alb*^{b4} locus to an interval between the markers z4492 and z4425, about 36–39 cM from the top of chromosome 21 (Figure 3A). By analyzing all annotated genes present in this genomic interval, we identified the 12-transmembrane domain transporter Slc45a2 as a probable candidate, which is also the causative disease gene of OCA4, has been implicated in human skin color variation and has been characterized as affected in the medaka *b* mutant (Fukamachi et al., 2001). The entire coding sequence localized to BAC CH211-71C16 (accession CR749169; Figure 3A). We sequenced the cDNA transcripts of *alb*^{b4} along with their wild-type siblings and identified a G to T transversion in exon 6, which leads to a premature stop codon after AA 461. Further analysis of strong alleles also revealed a nonsense mutation in *alb*^{ti20e} at AA 423 and a deletion of exon 6 in *alb*^{tnr52} causing a stop codon at AA 414 at the end of exon 5 (Figure 3A, C).

In the hypomorphic allele *alb*^{tm83a}, an in-frame deletion removing S62 was detected, as well as two missense mutations causing a G61R and a Q516R replacement, in the alleles *alb*^{ti225} and *alb*^{tnr39}, respectively. The missense mutation, *alb*^{ti225}, displays a glycine to arginine change at amino acid 61, thereby placing a much larger basic side chain directly next to a conserved serine. This mutation causes a strong phenotype, which might be explained by its interfering in interactions between the intravesicular chains that form an end of the transporter, this in turn might drastically perturb the protein's transporting function. To better visualize the location of the lesions in the various *alb* alleles, we used the known structure of the glycerol-3-phosphate transporter from *Escherichia coli*

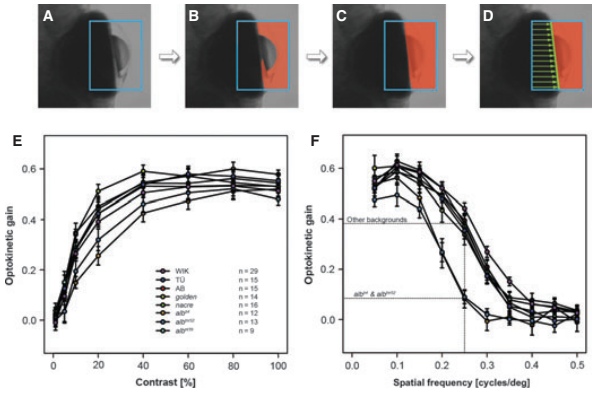

Figure 2. *alb* mutants display reduced visual ability. Schematic representation of the algorithm for detection of eye orientation (exemplified for the right eye). (A) a rectangle is drawn around the lens of the eye, (B) the area within the rectangle is thresholded to extract the brightest part, (C) the convex hull is drawn around the detected area, and (D) starting from the left side, the program searches for an approximately vertical edge, which corresponds to the rim of the right eye. In total, eight different strains were analyzed: three wild-type backgrounds WIK, TU, AB as well as homozygous mutants *nacre* (*mitfa*$^{-/-}$), *golden* (*slc24a5*$^{-/-}$), *albino*^{b4}, *albino*^{tnr52}, and *albino*^{tnr39}. Average temporal-to-nasal gain of the right eye of adult fish from the listed backgrounds measured with increasing contrast (E) and spatial frequency (F) of the optokinetic stimulation. Dotted lines emphasize the more than twofold difference in optokinetic gain between *albino* stops and other backgrounds.

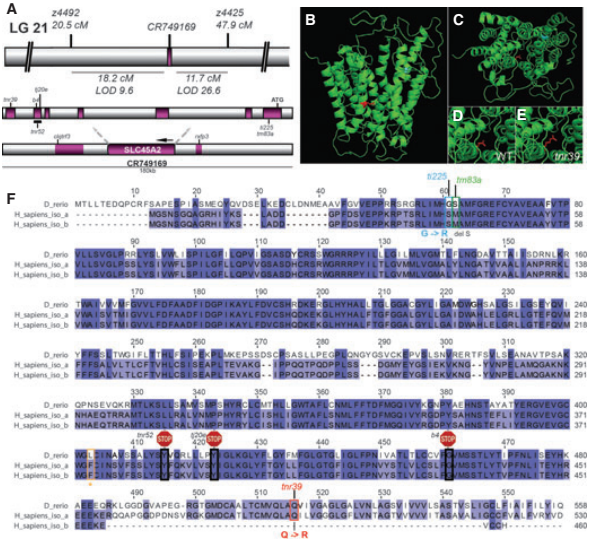

Figure 3. Mapping and positional cloning of the *alb* mutant reveal mutations in the solute carrier Slc45a2. The *alb*^{b4}, mutation was mapped to linkage group 21 using the presented microsatellite markers (above), which gave a predicted interval (below) of about 30 cM. The BAC CR74969 lies within this interval and contains all seven exons of the coding sequence of Slc45a2. Two additional transcripts, *clqtrf3* and *rxfp3*, are also contained within the BAC. The positions of the identified lesions of the *albino* mutants are displayed in reference to their positions among the exons. The deletion of exon 6 in *alb*^{tnr52} is represented by the black bar (A). The modeled 3D ribbon structure is shown in two orientations, and the missense mutations *alb*^{tnr39} (red) and *alb*^{ti225} (blue) are mapped onto the structure (B). A blow up looking through the central pore clearly displays how the side chain of R^{516}, in *alb*^{tnr39}, projects into the center of the pore (C, E) in contrast to Q^{516} in the wild type (D). The protein homology of *Danio rerio* as compared to the two known human isoforms is shown with each identified lesion mapped, respectively (F).

(1pW4_A) as a template (probability of true template 99.95%, E-value < 1.1e−24) to model the three-dimensional structure of SLC45A2 (Figure 3B). All 12-transmembrane domains fold in to form an almost pore-like structure. Interestingly, the three hypomorphic missense alleles (*alb*^{ti225}, *alb*^{tm83a}, and *alb*^{tnr39}) all show lesions in these transmembrane domains (Figure 3B, F). The position of all alleles as well as an alignment with the two known human isoforms is displayed in Figure 3F.

To further confirm that the identified lesions in *slc45a2* are causative for the *alb* phenotype, we intended to rescue the phenotype through BAC injections at the one cell stage. The entire *slc45a2* coding sequence is contained by the BAC along with two other genes, *clqtrf3* and *rxfp3*. Following injection, we identified several darkly pigmented melanophores in larval fish (Figure 4A, B). This indicates that the BAC contains the complete coding sequence of the responsible gene but also all the regulatory elements required to drive the gene's expression in the body melanophores.

Even though BAC injection was able to rescue *alb* melanophores in a mosaic fashion to a melanization level indistinguishable from wild type, there still remained at least two other complete coding sequences on the BAC. We therefore isolated and injected zebra fish *slc45a2* RNA that resulted in rescue of melanization of both melanophore and RPE by 48 hpf (Figure 4C). Next, we were interested whether human SLC45A2 RNA would also be able to rescue the zebra fish *albino* mutant. The 72 hpf larvae injected with human SLC45A2 RNA show a weak but distinguishable melanization (Figure 4D, E).

Furthermore, we then knocked down the *slc45a2* function through morpholino injection and noted a dose-dependent reduction in the melanophores' ability to pigment both RPE and NC-derived melanophores (Figure 4F–I).

Expression of *slc45a2* is restricted to melanophores

We carried out whole-mount in situ hybridization with *slc45a2* riboprobe on wild-type and *nacre* (*mitfa*$^{-/-}$) embryos at 24 and 48 hpf. In wild-type larvae, staining can be seen in the melanophores of the RPE as well as the melanophores of the migrating NC (Figure 4J, K). In *nacre* embryos, which lack all NC-derived melanophores but where the melanophores of the RPE and the other

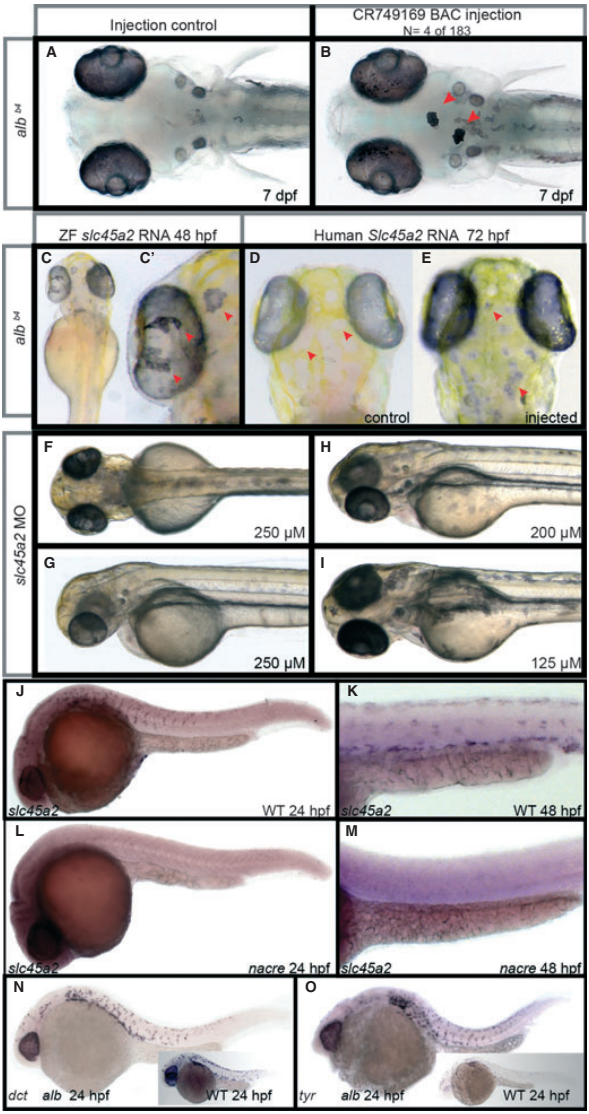

Figure 4. Rescue of melanocyte melanization, morpholino knockdown, and expression of *slc45a2* and melanoblast markers in *albino* mutants. BAC CR749169 injection shows complete rescue of melanophores (red arrows) on the dorsal aspect of the head (A, B). Injection of zebra fish wild-type *slc45a2* mRNA leads to melanization of melanophores of both the neural crest and retinal epithelium (RPE; red arrows; C and C'), while mRNA injection of human *Slc45a2* leads to weak melanization (red arrows D, E). Morpholino knockdown of the *slc45a2* transcript abolishes almost all melanin synthesis at a concentration of 250 µM, shown here at two different imaging angles (F, G), but some residual pale melanophores can still be seen. At lower morpholino concentrations, the melanophore intensity increases (H, I). Expression of *slc45a2* is in cells typical of melanoblasts of the migrating neural crest (NC) and RPE at 24 hpf (J) and still remains in melanophores of PTU-treated wild-type larvae at 48 hpf (K). Expression is abolished in the *nacre* mutant at both 24 and 48 hpf in NC-derived but not in RPE melanoblasts (L–M). Melanoblasts are otherwise present in *albino* mutants as the melanoblast-specific markers *dct* and *tyr* are still expressed at similar levels as in wild type (N, O).

chromatophore types are present, the expression of *slc45a2* in the NC–derived melanophores is abolished and no other cell type of the trunk expresses *slc45a2*, whereas expression remains in the RPE (Figure 4L, M). This shows that *slc45a2* is expressed in no other NC-derived tissue.

We were unable to identify multiple isoforms of *slc45a2*, leaving the most likely explanation for the

separate regulation of *slc45a2* in RPE and NC melanophores to be the result of the paralogs *mitfb* and *mitfa,* respectively. It would be of interest to further investigate whether in zebra fish, the expression in these cell types is mediated by two distinct promoter sequences, as has previously been shown in medaka (Fukamachi et al., 2008; Shimada et al., 2002) .

To confirm the presence of melanoblasts in *alb*^{b4}, the expression patterns of the melanoblast markers *dct* and *tyr* were investigated by whole-mount in situ hybridization. This experiment shows that in *alb*, NC-derived melanoblasts are present and distributed normally. The presence of melanophores lacking visible pigmentation persists in fully developed fish and mutant fish exhibit the typical zebra fish striping pattern, indicating that the basic cellular differentiation of the melanophores is normal but their ability to properly synthesize melanin is impaired (Figure 4N, O). Based on these data, we conclude that the function of Slc45a2 is specific to the melanophores and cells of the RPE.

Slc45a2 is vital for melanosome function and maturation but is not required for melanosome stability

We investigated the melanosomes of *alb* mutants at the ultrastructural morphological level. We chose to analyze the melanosomes of the RPE because of its compact nature and because the packing of melanosomes around the photoreceptor membranes allowed for a robust comparison between different mutants. In 3–4 dpf wild-type larvae, the melanosomes of the RPE have formed fully pigmented stage IV vesicles, which are completely filled with dense black melanin (Figure 5A–C). When sectioned and visualized by EM, the cylinder-shaped melanosomes appear for the most part transversely cut as round circles with some small chipping to their brittle melanin resulting in white gaps.

alb^{b4} mutant RPE forms vesicles resembling melanosome stages I–II in a slightly reduced number as compared to wild type with a slightly higher amount of variability in their size. These melanosomes appear almost empty; however, a very small amount of melanin, which is predominantly localized to the central regions of the vesicle, can be detected (Figure 5A–F). This is also obtained in the analysis of another premature stop allele *alb*^{ti20e} (Figure 5I). The stage II–III melanosomes of the weak *alb*^{ti225} allele contain slightly more melanin than *alb*^{b4}, but their pigment is also pale when compared to wild type (Figure 5G). The amount of melanization of the melanosomes increases in *alb*$^{b4/tnr39}$ with the central region becoming more densely filled and smaller circular satellite positions typical of stage III melanosomes also becoming melanized (Figure 5J). The amount of melanin production continues to increase in the stage III–IV melanosomes of the weaker *alb* hypomorphs but even the melanosomes of *alb*$^{b4/tm83a}$, the weakest *alb* allelic combination, still form highly irregularly sized and shaped melanosomes with reduced melanin accumulations (Figure 5H).

We also found that the *golden* (*slc24a5*) mutant exhibits weaker melanization with reduced melanosomes as previously described (Lamason et al., 2005). However, when compared to *golden* melanosomes (Figure 5K–M), all *alb* alleles show less pigmentation and higher variability, as well as lack of the regular structural characteristics of the late stages of melanosome maturation (stage III–IV).

Formation of melanosomes is tyrosinase dependent

To compare the melanosome morphology of *albino* to a tyrosinase-negative melanosome, we also examined the zebra fish *tyrosinase* mutant *sandy.* In contrast to *golden* and *albino*, the RPE cells of *sandy* mutants fail to form stage I melanosomes as well as any obvious lysosome- or melanosome-like vesicles (Figure 5N–P). In *sandy*, the photoreceptor membranes are also not developed properly at this time point. As tyrosinase's function is dependent on copper ions (Matoba et al., 2006), the copper chelator PTU is a frequently used chemical to inhibit the melanization of melanophores. Upon ultrastructural analysis of PTU-treated fish, we found that some stage I melanosomes are present but appear to be highly irregular and seemed to be in the process of collapsing (Figure 5Q–S). The photoreceptor membranes resembled those found in *sandy* mutants. Taken together, these results indicate that the presence of a functional tyrosinase is required for the formation and/or maintenance of melanosomes.

Knockdown of V-ATPase V1H1 subunit causes lightening of melanocytes in wild type and rescues melanization in albino

The V-ATPase complex had previously been described to play a role in the development and pigmentation of the zebra fish eye but we wanted to determine whether it was directly playing a role in melanosome biogenesis (Navarro et al., 2008; Nuckels et al., 2009). First, we assessed the function of *atp6v1h* by means of morpholino knockdown in wild-type fish. The V_1H protein has been shown to play a crucial role in the catalytic activity of the proton pump but does not play a role in the V_1 assembly (Nishi and Forgac, 2002). In this way, using a morpholino knockdown of the *atp6v1h* transcript, we are able to specifically inhibit the proton pump through genetic means without having an effect on the assembly of the V_1 complex. After injection, melanocytes initially appear paler and then begin to round up by 48 hpf when compared to controls (Figure 6A, B). Knockdown of *atp6v1h* carried out in the hypomorphic *alb*^{tnr39} allele showed noticeable darkening of the melanocytes at 48 hpf as well as the rounding up phenotype also seen in wild-type background. The null allele of *albino*^{b4} did not show a noticeable increase in melanin at 48 hpf (data not shown), but there was an obvious increase in melaniza-

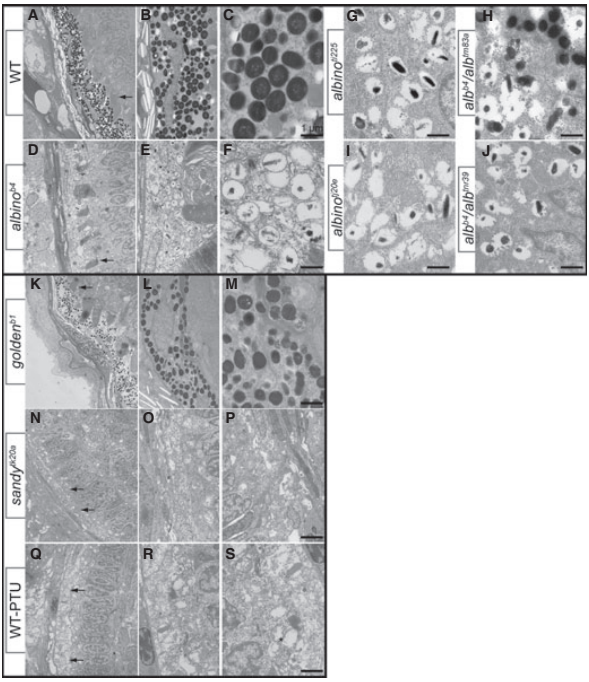

Figure 5. Melanosome ultrastructure reveals melanosomes of normal size and shape but dramatically reduced melanization in *alb* mutants. The melanosomes of the retinal epithelium (RPE) were investigated at 3.5 dpf on the ultrastructural level (A–S). Wild-type melanosomes of the RPE are tightly packed around the developing photoreceptor membranes and filled with dark electron dense melanin (A–C). The melanosomes of the *alb*^{b4} mutant are present in normal size and number but lack almost all melanin (D–F), and the photoreceptor membranes are of normal nature (arrows). Other *albino* alleles show varying degrees of melanin inside their melanosomes (G–J). For comparison, the *golden* mutant displays melanosomes of diminished melanin content (K–M). The *sandy* mutant completely lacks melanosomes and presents only very few vesicle-like structures (N–P) with abnormal developing photoreceptor membranes (arrows). The *sandy* phenotype is phenocopied through PTU treatment with some premelanosome-like vesicles (star; Q–S).

tion by 4 dpf when compared to injected controls (Figure 6E–H). By specifically knocking down the *atp6v1h* subunit, we show that it is possible to rescue the melanin producing capacity of both *albino* hypomorphs and null mutants.

V-ATPase inhibition through bafilomycin rescues melanization in albino mutants

To further confirm that the rescue of *albino* melanin production was specifically due to only the inactivation of the V_1 proton pump portion of the V-ATPase complex, we inhibited the pump through use of bafilomycin. Melanosomes are lysosome-related vesicles and are acidified through the activity of V-ATPases. These organelle acidifiers can be selectively inhibited through the application of bafilomycin that has previously been shown for zebra fish lysosomes (Peri and Nüsslein-Volhard, 2008) to increase the vesicle pH of their targets (Smith et al., 2004). We applied bafilomycin to 24 hpf developing *alb*^{b4} embryos over night at 25°C and found a dramatic melanization of both the NC-derived melanophores as well as the RPE (Figure 6J). Ultrastructural analysis of bafilomycin-treated embryos shows that the darkening seen in these embryos is indeed directly due to the increase in melanin within the melanosomes (Figure 6K). Therefore, we conclude that the melanosomes of *albino* fish are capable of producing melanin but lack the proper pH to do so. This suggests that the function of Slc45a2 is required for the expulsion of protons from the melanosomes in agreement with its previously proposed role as a proton exchanger. By increasing the pH of the melanosome, we suggest that the optimal pH of tyrosinase is approached and melanin production is resumed.

Discussion

The genetics of pigmentation and furthermore skin and coat color variation are highly complex and often involve multiple loci. A number of polymorphisms in the tyrosinase gene have been identified in humans but have failed to be convincingly associated with specific skin color variants. In recent years, the variation in human skin color has been shown to be tightly associated with the solute carriers SLC24A5 and SLC45A2. In the case of Slc45a2, the amino acid variation L374F can be found almost solely in people of European decent, while another polymorphism, E272K is more predominant in Japanese and Chinese populations. Positional cloning of the zebra fish

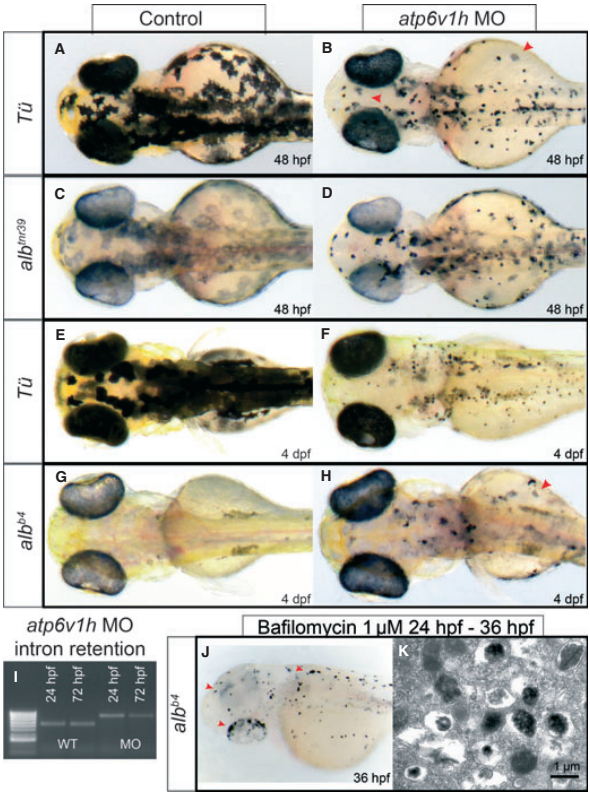

Figure 6. Knockdown or inhibition of V-ATPase complex causes rescue of *albino* melanization. Morpholino knockdown of *atp6v1h* was carried out in *Tü*, *alb*^{tnr39}, and *alb*^{b4} alleles and compared to injected controls. At 48 hpf, injected Tü fish have lighter melanocytes (arrowhead) that eventually round up and appear as small dots (A, B). The *alb*^{tnr39} shows a darkening of the melanocytes at 48 hpf as well as the rounding up seen in wild-type morphants (C, D). *atp6v1h* morphant phenotype persists at 4 dpf in wild-type larvae (E, F), and a noticeable darkening of melanocytes in the *alb*^{b4} morphant larvae can also be detected (arrowhead) before the rounding up of the melanocytes (G, H). *atpv1h1* morpholino specificity is demonstrated via intron retention at both 24 and 72 hpf. Treatment with bafilomycin at 24 hpf causes a dramatic increase in melanin in melanophores of both the body as well as the retinal epithelium (arrowheads) (H). Ultrastructural analysis of bafilomycin-treated embryos shows an increase in the content of melanin, which is found localized to the interior of the melanosomes (K).

golden mutant revealed the affected gene to encode the potassium-dependent sodium–calcium exchanger SLC24A5, leading to a reduction in melanosome size, number, and melanin density.

Here, we present evidence that a second solute carrier previously implicated in skin color variation, *slc45a2*, is the causative gene for the zebra fish *albino* phenotype. Three alleles exhibiting a premature stop codon (i.e. *alb*^{b4}, *alb*^{ti20e}, *alb*^{tnr52}) consistently show phenotypes that are indistinguishable from one another both as living fish and upon evaluation of the ultrastructural morphology of their melanosomes. *alb* nonsense alleles present a reduction in melanin density of the melanosomes themselves where the melanosomes of these *alb* alleles are highly similar to stage I melanosomes. Both also retain the ability to produce melanin albeit in the case of the *alb* stop alleles at very low levels.

This is in contrast to the more or less complete lack of melanosomes that we have observed in the tyrosinase mutant *sandy*. Furthermore, after treatment with PTU, which chelates copper ions required for the proper folding of tyrosinase protein, we also observe a similar drastic reduction in melanosomes. Taken together, this indicates that the formation and/or stability of the melanosomes is dependent on the transmembrane tyrosinase's presence but probably not on its function. The *sandy* mutant has been described to have a delayed ability to adapt to bright light when challenged with long periods of darkness during the day (Page-McCaw et al., 2004). This failure was thought to be localized to the retinal neural network, postsynaptic to the photoreceptors. Our ultrastructural analysis of *sandy* has shown an almost complete lack of melanosomes or vesicle-like structures in the RPE as well as improperly developed photoreceptor membranes. It has been proposed that L-DOPA, which is normally localized in the melanosomes, is also secreted from the RPE and is further processed to dopamine and acts in a paracrine fashion along with melatonin to modulate light

adaptation, providing a mechanism for the effect of *sandy*. Our observations suggest morphological changes in the RPE as an alternative mechanism that may at least contribute to this effect.

Through our analysis of various alleles, we show that modification of Slc45a2 can cause an intermediate reduction in melanosome melanization. The *alb*$^{b4/tnr39}$ allele replaces a glycine with a much larger and positively charged arginine, which based on structural predictions, projects into the channel. This extended side chain could then be in a position to inhibit the passage of the transporter's normal substrate.

V-ATPases are made up of two major subunits the V_1 and the V_0, which can be coupled and decoupled from each other. The V_0 is initially found in the vesicle membrane along with the associated protein AP1 where it plays a role in the sorting and fusing of vesicles. At a downstream time point, the V_1 can be coupled to the V_0 turning the entire complex into an ATP-dependent proton pump (Figure 7A). By means of our *atp6v1h1* knockdown, we also show that the V-ATPase is specifically responsible for the acidification of melanosomes and by means of rescue of the *albino* phenotype interaction with *slc45a2*. The *catastrophe* mutant, caused by mutations at the *atp6vo0d1* locus, has previously been shown to have significant ultrastructural melanosomal defects as well as to also be particularly sensitive to copper deprivation (Madsen and Gitlin, 2008).

The function of Slc45a2 has been proposed to be linked to the production of melanin in either of two different roles: first, the proper trafficking and sorting of tyrosinase to the melanosome, and second, the maintenance of a specific pH within the melanosomes themselves (Graf et al., 2005; Lucotte et al., 2010). Our findings support the second possibility.

The differentiation of melanosomes may require a dynamic range of pH and ionic conditions at different time points. Initially, a low pH may be required for the proper sorting required to form stage I melanosomes. As the melanosomes mature, a change in the pH and ionic conditions may be required in order for the optimal activity of tyrosinase to be achieved (Figure 7B). We have observed that the melanosomes of all *albino* alleles have in principle a normal structure, making a role for Slc45A2 in membrane trafficking less likely, but with varying degrees of hypopigmentation. Also, Konantz et al. (in preparation) have shown that Slc45a2 is specifically localized to the melanosomes. The activity of tyrosinase is known to be dependent on the secretion of H^+ from the melanosomes, so that varying the internal pH of the vesicle would have a direct effect on enzymatic activity. While the optimal pH of tyrosinase is 7.3, an acidic environment would render it almost inactive (Smith et al., 2004). It has been demonstrated that the activity of tyrosinase of light-colored melanocytes can be increased through the application of compounds such as bafilomycin, which block the activity of the organelle acidifier, V-

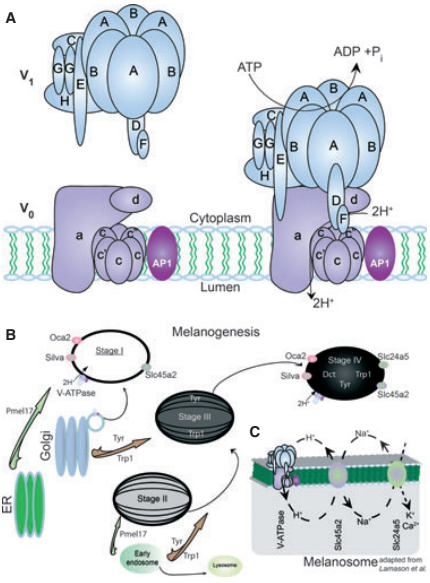

Figure 7. An overview of V-ATPase V_1, V_0 coupling, and melanosomal homeostasis. Initially, the V_0 subunit of the V-ATPase is found in the vesicle membrane where it plays a role in vesicle fusions and sorting. At a later point in vesicle maturation, it can reversibly bind the V_1 subunit. Together, both subunits form the complete V-ATPase complex capable of ATP-dependent proton pumping across the membrane (A). Melanosomes are thought to arise either directly from the ER itself or through a more complex post-Golgi, endocytic route. The maturing melanosomes are continually fused with vesicles as they pass stage I and stage II premelanosomes and begin to display the characteristic Pmel17 fibrils. As tyrosinase and Tyrp1 are added and becomes active in stage III melanosomes, the production of melanin is commenced until a fully mature and black granule is formed (B). Maintenance of ionic and pH conditions can be achieved through epistatic interactions on the melanosome membrane. By acting as a Na^+/H^+ exchanger, Slc45a2 plays both a role in maintaining the proper Ca^{2+} flux passing through Slc24a5 and in maintaining an optimal pH for the activity of tyrosinase (C).

ATPase, thereby raising the pH of the melanosomes (Smith et al., 2004). We show that increasing the pH of the melanosome through the use of bafilomycin or through knockdown of *atp6v1h* partially rescues the *albino* phenotype, suggesting that the functional role of Slc45a2 is related to the maintenance of melanosome pH. The Na^+/H^+ exchanger Slc45a2 removes H^+ from the melanosome by exchange with Na^+, which is then cycled back out of the melanosome by the cation exchanger Slc24a5 (Figure 7C). In this way, Slc45a2 plays a crucial role in the pH and ionic homeostasis within the melanosome. Our ultrastructural analysis of both *sandy*- and PTU-treated embryos highlights the importance of both

tryosinase and the copper that it requires to fold properly in melanosomal integrity. A reduction in the efficiency of Slc45a2 as an exchanger as seen in the *albino*^{tnr39} allele is expected to have a quenching effect on the activity of tyrosinase. At the same time, the integrity of the melanosomes is maintained in *albino* mutants avoiding the toxic effects of their disruption seen in *sandy* mutants. In this way, the activity of tyrosinase can be controlled and stabilized within the melanosomes in large part through the function of SLC45A2, which mediates the melanosome pH. A similar effect may be postulated for the European and African variants of the human Slc45a2 ortholog, providing a molecular basis for human skin color variation.

Methods

Zebra fish husbandry

Zebra fish were maintained as described (Nüsslein-Volhard, 2002).

Adult OKR

Optokinetic response of adult *alb*^{b4}, *alb*^{tnr52}, *alb*^{tnr39}, and other backgrounds zebra fish was measured as previously described (Mueller and Neuhauss, 2010). To enable automatic detection of the orientation of the unpigmented *alb*^{b4} eyes, the algorithm of the software had to be slightly modified (Figure 2). In addition, we used the projector (PLV-Z3000, SANYO Electric Co. Ltd., Osaka, Japan) to achieve better black values, higher contrast, and higher spatial resolution.

We measured temporal-to-nasal OKR slow-phase velocity of the right eye of adult fish in response to changing contrast or spatial frequency of the optokinetic stimulation. Angular velocity of the stimulation was left constant at 12 degree/s. In case of changing contrast, spatial frequency was held constant at 0.1 cycles/degree, and in case of changing spatial frequency, contrast was held constant at 70%.

Statistical analysis was performed using PASW Statistics 18 (SPSS Inc., Chicago, IL, USA). We used repeated measures ANOVAs with the contrast (repeated measures ANOVA, $F_{2,34} = 0.741$, $P = 0.484$) or the spatial frequency as within-subjects effect and the genotype as between-subjects effect (repeated measures ANOVA, $F_{2,34} = 4.840$, $P = 0.014$). Where appropriate, Dunnett's one-tailed post hoc test was used to compare the means of *alb*^{b4} and *alb*^{tnr39} fish against the wild-type control group (WIK).

Mapping and cloning of albino

Mapping of *albino* was carried out as described in Geisler et al. (2007). To validate candidate genes, total RNA was prepared from both wild-type and mutant embryos or clipped fins using TRIzol Reagent (Invitrogen, Darmstadt, Germany) with an added chloroform extraction before precipitation. For separation of phases, phase lock tubes (PLG 1.5 ml Heavy; Eppendorf, Hamburg, Germany) were used according to the manufacturer's protocol. Reverse transcription was performed using total RNA, oligo(dT) primer, and Superscript III reverse transcriptase (Invitrogen) according to standard procedures.

3D modeling using HHPRED

3D modeling was performed using HHPRED (http://toolkit.tuebingen.mpg.de/hhpred) with standard parameters. Briefly, eight iterations of PSI-BLAST were performed using the amino acid sequence of SLC45A2 from *Danio rerio* from the pdb70_24Apr10 database. A local alignment mode was used, and secondary structure was scored. The highest score was found for glycerol-3-phosphate transporter from *E. coli* (1pW4_A). This structure was used as a template for the 3D modeling. The model was visualized with MacPyMol (The PyMOL Molecular Graphics System, Schrödinger, LLC, New York, NY, USA).

Allele screen

Mutagenesis was performed as described before (Mullins et al., 1994) with the addition of clove oil to minimize stress (Rohner, unpublished). Mutagenesis was performed every week for a total of five times. Female albb4 were then crossed to ENU-treated males, and their progeny were then screened at 72 h for albino-like phenotypes. Those larvae were segregated, raised to adults, and then genotyped based on cDNA.

Morpholino injection

The antisense morpholinos for *slc45a2* and *atp6v1h* are both ATG morpholinos and were obtained from Gene Tools with the following sequences: *slc45a2*_atg:GCTGGTCCTCAGTAAGAAGAGTCAT and *atp6v1h*_atg:ATATTTAAGGAGCTGCTTCCTCTGC as well as the intron retention morpholino *atp6v1h1_2*ret3:CGGGAAGAATGCAATA TTAACCTGA. *atp6v1h1* knockdowns were primarily carried out using the *atp6v1h1_atg* morpholino, but all experiments were also repeated using the *atpv1h1_2ret3* morpholino to demonstrate transcript specificity.

BAC injection

The BAC CH211-71C16 (CR749169) was purified using the Large–Construct Kit (QIAGEN, Hilden, Germany) according to manufacturer's instructions and then injected into the one cell stage at a concentration of 20 ng/μl.

RNA rescue

The zebra fish *slc45a2* cDNA sequence BC154627 was used as a reference to design the following oligos: SLC(zeb)f1 5′-TCT TAC CAT CCA GAA CCA TGA CT-3′ and SLC(zeb)r1 5′-TTG AGG CTT ATT CTG TAC ATC ACA T-3′. The product was ligated into the pCS2^{+} vector. The resulting plasmid was verified by sequencing and was then linearized using NotI, and mRNA was produced using the mMESSAGE mMACHINE® SP6 Kit (Ambion, Kaufungen, Germany). Injections were carried out at the one cell stage at a concentration of 400 ng/μl. Rescue using the human RNA was performed exactly as above but with the following oligos for cloning: SLC(hum)f1-ACG TCA AAT CCA GTT TGA AAC AC and SLC(hum)r1-TCT GAG GTT AGG GTC ATT GTC TC.

In situ hybridization

An RT-PCR-based approach was used to generate probes for in situ hybridization. The PCR was carried out using an antisense primer, containing a T7 promoter sequence on its 5′-end. The PCR product then included the target sequence flanked by the T7 promoter sequence, so that an RNA riboprobe could be synthesized by in vitro transcription of the PCR product using the T7-RNA polymerase (Fermentas). The DNA oligos that were used are as follows: Slc45A2: 5′-tgtttggaagggaattctgc-3′ and 5′-TAATACGACTCACTATAGGcactccaaacatcaccacca-3′ along with 5′-cactccaaacatcaccacca-3′ and 5′-TAATACGACTCACTATAGGtgtttggaagggaattctgc-3′, which allows for the creation of both sense and antisense riboprobes. The *tyr* and *dct* riboprobes were generated using the following oligos: tyr-for-T7: 5′-TAATACGACTCACTATAGGGAGATGGTTTTGGCCAGATTTAGG-3′ tyr-rev: 5′-CAGCTCCTCAGCTCGTCTCT-3′; dct-for-T7: 5′-TAATACGACTCACTATAGGGAGAACATAGCCGGTCTGTTGTCC-3′ dct-rev: 5′-

ACTTCTTCGTCTGGCAGCAT-3′, respectively. Whole-mount in situ hybridization was carried out as previously described (Nüsslein-Volhard, 2002).

Ultrastructure analysis of melanosomes

For ultrastructural analysis by transmission electron microscopy (TEM), larvae were fixed in 4% formaldehyde and 2.5% glutaraldehyde in PBS (pH 7.2) at 4°C overnight. After postfixation with 1% osmium tetroxide, samples were rinsed with water, block stained with 1% uranyl acetate for 1 h on ice, dehydrated in a graded series of ethanol, infiltrated with Epon, and polymerized at 60°C for 48 h. Ultrathin sections stained with uranyl acetate and lead citrate were viewed in a Philips CM10 electron microscope at 60 kV. In addition, toluidine blue–stained Epon sections of 0.5 or 3 μm thickness were prepared for light microscopy.

Bafilomycin treatment

Bafilomycin was dissolved in DMSO according to Peri and Nüsslein-Volhard (2008) and was then applied to embryos in final concentrations ranging from 0.1 μM to 1 mM at 16, 24, 28, and 32 hpf overnight at 25°C to find the most effective condition, which was determined to be 1 μM applied at 16 hpf over night at 25°C.

Acknowledgements

C.D. and R.G. would like to acknowledge Ines Gehring for technical assistance as well as Simon Perathoner and Nicolas Rohner for providing mutagenized fish and Matthew Harris and Mitch Levesque for many enlightening discussions. The authors would also like to thank an anonymous reviewer for helpful comments on this manuscript. This work was supported by the European Commission's 6th Framework Programme (ZF-MODELS project, contract no. LSHG-CT-2003-503496) and 7th Framework Programme (ZF-HEALTH project, grant agreement HEALTH-F4-2010-242048).

Author contribution

C.D. conceived and designed the experiments. C.D., H.S., K.M., A. M., and M.K. performed the experiments. C.D., C.N.V., and R.G. analyzed the data. S.N. contributed reagents/materials/analysis tools. C.D., C.N.V., and R.G. wrote the manuscript.

References

Braasch, I., Schartl, M., and Volff, J.-N. (2007). Evolution of pigment synthesis pathways by gene and genome duplication in fish. BMC Evol. Biol. *7*, 74.

Brockerhoff, S.E., Hurley, J.B., Janssen-Bienhold, U., Neuhauss, S. C., Driever, W., and Dowling, J.E. (1995). A behavioral screen for isolating zebrafish mutants with visual system defects. Proc. Natl Acad. Sci. USA *92*, 10545–10549.

Dell'Angelica, E.C. (2003). Melanosome biogenesis: shedding light on the origin of an obscure organelle. Trends Cell Biol. *13*, 503–506.

Du, J., and Fisher, D.E. (2002). Identification of Aim-1 as the underwhite mouse mutant and its transcriptional regulation by MITF. J. Biol. Chem. *277*, 402–406.

Fernandez, L.P., Milne, R.L., Pita, G., Aviles, J.A., Lazaro, P., Benitez, J., and Ribas, G. (2008). SLC45A2: A novel malignant melanoma-associated gene. Hum. Mutat. *29*, 1161–1167.

Fukamachi, S., Shimada, A., and Shima, A. (2001). Mutations in the gene encoding B, a novel transporter protein, reduce melanin content in medaka. Nat. Genet. *28*, 381–385.

Fukamachi, S., Kinoshita, M., Tsujimura, T., Shimada, A., Oda, S., Shima, A., Meyer, A., Kawamura, S., and Mitani, H. (2008). Rescue from oculocutaneous albinism type 4 using medaka slc45a2 cDNA driven by its own promoter. Genetics *178*, 761–769.

Geisler, R., Rauch, G.-J., Geiger-Rudolph, S. et al. (2007). Large-scale mapping of mutations affecting zebrafish development. BMC Genomics *8*, 11.

Gentleman, R.C., Carey, V.J., Bates, D.M. et al. (2004). Bioconductor: open software development for computational biology and bioinformatics. Genome Biol. *5*, R80.

Graf, J., Hodgson, R., and van Daal, A. (2005). Single nucleotide polymorphisms in the MATP gene are associated with normal human pigmentation variation. Hum. Mutat. *25*, 278–284.

Graf, J., Voisey, J., Hughes, I., and van Daal, A. (2007). Promoter polymorphisms in the MATP (SLC45A2) gene are associated with normal human skin color variation. Hum. Mutat. *28*, 710–717.

Haffter, P., Odenthal, J., Mullins, M. et al. (1996). Mutations affecting pigmentation and shape of the adult zebrafish. Dev. Genes. Evol. *206*, 260–276.

Haug, M.F., Biehlmaier, O., Mueller, K.P., and Neuhauss, S.C. (2010). Visual acuity in larval zebrafish: behavior and histology. Front. Zool. *7*, 8.

He, L., Vasiliou, K., and Nebert, D.W. (2009). Analysis and update of the human solute carrier (SLC) gene superfamily. Hum. Genomics *3*, 195–206.

Hirata, M., Nakamura, K.-I., Kanemaru, T., Shibata, Y., and Kondo, S. (2003). Pigment cell organization in the hypodermis of zebrafish. Dev. Dyn. *227*, 497–503.

Kelsh, R.N., Brand, M., Jiang, Y.J. et al. (1996). Zebrafish pigmentation mutations and the processes of neural crest development. Development *123*, 369–389.

Lamason, R.L., Mohideen, M.-A.P.K., Mest, J.R. et al. (2005). SLC24A5, a putative cation exchanger, affects pigmentation in zebrafish and humans. Science *310*, 1782–1786.

Lister, J.A. (2002). Development of pigment cells in the zebrafish embryo. Microsc. Res. Tech. *58*, 435–441.

Lister, J.A., Robertson, C.P., Lepage, T., Johnson, S.L., and Raible, D.W. (1999). nacre encodes a zebrafish microphthalmia-related protein that regulates neural-crest-derived pigment cell fate. Development *126*, 3757–3767.

Lucotte, G., Mercier, G., Diéterlen, F., and Yuasa, I. (2010). A decreasing gradient of 374F allele frequencies in the skin pigmentation gene SLC45A2, from the north of West Europe to North Africa. Biochem. Genet. *48*, 26–33.

Madsen, E.C., and Gitlin, J.D. (2008). Zebrafish mutants calamity and catastrophe define critical pathways of gene-nutrient interactions in developmental copper metabolism. PLoS Genet. *4*, e1000261.

Matoba, Y., Kumagai, T., Yamamoto, A., Yoshitsu, H., and Sugiyama, M. (2006). Crystallographic evidence that the dinuclear copper center of tyrosinase is flexible during catalysis. J. Biol. Chem. *281*, 8981–8990.

Mueller, K.P., and Neuhauss, S.C.F. (2010). Quantitative measurements of the optokinetic response in adult fish. J. Neurosci. Methods *186*, 29–34.

Mullins, M., Hammerschmidt, M., Haffter, P., and NussleinVolhard, C. (1994). Large-scale mutagenesis in the zebrafish – in search of genes-controlling development in a vertebrate. Curr. Biol. *4*, 189–202.

Navarro, R.E., Ramos-Balderas, J.L., Guerrero, I., Pelcastre, V., and Maldonado, E. (2008). Pigment dilution mutants from fish models with connection to lysosome-related organelles and vesicular traffic genes. Zebrafish *5*, 309–318.

Newton, J.M., Cohen-Barak, O., Hagiwara, N., Gardner, J.M., Davisson, M.T., King, R.A., and Brilliant, M.H. (2001). Mutations

in the human orthologue of the mouse underwhite gene (uw) underlie a new form of oculocutaneous albinism, OCA4. Am. J. Hum. Genet. *69*, 981–988.

Nishi, T., and Forgac, M. (2002). The vacuolar (H+)-ATPases–nature's most versatile proton pumps. Nat. Rev. Mol. Cell Biol. *3*, 94–103.

Nuckels, R.J., Ng, A., Darland, T., and Gross, J.M. (2009). The vacuolar-ATPase complex regulates retinoblast proliferation and survival, photoreceptor morphogenesis, and pigmentation in the zebrafish eye. Invest. Ophthalmol. Vis. Sci. *50*, 893–905.

Nüsslein-Volhard, C., and Dahm, R. (2002). Zebrafish: A Practical Approach. (New York: Oxford University Press).

Page-McCaw, P.S., Chung, S.C., Muto, A., Roeser, T., Staub, W., Finger-Baier, K.C., Korenbrot, J.I., and Baier, H. (2004). Retinal network adaptation to bright light requires tyrosinase. Nat. Neurosci. *7*, 1329–1336.

Peri, F., and Nüsslein-Volhard, C. (2008). Live imaging of neuronal degradation by microglia reveals a role for v0-ATPase a1 in phagosomal fusion in vivo. Cell *133*, 916–927.

Raposo, G., and Marks, M.S. (2007). Melanosomes–dark organelles enlighten endosomal membrane transport. Nat. Rev. Mol. Cell Biol. *8*, 786–797.

Rees, J.L. (2003). Genetics of hair and skin color. Annu. Rev. Genet. *37*, 67–90.

Reischauer, S., Levesque, M.P., Nusslein-Volhard, C., and Sonawane, M. (2009). Lgl2 executes its function as a tumor suppressor by regulating ErbB signaling in the zebrafish epidermis. PLoS Genet. *5*, e1000720.

Sabeti, P.C., Varilly, P., Fry, B. et al. (2007). Genome-wide detection and characterization of positive selection in human populations. Nature *449*, 913–918.

Shimada, A., Fukamachi, S., Wakamatsu, Y., Ozato, K., and Shima, A. (2002). Induction and characterization of mutations at the b locus of the medaka, Oryzias latipes. Zool. Sci. *19*, 411–417.

Smith, D.R., Spaulding, D.T., Glenn, H.M., and Fuller, B.B. (2004). The relationship between Na(+)/H(+) exchanger expression and tyrosinase activity in human melanocytes. Exp. Cell Res. *298*, 521–534.

Streisinger, G., Singer, F., Walker, C., Knauber, D., and Dower, N. (1986). Segregation analyses and gene-centromere distances in zebrafish. Genetics *112*, 311–319.

Sturm, R.A., Teasdale, R.D., and Box, N.F. (2001). Human pigmentation genes: identification, structure and consequences of polymorphic variation. Gene *277*, 49–62.

Summers, C.G. (1996). Vision in albinism. Trans. Am. Ophthalmol. Soc. *94*, 1095–1155.

Supporting information

Additional Supporting Information may be found in the online version of this article:

Figure S1. Comparison of the phenotype of *alb*^{b4}/*alb*^{tm83a} transheterozygotes (A) and in late juveniles (12 mm) (B) with the phenotype of *alb*^{tm83a} homozygotes (C–D). In addition the adult *alb*^{tnr52} is shown (E).

Figure S2. Sequencing traces of all presented allele are presented here (A–F).

Publication 4:

Dooley, C.M., Mongera, A., Walderich, B., and Nüsslein-Volhard, C. (2013). **On the embryonic origin of adult melanophores: the role of ErbB and Kit signalling in establishing melanophore stem cells in zebrafish.** *Development* 140(5):1003-13

For this paper, which demonstrates the presence of a melanophore stem cell niche in association with the peripheral nervous system, I performed laser ablation of dorsal root ganglia in 3 dpf zebrafish larvae and showed that the absence of these reiterated structures leads to defects in adult pigment pattern formation.

Development 140, 1003-1013 (2013) doi:10.1242/dev.087007

On the embryonic origin of adult melanophores: the role of ErbB and Kit signalling in establishing melanophore stem cells in zebrafish

Christopher M. Dooley[1,2], Alessandro Mongera[1], Brigitte Walderich[1] and Christiane Nüsslein-Volhard[1,*]

SUMMARY

Pigment cells in vertebrates are derived from the neural crest (NC), a pluripotent and migratory embryonic cell population. In fishes, larval melanophores develop during embryogenesis directly from NC cells migrating along dorsolateral and ventromedial paths. The embryonic origin of the melanophores that emerge during juvenile development in the skin to contribute to the striking colour patterns of adult fishes remains elusive. We have identified a small set of melanophore progenitor cells (MPs) in the zebrafish (*Danio rerio*, Cyprinidae) that is established within the first 2 days of embryonic development in close association with the segmentally reiterated dorsal root ganglia (DRGs). Lineage analysis and 4D *in vivo* imaging indicate that progeny of these embryonic MPs spread segmentally, giving rise to the melanophores that create the adult melanophore stripes. Upon depletion of larval melanophores by morpholino knockdown of Mitfa, the embryonic MPs are prematurely activated; their progeny migrate along the spinal nerves restoring the larval pattern and giving rise to postembryonic MPs associated with the spinal nerves. Mutational or chemical inhibition of ErbB receptors blocks all early NC migration along the ventromedial path, causing a loss of DRGs and embryonic MPs. We show that the *sparse like* (*slk*) mutant lacks larval and metamorphic melanophores and identify *kit ligand a* (*kitlga*) as the underlying gene. Our data suggest that *kitlga* is required for the establishment or survival of embryonic MPs. We propose a model in which DRGs provide a niche for the stem cells of adult melanophores.

KEY WORDS: Kit ligand a, ErbB, Dorsal root ganglia, Melanophore stem cells

INTRODUCTION

Colour patterns are prominent features of many animals; they evolve rapidly and vary between closely related species, providing an important target for both natural and sexual selection (Darwin, 1871; Roulin, 2004; Hoekstra et al., 2006; Protas and Patel, 2008).

In vertebrates, all pigment cells of the body are derived from the neural crest (NC) except the pigmented retinal epithelium. The NC is an embryonic population of pluripotent migratory cells that contribute to a variety of organs and tissues. The NC is largely responsible for the emergence of many of the vertebrate-specific characteristics involved in head and body shape, protection and pattern diversity that evolved in this phylum over 550 million years (Gans and Northcutt, 1983).

The pigment patterns observed in birds and mammals are due to variations in melanin synthesis within a single type of chromatophore, the melanocyte. However, anamniotes and reptiles display several chromatophore types. In zebrafish, black melanophores, yellow xanthophores and silvery iridophores are arranged in distinct patterns in the hypodermis during larval and adult stages.

Although the early melanophores contributing to the larval pattern can be traced back directly to the migrating NC, the ontogeny of the melanophores that compose the continuously growing and expanding adult pattern during metamorphosis weeks later remains unclear. As the NC is no longer present, these cells must arise from hypothetical NC-derived stem cells that are set aside in the embryo (Rawls et al., 2001; Parichy et al., 2003; Yang and Johnson, 2006; Budi et al., 2011). These cells are quiescent during embryonic development but start to proliferate during juvenile development (Quigley et al., 2004; Mellgren and Johnson, 2004; Hultman et al., 2009).

Several zebrafish mutants in which melanophores are reduced or completely absent have been collected (Streisinger et al., 1986; Haffter et al., 1996; Kelsh et al., 1996; Lister et al., 1999). Mutations in the *colourless* (*cls*) gene, which encodes the HMG-box transcription factor Sox10, eliminate all three types of chromatophores as well as glia and the peripheral nervous system (Kelsh et al., 1996; Dutton et al., 2001). Mutations in genes such as *nacre* (*nac*; *mitfa* – Zebrafish Information Network), *sparse* (*spa*; *kita* – Zebrafish Information Network) and *sparse-like* (*slk*) specifically affect melanophores of the body whereas the other chromatophore types are present (Kelsh et al., 1996; Haffter et al., 1996; Lister et al., 1999). *mitfa* mutant fish lack all body melanophores throughout their lives. *mitfa* encodes a helix-loop-helix transcription factor (Elworthy et al., 2003). *mitfa* is expressed in melanoblasts at all stages of migration and differentiation (Lister et al., 1999). Interestingly, *mitfa* morphants, although completely deficient in early larval stripe formation, do recover and adopt normal larval and adult pigmentation (Mellgren and Johnson, 2004). This finding and evidence from temperature-sensitive *mitfa* alleles indicate that *mitfa* is not required for establishing or maintaining melanophore stem cells (Johnson et al., 2011). In juvenile fish, a population of postembryonic MPs expressing *mitfa* was described in the myotomes and associated with the Schwann cells of the spinal nerves and the DRGs (Budi et al., 2011). Although the proliferation and migration of these MPs ultimately gives rise to pigmented melanophores in the skin, the embryonic origin of postembryonic MPs remains unknown.

[1]Max-Planck-Institut für Entwicklungsbiologie, Spemannstr 35, 72076 Tübingen, Germany. [2]Wellcome Trust Sanger Institute, Wellcome Trust Genome Campus, Hinxton, Cambridge, CB10 1HH, UK.

*Author for correspondence (christiane.nuesslein-volhard@tuebingen.mpg.de)

Accepted 19 December 2012

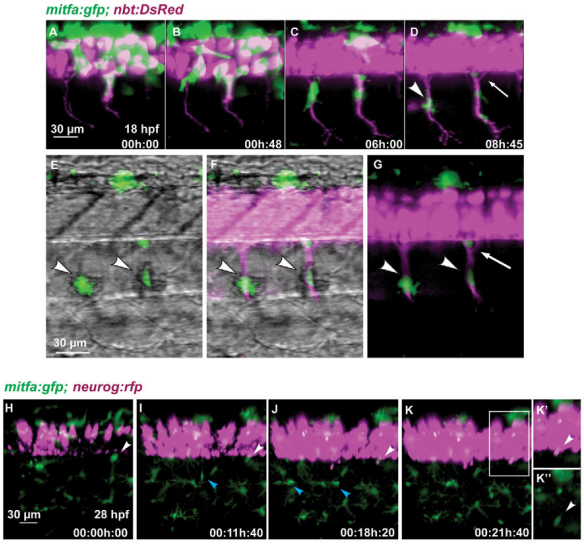

Fig. 1. Melanoblasts migrate along the motor neurons. (**A**-**G**) Time-lapse confocal imaging of a *Tg(mitfa:gfp;nbt:DsRed)* zebrafish embryo. Medially migrating GFP-positive cells (arrowhead in D) migrate along ventrally extending primary motor axons (DsRed) starting at 18 hpf. A portion of the area in D is shown in G, and in E,F with brightfield illumination. Arrowheads in E-G indicate melanoblasts melanising *in situ*. A GFP-positive cell remains at a ventral position of the neural tube (arrow in D,G). (**H-K″**) *Tg(mitfa:gfp;-8.4neurog1:nrfp)* embryo imaged starting at 28 hpf over a period of 22 hours. A GFP-positive cell (white arrowheads) located close to the ventral base of the neural tube remains at this position over the next 21 hours when the expression of nRFP marks the appearance of the DRG in the same region. A medially positioned cell (blue arrowhead in I) migrates out to the horizontal myoseptum and divides to form melanophores of the lateral stripe (blue arrowheads in J). (K′) Enlargement of the boxed region in K. (K″) Green channel only.

In adult *erbb3b* (also known as *hypersensitive*, *hps* and *picasso*) mutants, melanophores are drastically reduced but the larval melanophore pattern appears normal (Whitfield et al., 1996; Budi et al., 2008; Hultman et al., 2009; Hultman and Johnson, 2010). Mutations in *erbb3b* as well as in *erbb2* (*kitzelig*, *kiz*) not only cause defects in pigmentation, but also in the peripheral nervous system and lateral line glia (Lyons et al., 2005; Rojas-Muñoz et al., 2009). Morpholino and small molecule inhibitor studies show that both regenerating and adult melanophores require ErbB3b signalling during the first day of embryogenesis when NC cells delaminate and migrate (Budi et al., 2008; Hultman et al., 2009; Johnson et al., 2011; Budi et al., 2011). These findings support a model in which ErbB signalling is required in the early embryo to establish both the peripheral nervous system and the melanophore stem cells that later generate the adult melanophore pattern (Hultman et al., 2009; Hultman and Johnson, 2010).

kita mutant fish display a severe melanophore reduction. In larvae and juveniles, melanophores are almost completely absent. The adult fish display median longitudinal stripes that contain only ~15% of the normal number of melanophores (Johnson et al., 1995; Parichy et al., 1999; Hultman et al., 2007). In mice, mutations in *Kit* (also known as dominant-white spotting), in addition to a pigment phenotype, lead to an early failure in haematopoiesis, and homozygotes are embryonic lethal (Geissler et al., 1988). Similar phenotypes are observed in *Steel* (*Kitl*) mutant mice, which carry lesions at the *Kitlg* locus encoding the ligand of Kit. In mice, zebrafish and humans, *Kitlg* expression is required both for the migration and the survival of melanocyte precursors as well as later in the epidermis, where melanocyte precursors disperse throughout the entire embryo (Huang et al., 1992; Wehrle-Haller et al., 2001; Rawls and Johnson, 2003; Gu et al., 2009; Gu et al., 2011).

The *sparse like* (*slk*) mutant (Kelsh et al., 1996) displays a phenotype similar to that of *kita* mutants. We have positionally cloned *slk* and show that it encodes the zebrafish Kit ligand a. Both *kita* and *slk* (*kitlga*) mutants are viable and fertile; they display no defects in haematopoiesis, germ cell development or osteoclast development. The mutant phenotype of both genes suggests that larval and the majority of adult melanophores are Kitlga signalling dependent.

We present evidence for a distinct population of MPs associated with the DRGs. They require *slk* (*kitlga*) to function as stem cells. These melanophore stem cells are quiescent during larval life and activated in juveniles to give rise to the postembryonic MPs that distribute in a segmental fashion along the spinal nerves. Precocious activation is observed in embryos depleted of melanophores by *mitfa*-morpholino (MO) knockdown. Furthermore, their establishment, although not requiring Mitfa, depends on ErbB signalling in early embryonic development, which is required for migration of all NC cells including the MPs and DRG precursors along the ventromedial path. Our data suggest that DRGs serve as a niche for stem cells that generate melanophores contributing to the pigment pattern of adult fishes.

MATERIALS AND METHODS

Zebrafish husbandry and stocks

Zebrafish were maintained as described (Brand et al., 2002). Transgenic lines were provided by the following people: *Tg(mitfa:gfp)*^{w47} by James Lister, VCU Medical Center, Richmond, Virginia, USA; *Tg(−8.4neurog1:nRFP)*^{sb3}, *Tg(−4.9sox10:gfp)* by Robert Kelsh, University of Bath, Bath, UK; *Tg(nbt:DsRed)* by Madeleine van Drenth from the Max-Planck Institute for Developmental Biology, Tübingen, Germany. The following mutant alleles were used in this study: *alb*^{b4} (Streisinger et al., 1986), *erbb2*^{t20604} (*kiz*), *erbb3b*^{t21411} (*hps*) (Rojas-Muñoz et al., 2009), *mitfa*^{w2} (*nac*) (Lister et al., 1999), *kitlga*^{tc244b} (*slk*), *sox10*^{i3} (*cls*).

Mapping and cloning of *sparse like*

slk was mapped following Geisler et al. (Geisler et al., 2007) between markers z21055 (2.0 cM; LOD 63.1) and z3490 (2.3 cM; LOD 21.1) on

chromosome 25. *kitlga* maps within the same interval. RNA was isolated from 48 hours post fertilisation (hpf) *slk* embryos using TRIzol (Life Technologies, Frankfurt, Germany) and processed into cDNA with Transcriptor High Fidelity cDNA Synthesis Kit (Roche Diagnostics Deutschland, Mannheim, Germany). The *kitlga* transcript was amplified, subcloned into pGEM-T (Promega, Mannheim, Germany) and sequenced.

RNA *in situ* hybridisation

A RT-PCR-based approach was used to generate probes for RNA *in situ* hybridisation. The PCR was performed using an antisense primer containing a T7-promoter sequence on its 5′-end. The DNA oligonucleotides used were: *kitlga*, 5′-TCTCGTTCCATATGAAGAAGTCAA-3′ and 5′-TAATACGACTCACTATAGGTCAGATATCCCCACATCTAATGG-3′ (Hultman et al., 2007). The PCR product included the target sequence flanked by the T7-promoter sequence, enabling us to synthesise an RNA riboprobe by *in vitro* transcription of the PCR product using T7-RNA polymerase (Fermentas, St Leon-Rot, Germany). Whole-mount *in situ* hybridisation (Thisse and Thisse, 2008) and antibody staining (Schulte-Merker, 2002) were performed as described. Anti-HuC/HuD (Honjo et al., 2008) was obtained from Life Technologies.

Generation of chimeric fish

Rhodamine dextran (Life Technologies) was injected into *Tg(mitfa:gfp)* donor eggs at the one-cell stage and about ten cells were transplanted at the blastula stage into *alb* recipients of the same age. The *alb* recipients had been injected at the one-cell stage with *mitfa* MO. Chimeric embryos were scored at 3 days post-fertilisation (dpf) and imaged using the LSM5 Live, Carl Zeiss Microimaging, Jena, Germany. Chimeras displaying donor-derived melanophores at the horizontal myoseptum were individually raised to adulthood and scored for darkly pigmented melanophores in the pale *alb* background.

Morpholino injection

MO injections were carried out as described (Nasevicius and Ekker, 2000) with the following amounts: *mitfa* 5.0 ng (*mitfa*-MO, 5′-CATGTTCAACTATGTGTTAGCTTC-3′), *kitlga* 5.0 ng (*kitlga*-MO, 5′-CTGGATAACAACACTCACCACTTCT-3′) (Hultman et al., 2007) and *erbb3b* 2.0 ng (erbb3b, 5′-TGGGCTCGAACTGGGTGGAAACAA-3′) (Budi et al., 2008). All MOs were obtained from Gene Tools LLC, Philomath, USA.

Inhibitor treatment

Embryos at somitic stages were dechorionated and placed in 10 μM of ErbB inhibitor (PD168393, Calbiochem, Merck KGaA, Darmstadt, Germany) at 28°C for 4 hours. Embryos were mounted in agarose (also containing 10 μM PD168393) and imaged for 24 hours.

DRG ablation

Tg(−8.4neurog1:nrfp)^{sb3} embryos at 3 dpf were anaesthetised and mounted in 0.6% low temperature melting agarose on glass-bottom dishes. Embryos were mounted laterally and four to eight DRGs of consecutive metamers were ablated using a 351-nm 100-Hz pulsed laser line on a FV1000 Olympus confocal microscope (Olympus Europa Holding, Hamburg, Germany).

TUNEL assay

Embryos were dechorionated and then fixed in 4% paraformaldehyde overnight at 4°C. Apoptosis staining was performed using the *In Situ* Cell Death Detection Kit (Roche Diagnostics Deutschland) according to the manufacturer's protocol.

Imaging

Embryos were dechorionated, anaesthetised in 0.004% tricaine and mounted in 0.6% low temperature melting agarose on glass-bottom dishes at 28°C. Live imaging was performed using a LSM5 Live confocal microscope (Carl Zeiss Microimaging). The data were analysed using IMARIS 6.1 software (Bitplane A6, Zurich, Switzerland). In some imaging experiments, the medial crest population was identified after removing the superficial optical sections with the function 'Crop 3D'. Adult fish were imaged using a Canon EOS 5d mark II (Canon Deutschland, Krefeld, Germany).

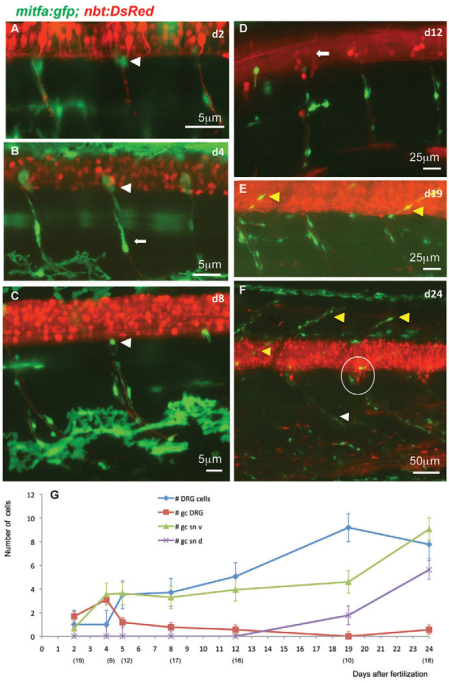

Fig. 2. Stationary MPs located at the DRGs give rise to MPs located along the spinal nerves. (**A-F**) Time-lapse confocal imaging of *Tg(mitfa:gfp;nbt:DsRed)* zebrafish individuals during larval development of consecutive ages. GFP-positive cells at the exit point of the spinal nerves (white arrowheads in A-C) appear to be stationary. Other GFP-positive cells of more elongated shapes are observed along the spinal nerves (e.g. arrow in B). Until 12 dpf (D), no GFP-positive cells can be seen along the dorsally extending spinal nerves (arrow in D), whereas at metamorphic stages (E,F) both the dorsally extending (yellow arrowheads) and the ventrally extending (white arrowhead) spinal nerves show an increased number of associated GFP-positive cells. The number of cells in each DRG (circled in F) has increased to about eight. (**G**) Average numbers of GFP-positive cells per hemisegment located at the DRGs, the ventral and dorsal spinal nerves as well as DRGs at increasing larval age (dpf). The numbers of hemisegments counted is indicated below the respective time points. gc DRG, green cells at DRG; gc sn v, green cells at spinal nerves ventral; gc sn d, green cells at spinal nerves dorsal.

RESULTS

Stationary MPs are associated with DRGs

A transgenic line expressing GFP under the control of the *mitfa* promoter (Lister, 2002) allows the 4D imaging and tracing of melanoblasts in early development. *mitfa:gfp* is initially broadly expressed among NC cells. Subsequently, its expression becomes more and more restricted to melanoblasts although it is also observed in other chromatophore types and glia (Curran et al., 2009). In the trunk, NC cells migrate along the ventromedial path

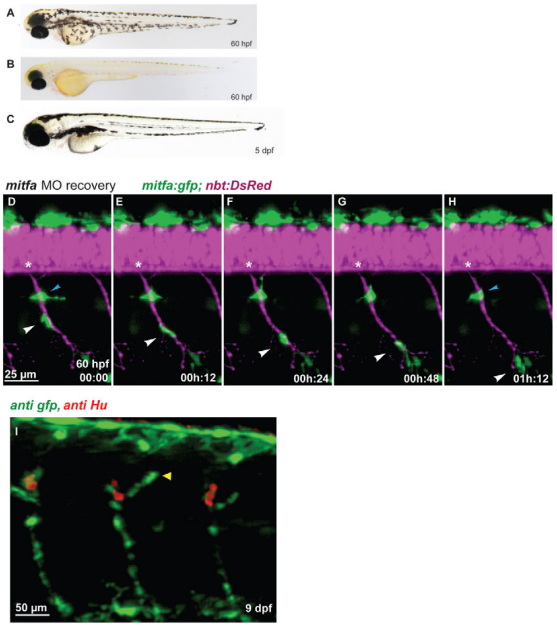

Fig. 3. Regenerating MPs emerge at the site of the DRGs and travel along the spinal nerves. (**A-C**) In contrast to wild type (A), *mitfa*-MO-treated zebrafish embryos (B) lack larval melanophore pigmentation until 60 hpf, but regenerate the larval melanophore stripes completely by day 5 (C). (**D-H**) *Tg(mitfa:gfp; nbt:DsRed)* embryo previously treated with *mitfa*-MO imaged for several hours starting at 60 hpf (digital sectioning). A GFP-positive cells (white arrowhead) migrates along the spinal nerve. Another cell remained stationary (blue arrowhead) but was later observed to migrate away. Asterisks indicate the position of the DRG. (**I**) In *mitfa* morphant larvae (9 dpf), the regenerating MPs form a string of *mitfa*-positive cells along the spinal nerves associated with the DRGs both dorsally (arrowhead) and ventrally.

in close association with primary motor neurons, labelled in Fig. 1A-G with a transgene expressing DsRed under the control of a neuron-specific promoter (*nβt:DsRed*) (supplementary material Movie 1). We identified some of the migrating GFP-positive cells as melanoblasts because they undergo melanisation while still associated with primary motor axons (Fig. 1E,F). We observe round stationary cells remaining at the motor axon exit point (Fig. 1G, arrow).

We followed *mitfa:gfp*-labelled cells together with RFP-labelled cells of neuronal origin under the control of a neurogenin promoter (*neurog:rfp*). Melanophores forming the lateral stripe also originate from *mitfa:gfp* cells following the ventromedial path at ~40 hpf, turning into the horizontal myoseptum and migrating towards the skin (Fig. 1H-K, blue arrowheads). Fig. 1K shows the appearance of the DRG precursor cell at 48 hpf located next to a *mitfa:gfp*-labelled cell that resided at this position for at least 21 hours.

The larval set of melanophores has differentiated by 3 dpf and GFP expression has largely ceased. Interestingly, at later time points we still observe GFP-labelled cells located close to the DRGs (Fig. 2A-C, arrowheads) and along the ventral motor neurons (Fig. 2B, arrow). Their elongated shape suggests that they are, at least in part, Schwann cells. Schwann cells along the lateral line also retain the *mitfa:gfp* label until late larval stages (data not shown).

Imaging larvae until metamorphosis (Fig. 2A-F) shows that the number of stationary cells at the site of the DRG expressing *mitfA:gfp* remains at the level of zero to one labelled cell per hemisegment. The number of labelled cells along the ventral spinal nerve (Fig. 2B, arrow) remains about four throughout larval development (Fig. 2G). No labelled cells along the dorsal spinal nerves (Fig. 2D, arrow) can be observed until metamorphosis, when the number of *mitfa:gfp*-labelled cells increases along the spinal nerves both dorsally and ventrally (Fig. 2E,F, arrowheads). This suggests that these are MPs emerging from the stationary cells at the DRG.

We propose that the DRG-associated stationary cells include melanophore stem cells producing MPs that later give rise to adult melanophores.

Recovering melanoblasts emerge at the DRG and migrate along the spinal nerves

Larval melanophores can regenerate if chemically or genetically ablated (Yang and Johnson, 2006; Hultman et al., 2009; Tryon et al., 2011). To investigate whether these newly formed melanophores originated from the putative DRG-associated stem cells, we depleted the directly differentiating melanophores with a *mitfa*-morpholino. (Mellgren and Johnson, 2004) and traced melanophore renewal by 4D *in vivo* imaging in the *Tg(mitfa:gfp)* line.

In the first 60 hpf, knockdown of Mitfa faithfully phenocopies the *nac* mutant phenotype as the *mitfa*-MO-treated embryos do not show pigmented melanophores. Strikingly, in subsequent stages, larval melanophore pigmentation recovers and by 5 dpf the larval melanophore pattern is completely restored (Mellgren and Johnson, 2004) (Fig. 3A-C). This indicates that knockdown of Mitfa during early development affects melanoblasts committed to direct differentiation, whereas the melanoblast population that restores the pattern is derived from melanophore stem cells that did not require Mitfa early in development (Hultman and Johnson, 2010).

In *mitfa*-MO embryos between 60 and 80 hpf, new *mitfa:gfp*-labelled melanoblasts appear. In time-lapse movies, we captured melanoblasts originating at the site of the DRG and migrating along the spinal nerves (Fig. 3D-H). We were able to follow *mitfa:gfp*-labelled cells in *mitfa*-MO individuals until late larval stages. Fig. 3I shows a stereotyped pattern of GFP-positive cells associated with DRG neurons (red) notably following both the dorsal (arrowhead) and ventral projections. This pattern resembles that observed later in juvenile wild-type fish, when *mitfa:gfp*-positive cells appear in close contact with the spinal nerves (Fig. 2E,F) (Budi et al., 2011).

To trace the migration and cell lineage of individual regenerating melanoblasts, we transplanted cells from *mitfa:gfp* embryos into *albino* (*slc45a2* – Zebrafish Information Network) mutant embryos treated earlier with *mitfa*-MO. This enabled us to select embryos in which donor cells (rhodamine-tracer positive) contributed to the DRGs. We imaged GFP-positive cells appearing at the location of donor-derived DRGs for 28 hours starting at 60 hpf. Fig. 4A-E (see also supplementary material Movies 2, 3) shows the migration of GFP-positive cells dividing several times while travelling along the sensory projections labelled in red. These cells originated from a single unlabelled cell that resides close to a DRG, begins to express GFP and undergoes a division giving rise to one daughter cell that remains at this location. The other daughter cell moves away, divides again and melanises once it reaches the ventral side of the myotome. In this clone, the migration of individual progeny of silent MPs could be traced along DRG-derived neurons to a location in the ventral stripe as well as into the dorsal stripe to differentiate into darkly pigmented melanophores (Fig. 4F-H).

We traced several GFP-labelled melanoblasts (n=8) that originate from the site of the DRGs, migrate along the spinal nerves and give rise to melanophores of larval stripes. We thus identified the MPs residing close to the DRG as progenitors of regenerating melanoblasts. From these transplantation experiments we selected chimeric animals displaying donor-derived melanophores located at the horizontal myoseptum and individually raised these to adulthood. In three out of five such cases, adult melanophores developed at the same location as the regenerated larval pigmentation (Fig. 4I,J). The chimeras displayed donor-derived melanophores in vertical streaks often spanning the entire pattern from dorsal to ventral. This indicates that MPs that give rise to the regeneration of the larval pigmentation also generate the adult melanophore pattern.

We conclude that in *mitfa*-MO-treated embryos the absence of differentiated melanophores induces premature activation of embryonic MPs located in close proximity to DRGs. This results in proliferation and migration of MPs that first restore a larval pattern, and eventually produce adult melanophores.

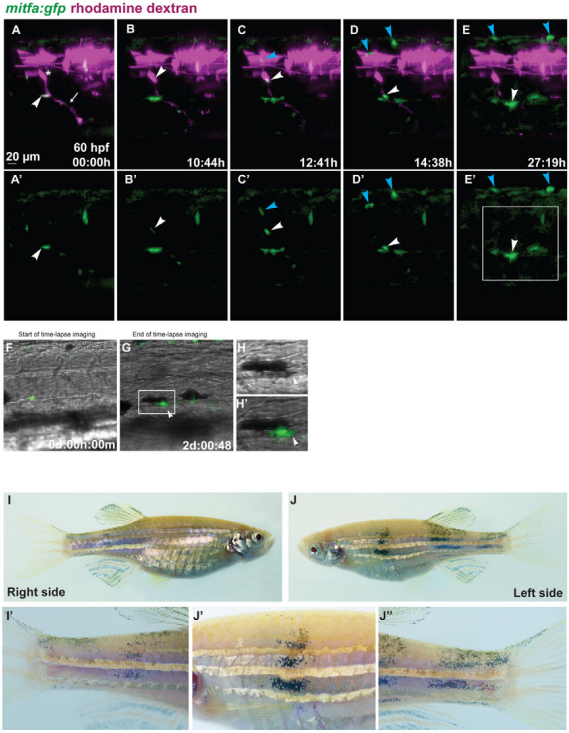

Fig. 4. Tracing individual MPs during regeneration in chimeric animals. Blastula transplantations were performed with *Tg(mitfa:gfp)* zebrafish embryos injected with rhodamine dextran as donors and *alb* embryos injected with *mitfa*-MO as recipients. (**A-E′**) Red and green channel are shown in A-E, green channel only in A′-E′. Starting at 60 hpf (A,A′), we imaged a clone appearing at the site of a rhodamine-labelled DRG (asterisk) from which a peripheral axon extends ventrally (arrow). The arrowhead in A,A′ points to a GFP-positive cell located at the ventral side of the myotome. Another labelled cell appears at 70 hpf at the site of the DRG (arrowhead in B,B′). This cell divides, and the two daughter cells migrate dorsally (blue arrowhead) and ventrally (white arrowhead) along a spinal nerve (C,C′). The dorsally migrating cell divides once (blue arrowheads in D-E′), its progeny arrive at the dorsal side of the larva. The ventrally migrating cell divides once (white arrowheads in D-E′). (**F-H′**) The daughter cells, after reaching a position along the ventral stripe close to a cell that arrived there earlier, melanise (arrowheads in G-H′). Complete time-lapse imaging is shown in supplementary material Movies 2, 3. The region marked in E′ is shown in more detail in G, and the boxed area in G is enlarged in H,H′. (**I-J″**) Chimeric adult fish that had developed several donor-derived melanophores at the lateral stripe in late larval stages. These display vertical streaks of donor-derived melanophores spanning the entire flank from dorsal to ventral, including the fins, enlarged in I′,J′,J″. These streaks appeared in the same rostrocaudal position as the larval melanophores.

ErbB receptors are required for the migration of all NC cells along the ventromedial path

To learn more about the role of DRGs in melanophore development, we examined mutants of the neuregulin receptors ErbB3b (also known as *hypersensitive*, *hps*) and ErbB2 (*kitzelig*, *kiz*) that lack DRGs and glia (Lyons et al., 2005; Honjo et al., 2008; Budi et al., 2008; Rojas-Muñoz et al., 2009). Whereas *erbb2* mutants are larval lethal, the *erbb3b* alleles are hypomorphs with variable expressivity and viability and mutant fish may survive to adulthood. Strikingly, large portions of the flank of *erbb3b* fishes are devoid of melanophores (Budi et al., 2008) (Fig. 5A). Small molecule inhibitor studies indicated that ErbB3b/ErbB2 signalling is required during the first day of embryogenesis for the subsequent development of metamorphic melanoblasts (Budi et al., 2008). A close correlation between the position of defects along the anteroposterior pattern in the adult fishes and the time window of inhibition coinciding with the developmental stage at which NC delaminates and migrates in the respective segments was shown by Budi et al. (Budi et al., 2008) in *sparse* (*kita*) mutant embryos for Kit-independent melanophores. We confirmed this correlation for wild type (Fig. 5B-E).

Honjo et al. (Honjo et al., 2008) reported that the lack of DRGs in *erbb3b* mutant embryos resulted from a failure of the NC cells to pause during migration towards the ventral side of the embryo. We performed 4D time-lapse imaging of NC labelled with *sox10:gfp* and neural tissue labelled with *nβt:DsRed*. In wild-type embryos, *sox10:gfp*-positive NC cells, after reaching the ventral side of the neural tube, continue to migrate in the conspicuous segmental streams along the primary motor neurons towards the ventral side of the embryo (Fig. 6A-A″). By contrast, no migration occurs in embryos treated with small molecule inhibitors of ErbB receptors, and NC cells are arrested dorsally to the neural tube (Fig. 6B-B″). The motor neurons remain uncovered by glial cells. A close-up at 36 hpf shows that embryonic *mitfa:gfp*-positive MPs are absent in inhibitor-treated embryos (Fig. 6C,D). Imaging of *mitfa:gfp* cells in the *erbb2* mutants showed that no NC migration occurs along the ventromedial path (supplementary material Movie 4). In *erbb3b* mutant embryos, some segments are completely devoid of migrating NC, whereas in others migration is normal (data not shown). Notably, migration of NC cells along the dorsolateral path is normal in *erbb* mutants or inhibitor-treated embryos (Fig. 6B′; supplementary material Movie 4). These observations indicate that ErbB signalling is required for NC migration specifically along the ventromedial path.

We investigated the recovery of melanoblasts in partial MO knockdowns of ErbB3b in *mitfa* morphants. We observed that some segments completely recovered the stream of GFP-positive cells associated with the DRG neurons, whereas others had a complete lack of such cells (Fig. 6E). There is a strong correlation between the presence of DRGs and recovered *mitfa:gfp*-positive cells whereas segments lacking a DRG do not usually display them (Table 1).

To examine further the role of DRGs, eight DRGs were laser ablated in wild-type larvae at 3 dpf. We observed a lower number of melanophores in the corresponding segments of the flank of the respective adult fishes and, thus, mild phenocopies of the *hps*/*picasso* mutant phenotype in eight out of ten cases (Fig. 5F).

These experiments support the notion that DRGs provide a niche for melanophore stem cells.

Fig. 5. The Role of ErbB signalling and the DRGs for adult melanophore pigmentation. (**A**) *hps/erbb3b*^{t21411} adult fish showing a dramatic regional reduction of melanophores. (**B-E**) Adult fish treated at successive stages of somitogenesis (left) with the ErbB inhibitor PD168393. The later the inhibitor was applied, the more posterior is the position of the defect (brackets). (**F**) Adult fish in which eight consecutive DRGs were laser-ablated at 3 dpf.

sparse like encodes Kit ligand a

We next investigated the role of Kitlga signalling in the establishment of melanophore progenitors. *spa* (*kita*) is required for the survival, migration and differentiation of melanoblasts at all stages of development. We identified the mutant *sparse like* (*slk*), (Kelsh et al., 1996) (Fig. 7) as affected in *kit ligand a* (*kitlga*) (Hultman et al., 2007). In both *spa* and *slk* mutants, late larval and metamorphic melanophores are absent (Fig. 7F-H). A population of Kitlga signalling-independent melanophores appears in adult fish (Fig. 7J). The mutant *slk* carries a stop codon in the *kitlga* gene (Fig. 8A). *kitlga* is expressed at very low levels in early embryos at the site of premigratory NC (Hultman et al., 2007) (data not shown). Its expression persists in segmental patches in cells under the epidermis on the dorsal side as well as in segmentally repeated expression domains close to the notochord (Hultman et al., 2007). This *kitlga* expression domain is absent in *sox10* mutant embryos and includes a subset of neural crest at the site of the developing PNS (Fig. 8B-D).

Table 1. Quantification of the association of DRGs and GFP-positive cells as shown in Fig. 6F

	Count	
DRG staining	Control	*erb3b*MO+*mitfa*MO
Hu+; *mitfa*:GFP+	190	138
Hu+; *mitfa*:GFP–	40	30
Hu–; *mitfa*:GFP+	2	5
Hu–; *mitfa*:GFP–	4	77
Total	236	250

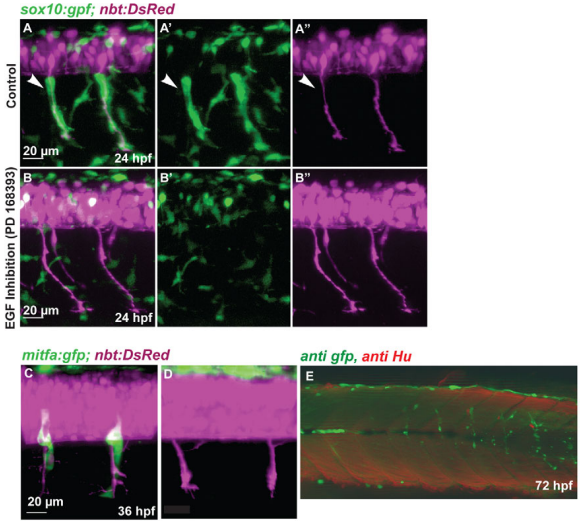

Fig. 6. NC migration along the ventromedial path is blocked by inhibition of ErbB receptors. (**A-B″**) *Tg(sox10:gfp; nbt:DsRed)* zebrafish embryos at 24 hpf. (A,B) Red and green channel (merge); (A′,B′) green channel; (A″,B″) red channel. Medial NC cells (green) covering the primary motor axons (white arrowheads, A-A″) are absent after treatment with the ErbB inhibitor PD168393 (B-B″). (**C**,**D**) Confocal images of 36 hpf *Tg(mitfa:gfp; nbt:DsRed)* embryos. (C) Wild-type embryo. (D) Embryo treated with ErbB inhibitor at 16 hpf. (**E**) *Tg(mitfa:gfp)* embryos were injected with a double MO combination against *mitfa* and *erbb3b*. Larvae were stained at 8 dpf using anti-GFP (green) and anti-HU (red) antibody (white arrowheads). The association of DRGs (red) and GFP-positive cells was quantified (Table 1). In double *mitfa* and *erbb3b* knockdowns, of 82 metamers lacking HU positive cells only five (6%) develop a string of GFP-positive cells.

Kitlga signalling is required for embryonic MP formation

We imaged the site of DRG formation in *slk* embryos at 48 hpf. Fig. 9A-D shows the presence of *mitfa:gfp*-labelled cells located close to the progenitors of the DRGs. However, these cells often appear elongated and detached in *slk* mutants (Fig. 9B,D, arrowhead), suggesting that the stationary MPs are reduced or missing but *mitfA:gfp*-positive glia cells are retained. We observed the *mitfa:gfp*-labelled cells located along the spinal nerves in wild-type (Fig. 2) and *slk* mutant (data not shown) fish until metamorphosis. Although reduced in number, we do not observe a significant qualitative difference, presumably because the labelled cells are mostly glia. Interestingly, like in wild type, in *slk* mutants labelled cells along the dorsal spinal nerve are not observed before metamorphosis (data not shown). This indicates that in *slk* mutants, despite the absence of melanophores there is no precocious activation of MPs to produce regenerating melanoblasts, as seen in *mitfA*-MO-treated embryos (Fig. 3I). Embryos treated with *kitlga* MO do not show melanophore pigmentation and faithfully copy the mutant phenotype until late stages of larval development (Fig. 9G,H). Thus, in contrast to *mitfa*, *kitlga* morphants do not regenerate the larval melanophore population. This indicates that in

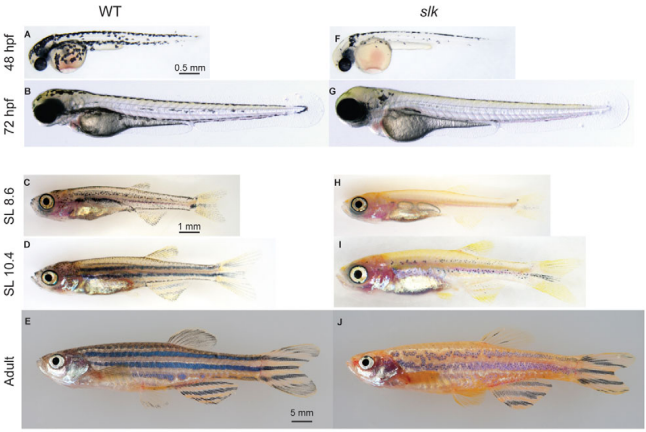

Fig. 7. The phenotype of *sparse like*^{tc244b} fish at different developmental stages. (**A-J**) The phenotype of wild-type (A-E) and *sparse like* (F-J) fish at different developmental stages. Unlike wild-type fish (C), *slk* fish are almost completely devoid of melanophores at the beginning of metamorphosis (H). Adult *slk* mutants (J) form stripes with strong reduction in melanophore number compared with wild-type siblings (E). SL, standard length.

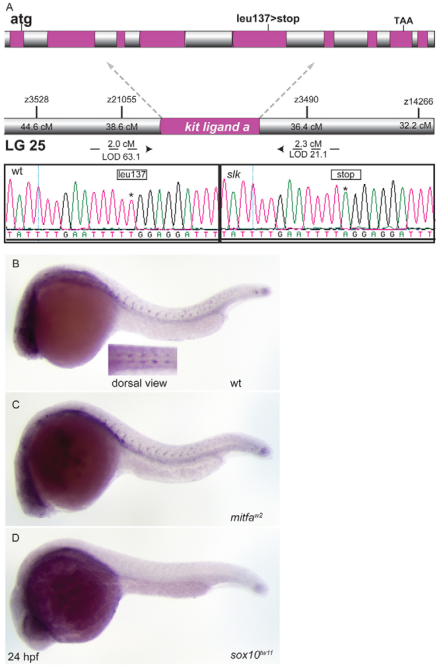

Fig. 8. *slk* encodes Kitlga and is expressed in NC cells. (**A**) *slk* mutants reveal a T to A base substitution in exon 5 of the *kitlga* transcript causing a premature stop codon. (**B-D**) *kitlga in situ* hybridisation. At 24 hpf, *kitlga* is expressed in NC cells migrating along the medial path. This expression domain is maintained in *mitfa* mutants (C) but not in *sox10* mutant embryos (D).

kitlga mutant embryos, embryonic MPs located at the DRG are missing or fail to function as stem cells. It also suggests that in normal development MPs are established during the first few days of embryogenesis when the MO knockdown is effective, under the control of Kitlga signalling.

In *slk* embryos, we do observe that *mitfa:gfp* cells undergo apoptosis before NC migration commences (Fig. 9C,D), reflecting the *slk* phenotype. This observation supports the notion that there is a population of melanoblasts in this dorsal location that is specified before migration along the dorsolateral route and that requires Kitlga signalling for its survival.

DISCUSSION

Identification of melanophore stem cells

Although the presence of embryonic melanophore stem cells (MSCs) had already been postulated (Budi et al., 2008; Johnson et al., 2011), their location remained elusive. We demonstrate that the embryonic MPs we observe during early development closely associated with the emerging DRGs are MSCs. These MSCs can be activated prematurely using MO knockdown of Mitfa to remove larval melanophores. The progeny of activated MSCs can be traced as they express *mitfa:gfp* and are mitotically active. They can regenerate all components of the larval melanophore pattern. Moreover, during migration along spinal nerves they form a chain of GFP-expressing cells, closely resembling postembryonic MPs reported by Budi et al. (Budi et al., 2011). Melanoblasts originating from these MPs migrate into the skin, melanise and arrange themselves in the striped pattern of the adult (Fig. 4). During normal development, activation of the quiescent melanophore stem cells occurs in late larval and juvenile stages (Fig. 2), giving rise to the adult melanophore pattern.

MSCs require ErbB signalling and are associated with the DRGs

Our live imaging confirms that NC migration along the ventromedial path occurs in close association with the extending primary motor axons (Banerjee et al., 2011). Melanoblasts of the larval pattern also migrate along this path, as shown by the direct tracing of *mitfa:gfp* cells that undergo melanisation (Fig. 1E,F). Mutations in *erbb2b* or treatment with drugs inhibiting ErbB receptors inhibit migration of NC cells along the ventromedial path. The close correlation between the position of adult pigmentation defects along the rostrocaudal axis and the time window of inhibiting migration of NC cells (Budi et al., 2008) (Fig. 5B-E) strongly supports the notion that the MSCs are also affected by the inhibitor. Both glia and melanoblasts express ErbB receptors (Lyons et al., 2005; Budi et al., 2008). Unlike glia, which require ErbB signalling during migration, proliferation and differentiation, in the case of the melanophores, once this migration has occurred, ErbB signalling is no longer required for the development of adult melanophores.

The stem cells we have identified are associated with the DRGs of the peripheral nervous system. ErbB-dependent NC migration also affects DRGs when perturbed. The progenitor cells of the DRGs settle at the exit point of the primary motor neurons adjacent to the ventral spinal cord (Carney et al., 2006). We found a close association of MSCs with the DRGs. Through ablation in the embryo we have provided evidence of the role of DRGs in the establishment of melanophore stem cells either as a niche, a source for the peripheral nerves on which MPs travel to the surface, or both.

So far, although we have ample evidence from lineage tracing that MSCs are located at the site of the DRGs, we do not exclude additional sites. Some of the *mitfa:gfp*-positive cells along ventral spinal nerves in larval stages (Fig. 2) might also function as MPs.

Kitlga signalling specifically affects melanophore stem cells

Our data indicate that the Kitlga pathway is specifically required for a progenitor population of melanophores whereas other NC-derived cell types are not affected. In *kitlga* embryos, the DRGs are formed and *mitfa:gfp*-positive cells are seen close to them and along the spinal nerves. Most, if not all, of these cells are presumably glial cells, and from the morphology we cannot unequivocally distinguish embryonic MPs and glia cells. These cells may include progenitors of Kitlga-independent adult melanophores that also migrate along the ventromedial path (Budi et al., 2008). The failure of the melanophore population to regenerate after *kitlga*-MO treatment means that they do not function as MSCs, and that MSCs require Kitlga signalling very early for their establishment. We observe cells that undergo apoptosis at a dorsal location, indicating that they are specified as

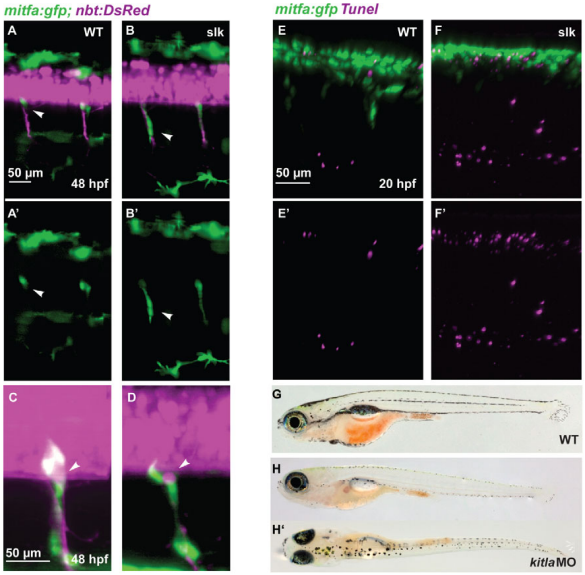

Fig. 9. Abnormal NC migration and apoptosis in *slk* embryos. (**A-B′**) GFP-positive cells in double transgenic *Tg(mitfa:gfp; nbt:DsRed)* wild-type (A,A′) and *slk* mutant (B,B′) embryos at 48 hpf. In the wild-type embryo, GFP-positive NC cells remain at the position of the DRG and have a rounded morphology (white arrowhead in A,A′) whereas in *slk* mutants they are stretched along the nerves and appear to be migratory (white arrowheads in B,B′). A′, B′ show green channel only. (**C**,**D**) Magnification showing *mitfa:gfp*-labelled cells at the exit point of the spinal nerves at 48 hpf of wild-type (C) and *slk* mutant (D) embryos. The arrowheads point to DRGs. (**E-F′**) TUNEL staining in *Tg(mitfa:gfp)* embryos in wild-type (E,E′) and *slk* (F,F′) embryos at 20 hpf. E′,F′ show red channel only. (**G-H′**) Wild type (G) and *slk* morphant (H,H′) at 20 dpf (5.7 mm SL).

melanoblasts prior to migration. Presumably most of these cells are melanoblasts destined to migrate along the dorsolateral route. *kitlga* is expressed early in NC cells located at the site of the future DRG and associated glia. It is tempting to speculate that, in addition to survival and migration, Kitlga has the function of a niche factor of MSCs. In this context, it is interesting to note that in mice, kit ligand (also known as steel factor) provides a niche factor for survival and migration of primordial germ cells (Gu et al., 2009).

We note that at the early time point, *kitlga* function distinguishes the various NC fates as in *slk* mutants only the melanophores are strongly reduced but there is no evidence that glia, peripheral nervous system or other chromatophore types are affected.

Melanophore progenitors migrate along a vertical path

In zebrafish, 4D imaging allows tracing of migrating cells and tissue with high resolution in time and space during embryonic and larval life. The premature activation of quiescent stem cells after *mitfa*-MO knockdown has enabled us to study the origin and migration of postembryonic regenerating MPs already in late larval stages. Regenerating melanophores are responsive to ErbB inhibition in the same time window in early development as adult melanophores (Hultman and Johnson, 2010; Johnson et al., 2011). Tracing regenerating melanophores in larval and adult chimeras confirmed the notion that both populations arise from the same stem cells (Fig. 4).

During metamorphosis, MPs originate at the DRGs and move along the spinal nerves both dorsally and ventrally. These cells populate individual segments with MPs that form a stream of labelled cells (Fig. 2E,F). In chimeric animals, during metamorphosis donor MPs populate the skin of albino recipients with melanophores in vertical streaks running from dorsal to ventral (Fig. 4; data not shown). This suggests that a segmental melanophore streak results from a single or a very small number of stem cells being seeded and that these can give rise to the entire population of MPs of a segment by spreading along the segmental spinal nerves, whereas little lateral spreading occurs. Fig. 10 illustrates schematically the paths taken by melanophore progenitors during embryogenesis (Fig. 10A-C) and metamorphosis (Fig. 10D-F).

Distinct classes of melanophore progenitors

On the basis of these observations, several classes of MPs can be distinguished. On the first day of development, a small number of MSCs that reside close to the DRGs in each segment is established. These are normally quiescent throughout larval life and do not require *mitfa*. They are dependent on Kitlga signalling for their function as MSCs. The development of MSCs depends on migration of NC cells along the ventromedial path and the establishment of the DRGs. This process requires ErbB2/3b receptor signalling during the first 18-24 hours of development.

In later larval and juvenile stages, another class of MPs appears as progeny of activated MSCs. These postembryonic MPs express *mitfa:gfp*, originate from the DRGs, proliferate and migrate along the spinal nerves. We do see melanising cells along the peripheral nerves in adult fishes, and propose that the MPs observed in extra hypodermal space (Budi et al., 2011) are in fact associated with nerve bundles running along myosepta. Both classes of MPs are present in *mitfa* mutants.

The DRG-associated MSCs give rise to the melanophores of the adult pattern. We presume but have not yet directly shown that these

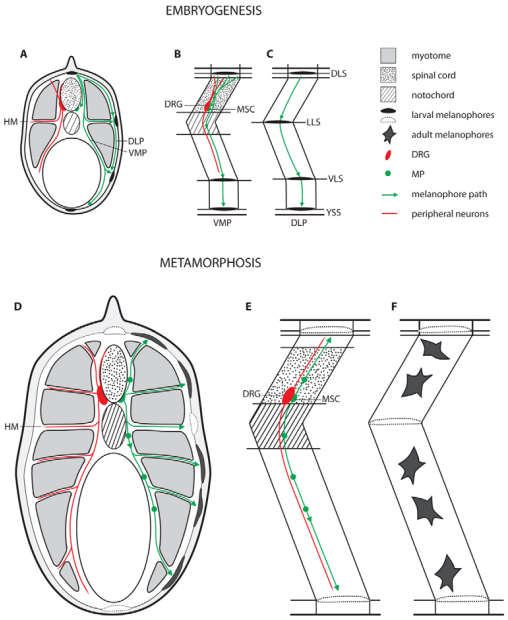

Fig. 10. Model of migration of melanophore progenitors during embryogenesis and metamorphosis. (**A**) Schematic cross-section through a trunk segment indicating the path of the peripheral neurons emerging from the DRG (left side). The migratory route taken by the melanoblasts along the ventromedial path (VMP) and the dorsolateral path (DLP) (right side). (**B**) Side view of the ventromedial path showing that melanoblasts contribute to the ventral larval stripes (VLS), they migrate through the horizontal myoseptum (HM) to form the lateral larval stripe (LLS). (**C**) Melanoblasts traveling along the dorsolateral path between somites and epidermis contribute to all three stripes. DLS, dorsal larval stripe; YSS, yolk sac stripe. (**D-F**) During metamorphosis adult melanophores arrive in the skin originating from melanophore progenitors (MPs) associated with the spinal nerves (red) that innervate the myotome via myosepta. These MPs are derived from embryonic melanophore stem cells (MSCs) located at the DRGs. The larval melanophores (dotted) later disappear.

have the capacity of self-renewal, as anticipated from stem cells. Failure in the establishment of MSCs cannot easily be repaired, as seen in the long-lasting effects of the early transient inhibition of the receptors of the ErbB signalling system, the DRG ablation, and the failure to recover the melanophore pattern in *kitlga* morphants. We propose that stem cell maintenance depends on the microenvironment provided by the DRG and associated glia as a stem cell niche, and speculate that one function of Kitlga signalling is to attract and to maintain them in this niche. The postembryonic MPs may be regarded as transient amplifying cells as they proliferate and provide the adults with the necessary supply of melanophores during stripe formation, growth and regeneration.

It is important to note that most, but not all, adult melanophores originate from these Kitlga signalling-dependent stem cells. During adulthood, *spa* and *slk* mutants develop a striped pattern displaying melanophores that do not require Kitlga signalling. Budi et al. (Budi et al., 2011) presented evidence for the existence of melanophore progenitor cells that develop from cells co-expressing *foxd3* and *mitfa*, possibly shared Schwann cell progenitors. A Schwann cell precursor origin of melanocytes derived from the ventromedial path of NC migration has also been observed in amniotes such as mice and chicken (Adameyko et al., 2009). Clonal analysis in adult zebrafish indicates that some melanophores share a lineage with iridophores (A. Singh, A.M. and C.N.-V., unpublished). Kitlga signalling-independent adult melanophores, however, require ErbB signalling at the same early time interval as the Kit-dependent MSCs (Budi et al., 2008), suggesting that these melanophore progenitors also travel along the ventromedial path. We do not yet know the embryonic origin of adult xanthophores or iridophores.

Although dorsolateral migration holds for some of the larval melanophores in zebrafish, adult melanophores arise from migration along nerves in a similar manner to the melanocyte progenitors described by Adameyko et al. (Adameyko et al., 2009) in mouse and chicken. We present evidence for a stem cell population that resides at the DRGs and that appears to be specific to melanophores. Although we expect the embryonic origin of adult melanophores to be common to fishes, it will be interesting to ascertain whether stem cells with a similar origin are also present in the amniotic vertebrates.

Acknowledgements
Sören Alsheimer, Ajeet Singh, Virgilio Failla and Christian Liebig provided excellent support in confocal microscopy and image processing. We thank Andrey Fadeev for assistance in adult fish photography. Robert Geisler and Ines Gehring provided technical support in the mapping of *slk*. We thank Jana Krauss and Ajeet Singh for discussion, and Robert Kelsh, Darren Gilmour, Simon Perathoner for valuable comments on earlier versions of the manuscript.

Funding
This research was funded by the Max-Planck Society, Germany.

Competing interests statement
The authors declare no competing financial interests.

Supplementary material
Supplementary material available online at
http://dev.biologists.org/lookup/suppl/doi:10.1242/dev.087007/-/DC1

References

Adameyko, I., Lallemend, F., Aquino, J. B., Pereira, J. A., Topilko, P., Müller, T., Fritz, N., Beljajeva, A., Mochii, M., Liste, I. et al. (2009). Schwann cell precursors from nerve innervation are a cellular origin of melanocytes in skin. *Cell* **139**, 366-379.

Banerjee, S., Gordon, L., Donn, T. M., Berti, C., Moens, C. B., Burden, S. J. and Granato, M. (2011). A novel role for MuSK and non-canonical Wnt signaling during segmental neural crest cell migration. *Development* **138**, 3287-3296.
Brand, M., Granato, M. and Nuesslein-Volhard, C. (2002). Raising and keeping zebrafish. In *Zebrafish: a Practical Approach* (ed. C. Nuesslein-Volhard and R. Dahm). Oxford: Oxford University Press.
Budi, E. H., Patterson, L. B. and Parichy, D. M. (2008). Embryonic requirements for ErbB signaling in neural crest development and adult pigment pattern formation. *Development* **135**, 2603-2614.
Budi, E. H., Patterson, L. B. and Parichy, D. M. (2011). Post-embryonic nerve-associated precursors to adult pigment cells: genetic requirements and dynamics of morphogenesis and differentiation. *PLoS Genet.* **7**, e1002044.
Carney, T. J., Dutton, K. A., Greenhill, E., Delfino-Machín, M., Dufourcq, P., Blader, P. and Kelsh, R. N. (2006). A direct role for Sox10 in specification of neural crest-derived sensory neurons. *Development* **133**, 4619-4630.
Curran, K., Raible, D. W. and Lister, J. A. (2009). Foxd3 controls melanophore specification in the zebrafish neural crest by regulation of Mitf. *Dev. Biol.* **332**, 408-417.
Darwin, C. (1871). *The Descent of Man, and Selection in Relation to Sex*. John Murray, London.
Dutton, K. A., Pauliny, A., Lopes, S. S., Elworthy, S., Carney, T. J., Rauch, J., Geisler, R., Haffter, P. and Kelsh, R. N. (2001). Zebrafish colourless encodes sox10 and specifies non-ectomesenchymal neural crest fates. *Development* **128**, 4113-4125.
Elworthy, S., Lister, J. A., Carney, T. J., Raible, D. W. and Kelsh, R. N. (2003). Transcriptional regulation of mitfa accounts for the sox10 requirement in zebrafish melanophore development. *Development* **130**, 2809-2818.
Gans, C. and Northcutt, R. G. (1983). Neural crest and the origin of vertebrates: a new head. *Science* **220**, 268-273.
Geisler, R., Rauch, G.-J., Geiger-Rudolph, S., Albrecht, A., van Bebber, F., Berger, A., Busch-Nentwich, E., Dahm, R., Dekens, M. P. S., Dooley, C. et al. (2007). Large-scale mapping of mutations affecting zebrafish development. *BMC Genomics* **8**, 11.
Geissler, E. N., Ryan, M. A. and Housman, D. E. (1988). The dominant-white spotting (W) locus of the mouse encodes the c-kit proto-oncogene. *Cell* **55**, 185-192.
Gu, Y., Runyan, C., Shoemaker, A., Surani, A. and Wylie, C. (2009). Steel factor controls primordial germ cell survival and motility from the time of their specification in the allantois, and provides a continuous niche throughout their migration. *Development* **136**, 1295-1303.
Gu, Y., Runyan, C., Shoemaker, A., Surani, M. A. and Wylie, C. (2011). Membrane-bound steel factor maintains a high local concentration for mouse primordial germ cell motility, and defines the region of their migration. *PLoS ONE* **6**, e25984.
Haffter, P., Odenthal, J., Mullins, M., and Lin, S. (1996). Mutations affecting pigmentation and shape of the adult zebrafish. *Dev. Genes Evol.* **206**, 260-276.
Hoekstra, H. E., Hirschmann, R. J., Bundey, R. A., Insel, P. A. and Crossland, J. P. (2006). A single amino acid mutation contributes to adaptive beach mouse color pattern. *Science* **313**, 101-104.
Honjo, Y., Kniss, J. and Eisen, J. S. (2008). Neuregulin-mediated ErbB3 signaling is required for formation of zebrafish dorsal root ganglion neurons. *Development* **135**, 2615-2625.
Huang, E. J., Nocka, K. H., Buck, J. and Besmer, P. (1992). Differential expression and processing of two cell associated forms of the kit-ligand: KL-1 and KL-2. *Mol. Biol. Cell* **3**, 349-362.
Hultman, K. A. and Johnson, S. L. (2010). Differential contribution of direct-developing and stem cell-derived melanocytes to the zebrafish larval pigment pattern. *Dev. Biol.* **337**, 425-431.
Hultman, K. A., Bahary, N., Zon, L. I. and Johnson, S. L. (2007). Gene duplication of the zebrafish kit ligand and partitioning of melanocyte development functions to kit ligand a. *PLoS Genet.* **3**, e17.
Hultman, K. A., Budi, E. H., Teasley, D. C., Gottlieb, A. Y., Parichy, D. M. and Johnson, S. L. (2009). Defects in ErbB-dependent establishment of adult melanocyte stem cells reveal independent origins for embryonic and regeneration melanocytes. *PLoS Genet.* **5**, e1000544.
Johnson, S. L., Africa, D., Walker, C. and Weston, J. A. (1995). Genetic control of adult pigment stripe development in zebrafish. *Dev. Biol.* **167**, 27-33.
Johnson, S. L., Nguyen, A. N. and Lister, J. A. (2011). mitfa is required at multiple stages of melanocyte differentiation but not to establish the melanocyte stem cell. *Dev. Biol.* **350**, 405-413.
Kelsh, R. N., Brand, M., Jiang, Y. J., Heisenberg, C. P., Lin, S., Haffter, P., Odenthal, J., Mullins, M. C., van Eeden, F. J., Furutani-Seiki, M. et al. (1996). Zebrafish pigmentation mutations and the processes of neural crest development. *Development* **123**, 369-389.
Lister, J. A. (2002). Development of pigment cells in the zebrafish embryo. *Microsc. Res. Tech.* **58**, 435-441.
Lister, J. A., Robertson, C. P., Lepage, T., Johnson, S. L. and Raible, D. W. (1999). nacre encodes a zebrafish microphthalmia-related protein that regulates neural-crest-derived pigment cell fate. *Development* **126**, 3757-3767.
Lyons, D. A, Pogoda, H.-M., Voas, M. G., Woods, I. G., Diamond, B., Nix, R., Arana, N., Jacobs, J., and Talbot, W. S. (2005). Erbb3 and Erbb2 are essential for schwann cell migration and myelination in zebrafish. *Curr. Biol.* **15**, 513-524.
Mellgren, E. M. and Johnson, S. L. (2004). A requirement for kit in embryonic zebrafish melanocyte differentiation is revealed by melanoblast delay. *Dev. Genes Evol.* **214**, 493-502.
Nasevicius, A. and Ekker, S. C. (2000). Effective targeted gene 'knockdown' in zebrafish. *Nat. Genet.* **26**, 216-220.
Parichy, D. M., Rawls, J. F., Pratt, S. J., Whitfield, T. T. and Johnson, S. L. (1999). Zebrafish sparse corresponds to an orthologue of c-kit and is required for the morphogenesis of a subpopulation of melanocytes, but is not essential for hematopoiesis or primordial germ cell development. *Development* **126**, 3425-3436.
Parichy, D. M., Turner, J. M. and Parker, N. B. (2003). Essential role for puma in development of postembryonic neural crest-derived cell lineages in zebrafish. *Dev. Biol.* **256**, 221-241.
Protas, M. E. and Patel, N. H. (2008). Evolution of coloration patterns. *Annu. Rev. Cell Dev. Biol.* **24**, 425-446.
Quigley, I. K., Turner, J. M., Nuckels, R. J., Manuel, J. L., Budi, E. H., MacDonald, E. L. and Parichy, D. M. (2004). Pigment pattern evolution by differential deployment of neural crest and post-embryonic melanophore lineages in Danio fishes. *Development* **131**, 6053-6069.
Rawls, J. F. and Johnson, S. L. (2003). Temporal and molecular separation of the kit receptor tyrosine kinase's roles in zebrafish melanocyte migration and survival. *Dev. Biol.* **262**, 152-161.
Rawls, J. F., Mellgren, E. M. and Johnson, S. L. (2001). How the zebrafish gets its stripes. *Dev. Biol.* **240**, 301-314.
Rojas-Muñoz, A., Rajadhyksha, S., Gilmour, D., van Bebber, F., Antos, C., Rodríguez Esteban, C., Nüsslein-Volhard, C. and Izpisúa Belmonte, J. C. (2009). ErbB2 and ErbB3 regulate amputation-induced proliferation and migration during vertebrate regeneration. *Dev. Biol.* **327**, 177-190.
Roulin, A. (2004). The evolution, maintenance and adaptive function of genetic colour polymorphism in birds. *Biol. Rev. Camb. Philos. Soc.* **79**, 815-848.
Schulte-Merker, S. (2002). Looking at Embryos. In *Zebrafish: a Practical Approach* (ed. C. Nuesslein-Volhard and R. Dahm), pp. 39-58. Oxford: Oxford University Press.
Streisinger, G., Singer, F., Walker, C., Knauber, D. and Dower, N. (1986). Segregation analyses and gene-centromere distances in zebrafish. *Genetics* **112**, 311-319.
Thisse, C. and Thisse, B. (2008). High-resolution in situ hybridization to whole mount zebrafish embryos. *Nat. Protoc.* **3**, 59-69.
Tryon, R. C., Higdon, C. W. and Johnson, S. L. (2011). Lineage relationship of direct-developing melanocytes and melanocyte stem cells in the zebrafish. *PLoS ONE* **6**, e21010.
Wehrle-Haller, B., Meller, M. and Weston, J. A. (2001). Analysis of melanocyte precursors in Nf1 mutants reveals that MGF/KIT signaling promotes directed cell migration independent of its function in cell survival. *Dev. Biol.* **232**, 471-483.
Whitfield, T. T., Granato, M., van Eeden, F. J., Schach, U., Brand, M., Furutani-Seiki, M., Haffter, P., Hammerschmidt, M., Heisenberg, C. P., Jiang, Y. J. et al. (1996). Mutations affecting development of the zebrafish inner ear and lateral line. *Development* **123**, 241-254.
Yang, C.-T. and Johnson, S. L. (2006). Small molecule-induced ablation and subsequent regeneration of larval zebrafish melanocytes. *Development* **133**, 3563-3573.

Typeset with LaTeX